SYNTHESIS OF HYDROXYAPATITE NANORODS BY REFLUXING AND HYDROTHERMAL METHODS

PAKVIPAR CHAOPANICH

A THESIS SUBMITTED IN PARTIAL FULFILLMENT OF THE
REQUIREMENT FOR THE DEGREE OF DOCTOR OF PHILOSOPHY
(APPLIED CHEMISTRY)
DEPARTMENT OF CHEMISTRY, FACULTY OF SCIENCE
KING MONGKUT'S INSTITUTE OF TECHNOLOGY LADKRABANG
YEAR 2018

KMITL- 2018-SC-D-010-038

Thesis Title	Synthesis of Hydroxyapatite Nanorods by Refluxing and Hydrothermal Methods
Student Name	Miss Pakvipar Chaopanich
Student ID	53650305
Degree	Doctor of Philosophy (Applied Chemistry)
Department	Chemistry
Faculty	Science
University	King Mongkut's Institute of Technology Ladkrabang (KMITL)
Year	2018
Thesis Advisor	Asst. Prof. Dr. Punnama Siriphannon

Abstract

This thesis aims to study the synthesis of hydroxyapatite nanoparticles by facile low temperature refluxing and hydrothermal methods (nHAp) using calcium nitrate tetrahydrate ($Ca(NO_3)_2{\cdot}4H_2O$) and diammonium hydrogen phosphate ($(NH_4)_2HPO_4$) as starting materials, in which the Ca/P molar ratio was controlled at 1.67. The synthesis parameters were varied, i.e. sodium polystyrene sulfonate (PSS) template addition, reaction pH and reaction times. In the refluxing method, the nHAp was synthesized using various concentrations of PSS template, i.e. 0.00, 0.05, 0.20 and 0.30 w/v%. The higher PSS concentration, the shorter rod-liked crystallite size of nHAp was obtained. When the reaction pH for synthesizes of nHAp was varied, i.e. 8.5, 9.5 and 10.5, the shorter rod-liked nHAp crystals were created with the increase of reaction pH. When the refluxing time was increased from 1 hr to 6 hrs, the crystallite size of *002*-plane of nHAp would increase. In the hydrothermal synthesis, the reaction was performed at 100°C for various reaction times, i.e. 0, 0.5, 1, 2 and 3 hrs. The longer hydrothermal treatment times, the larger rod-liked nHAp crystals were obtained. In the PSS free system, the hydrothermal reaction pH increase from 8.5 to 9.5 and 10.5 resulted in the reduction of crystallite size of rod-liked nHAp crystals. However, the longer rod-liked nHAp crystals were obtained in the hydrothermal synthesis with PSS adding. In refluxing method, the surface charge of the synthesized nHAp showed the positive ζ value, preferably bonding with the negatively charged aspartic acid than the positively charged arginine. Conversely, the surface of nHAp particles synthesized by hydrothermal method possessed the negative ζ value, thus, they preferably bond with the positively charged arginine. Moreover, the nHAp synthesized by refluxing and hydrothermal methods with and

without PSS template presented the low percentage of cytotoxicity against Vero cells and effective inhibition of *S.aureus* microorganism.

Keywords: sodium polystyrene sulfonate, refluxing, biomaterials, hydroxyapatite, hydrothermal

Acknowledgement

The author would like to take this opportunity to express sincere thanks to her advisors and people who useful advice and full support in this research.

The author wishes to express deep gratitude to Asst. Prof. Dr. Punnama Siriphannon for her valuable guidance and encouragement throughout this research. It goes without saying to the thesis committee, Asst. Prof. Dr. Dujreutai Pongkao Kashima, Asst. Prof. Dr. Chonlada Ritvirulh, Asst. Prof. Dr. Panpailin Seeharaj and Dr. Kittisak Choojun for reading and criticizing the manuscript.

The author deeply appreciates the Office of the Higher Education Commission, Ministry of Education, Thailand under the research project title "Higher Education Research Promotion" for financial support.

Special thanks to Scientific Instrument Service Center at Faculty of Science at King Mongkut's Institute of Technology Ladkrabang, Scientific Equipment and Research Division (KURDI) at Kasetsart University and National Metal and Materials Technology Center (MTEC) for helping in analysis with special instruments. In addition, thanks also to Department of Chemistry, Faculty of Science, King Mongkut's Institute of Technology Ladkrabang for laboratory instruments and instrument analysis.

The author would like to give the special thanks to all of her friends who have been helping while studying the Ph.D. program.

Miss Pakvipar Chaopanich

Table of Contents

Table of Contents (Continued)

Table of Contents (Continued)

List of Tables

List of Tables (Continued)

Table Page

List of Figures

List of Figures (Continued)

Abbreviations/Symbols

Hydroxyapatite	HAp
Sodium polystyrene sulfonate	PSS
Phosphate buffer saline	PBS
Aspartic acid	Asp
Arginine	Arg
X-ray diffraction spectroscopy	XRD
Fourier transform infrared spectroscopy	FT-IR
Transmission electron microscopy	TEM
Selected area of electron diffraction pattern	SAED
Full width at half-maximum	FWHM
(3-(4,5-dimethythiazoly-2)-2,5-diphenyltetrazodium bromide	MTT
Stephylococus	*S.aureus*
Esherichia	*E.coli*
Zeta potential	ζ

Chapter 1

Introduction

1.1 Research Motivation

Hydroxyapatite (HAp, $Ca_{10}(PO_4)_6(OH)_2$) is identified as an inorganic biomaterial containing calcium phosphate as a basic substance, i.e. bone and teeth. The HAp possesses some interesting properties for medical applications such as biocompatibility, non-toxicity and bioactivity. A small fracture toughness and a flexural strength of HAp are drawback properties of this materials [1-2]. Then, the use of this materials are in the form of powder, coating and non load bearing applications. Forthermore, there are some reports informing about the characteristic of the Hap, which has plate-like or rod-like crystalline forms with particle size smaller than 100 nm and it has similar structure of physical rigid tissues [3-4]. Therefore, this special characteristic of the nanosized HAp is considered to be the best material for long term using in medical applications [5-6]. In addition, the nanosized HAp also showed much higher bioactivity than the microsized HAp [7-9]. Besides, the HAp can be used in various fields of applications, such as wastewater treatment [10], gas sensor [11], chromatography [12], etc.

The developments of synthetic methods including mechanochemical process [13], sol-gel process [14] and solid-state reaction [15] have been purposed by various researchers to produce the HAp nanosized material. However, these methods still have some drawbacks such as multi-tep procedure with high firing temperature and product impurity. To overcome these drawbacks, a hydrothermal reaction has been used for synthesis of HAp nanoparticles [16]. Moreover, this method could perform in the closed system using the aqueous media, classifying as the environmentally friendly process. Although this method is one good way for synthesis the HAp nanoparticles, but it requires an expensive equipment to control the pressure. Therefore, it is a main limitation to be used for large-scale.

From the above mentioned points, this research aimed to study and develop an effectively facile refluxing method for synthesis of HAp nanorods, in which it will be in comparison with the hydrothermal method. The refluxing method is considered to be safe, economic and convenient method for indrustrial manufacture. Moreover, the macromolecular template is added into the synthesis system for control of the size distribution and morphology of HAp nanoscale particles. It is because some macromolecular templates, e.g. chondroitin sulfate (ChS) [17], ethylenediamine tetraacetic acid (EDTA) [18], etc., have been reported that they act

as the effective promoters for nucleus formation and development of HAp crystals and/or preventing HAp agglomeration. In this research, sodium polystyrene sulfonate (PSS) has been used as the macromolecular template because it is strong anionic polyelectrolytes possessing the negative charges on its backbone when it is dissolve in water. Particularly, it is non-toxic and commonly used in biomedical applications, e.g. drug delivery [19], biosensor [20], etc. Moreover, the PSS has been reported that it could enhance the cell adhesion in the *in vivo* tests [21], indicating its biosafety property for biomaterials. Therefore, this research will study the effect of PSS on size, morphology and properties of HAp synthesized by environmentally friendly refluxing and hydrothermal systems. In addition, the biological activities of the synthesized HAp were investigated in order to determine the possibility for biomedical usages.

1.2 Objectives of the study

1) To study the effect of preparation parameters on structure, morphology and properties of HAp.

2) To investigate the biological activities of synthesized HAp.

1.3 Scopes of the study

1) The HAp nanoparticles are synthesized by refluxing method using various preparation parameters as followed;

- PSS concentration; i.e. 0.00, 0.05, 0.20 and 0.30 w/v%
- pH of reaction; i.e. 8.5, 9.5 10.5 11.5 and 12.5
- Refluxing times; i.e. 0, 1, 3 and 6 hrs

2) The HAp nanoparticles are synthesized by hydrothermal method using various preparation parameters as followed;

- Hydrothermal times; i.e. 0, 0.5, 1, 2 and 3 hrs
- PSS concentration; i.e. 0.00 and 0.20 w/v%
- pH of hydrothermal reaction; i.e. 8.5, 9.5 and 10.5

3) The synthesized HAp surfaces are developed using two types of amino acid, i.e. aspartic acid (negative charge) and arginine (positive charge).

4) The synthesized HAp nanoparticles and the develop HAp are characterized by XRD, FT-IR, TEM and Zeta potential analyzer.

5) *In vitro* MTT cytotoxicity and anti-bacterial activity of the synthesized HAp nanoparticles and the modified HAp are investigated.

1.4 Benefits of the study

1) HAp nanoparticles can be synthesized using suitable preparation parameters by facile refluxing method. This method will be the tentative candidate for industrial production.

2) The knowledge about the influence of PSS pattern on the mechanism of HAp crystal development can facilitate the controlling of structure, size and morphology of HAp to fulfill the medical uses.

3) The knowledge about biological activities of the synthesized HAp nanorods can conduce to develop new biological and/or biomedical applications.

Chapter 2

Theory and Literature Reviews

2.1 Biomaterials

An interesting function of biomaterials is used for connecting with biological process including evaluating, treatment augment or reimburse some tissues, organ or specific operation in human body. [22-23] Therefore, the research about biomaterials and their interactions in biological conditions become important for future applications.

An improvement of human heath by using biomaterials is an essential aim of various research and outcome applying use in human body. It is necessary to clarify about characteristics of biological materials such as structures, properties and biological functions. Therefore, there insight knowledges of biomaterials could be stated such as biological materials, implant materials and interaction between materials and physiological environment in the body. [22, 24] From the relationship mentioned above, material with unique structure and properties have been designed and developed in order to fulfill the specific applications in medical uses.

2.1.1 Classification of biomaterials

Biomaterials are commonly classified based on types of materials and interaction between materials and environment as follows:

(A) Types of materials [25]

- **Metals** are classified as inorganic materials having non-direction bonds of metals with extremely transferring electrons. These materials are suitable materials to apply for orthopedic and dental applications such as hip replacements and dental filling, respectively.
- **Polymers** are identified as organic materials containing huge network structures which are bridged together through directional covalent bonds. Polymers are widely used in the human's body applications such as in ophthalmology, skin wound treatments and soft tissue implants.
- **Ceramics** are set in the group of inorganic materials presenting non-directional ionic bonds through the mechanism of donation and acception of electrons. These materials most often employed in biological applications such as implant coating, bone graft substitution and bone cement.

(B) Interaction between materials and environment [25-27]

- **Bioinert materials** preserve both physical characteristic and mechanical properties under the interaction with the neighboring tissues, in which they do not form a bond with surrounding tissues and/or bone. In addition, they should not release any toxic substance into the physiological environment and damage the neighboring tissues, such as alumina, zirconia, titanium, etc.
- **Bioactive materials** form surface bonding with the neighboring tissues and/or bone *via* chemical reactions. The common examples of these materials are hydroxyapatite and bioactive glasses.
- **Bioresorbable materials** are designed to degrade slowly by time and substituted with natural tissues, in which they introduce to the reconstruction of tissues substuting their replacement, e.g. porour hydroxyapatite, tricalcium phosphates, calcium sulfate, etc.

2.1.2 Bioceramics

Ceramics have been developed and used in medical applications in order to develop the well being of human daily life due to their similarities in chemical properties to natural bones. Therefore, the ceramics are most often used for the repair and reconstruction as a part of orthopedic implants and dental materials, which are called "bioceramics". [26] In addition, the bioceramics are manufactured in different patterns, phases and functions for the repair of the human body listed in Table 2.1.

Table 2.1 Characteristic of bioceramic, Form, Phase and Fuction [26]

Form	Phase	Function
Powder	Polycrystalline, Glass	Space-filling, therapeutic treatment, regeneration of tissues
Coating	Polycrystalline, Glass, Glass-Ceramic	Tissue bonding, corrosion protection
Bulk	Single Crystal, Polycrystalline, Glass, Glass-Ceramic, Composite (Multi-Phase)	Replacement and augmentation of tissue

2.2 Hydroxyapatite (HAp)

Hydroxyapatite (HAp) is a major type of calcium-phosphate mixed bioceramic, presenting in the form of $Ca_{10}(PO_4)_6(OH)_2$, in which it is primarily used in the rigid tissue replacement, such as bone and teeth. [28] The HAp has special characteristic including bioactive, osteoconductive, non-toxic and non-immunogenic activities. Additionally, its structure displays crystallographically similar to bone materials. Some of the physiochemical properties of HAp are illustrated in Table 2.2. [29]

Table 2.2 General Properties of Hydroxyapatite [29]

Properties	Data
Chemical Composition	$Ca_{10}(PO_4)_6(OH)_2$
Ca/P molar	1.67
Color	White
Space group	Hexagonal
Cell dimensions (Å)	$a = b = 9.42$, $c = 6.88$
Young's modulus (GPa)	80-110
Elastic modulus (GPa)	114
Compressive strength (MPa)	400-900
Bending strength (MPa)	115-200
Density (g/cm^3)	3.16
Relative density (%)	95-99.5
Fracture toughness ($MPa \cdot m^{1/2}$)	0.7-1.2
Vickers harness	600
Decomposition temp. (°C)	>1000
Melting point (°C)	1614
Dielectric constant	7.40-10.47
Thermal conductivity (W/cm·K)	0.013

The HAp primarily belongs to the hexagonal system of $P6_3/m$ space group, consisting of six fold symmetry axis with a threefold spiral and a microplane. The crystal pattern of HAp is shown in Fig. 2.1. The chemical composition of HAp can be written as $Ca_4(I)Ca_6(II)(PO_4)_6(OH)_2$, where the Ca atoms involve two series of unequivalent sites. The Ca(I) atoms are in the four fold symmetry positions and the Ca(II) atoms present in the six fold symmetry positions. The disordered position are occupied by OH group on the top or under of the triangles generated by the Ca(II) atoms. Four atoms of Oxygen (O) around phosphate (P) atom produce a tetrahedron in which it is practically regular with only small distortion. The structure of purposed

crystal and the behavior of crystallization of HAp are energetically depend upon the exchanging nature of the ionic species and the sequence. The crystalline structure of HAp can be modified by administration of the calcium to phosphorus (Ca/P) molar ratio. [29]

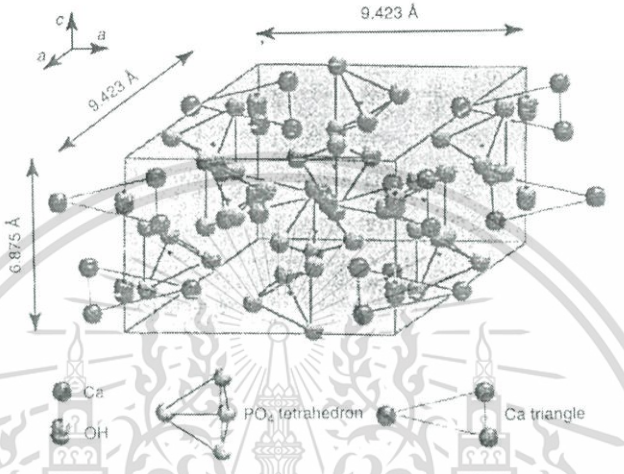

Figure 2.1 Crystal structure of diagonally viewed HAp [29]

In general, the biomaterials with nanostructure commonly possess higher bioactivity than those with larger particle size, therefore, the HAp nanostructure has attracted a lot of attention than the coarser crystals. [30] Among the various HAp nanostructures, the plate-liked biological apatite crystal occurs in bone orientated along the *c*-axes which is different from that in dentin and enamel in teeth. Particularly, the enamel is composed of rod-like apatite crystals with 25-100 nm in length.

2.2.1 Preparation of hydroxyapatite

The HAp can be prepared by many techniques, including rigid/ solid state reaction, mechanochemical method, solvent based chemical process, template-assisted method, etc. The preparation methodology and key ingradients used in the synthesis can affect the morphologic characteristics, stoichiometry, crystallinity and properties of the HAp products. [29]

2.2.1.1 Solid state reaction

Rigid or Solid state reaction has basically been applied for the production of ceramic fine grained at high temperature. The HAp powders prepared

by using this method usually have irregular shapes with large grain size, in which they quite often exhibit heterogeneity in their phase compositions. It is because the differences in chemical reactions developing from small diffusion coefficients of ions within the structure of solid. The basic manufacture of HAp through solid state method is done by the following reaction in equation (2.1) at 1000 to 1300°C: [29]

$$CaHPO_4{\cdot}2H_2O + 4CaCO_3 \longrightarrow Ca_{10}(PO_4)_6(OH)_2 + 4CO_2 + 14H_2O \quad (2.1)$$

The significant parts of this reaction are fundamentally occurred in solid phase acting as Ca and P ancestor for preparation of HAp. [29] In addition, the HAp can also be produced by solid state reactions in equation (2.2-2.3) as follows:

$$6CaHPO_4 + 4Ca(OH)_2 \longrightarrow Ca_{10}(PO_4)_6(OH)_2 + 6H_2O \quad (2.2)$$

$$3Ca_3(PO_4)_2 + Ca(OH)_2 \longrightarrow Ca_{10}(PO_4)_6(OH)_2 + H_2O \quad (2.3)$$

2.2.1.2 Mechanochemical method

The mechanochemical process is the strategy in the conventional process of particle manufacture. The nanoscale particles are produced by gradual cracking down bulk raw materials until they become nanosize. [31] This method usually known as mechanical alloying is a basic drying process for fabrication various complicated materials, such as nanosized crystalline alloys and ceramics. [32] The process not only involves physical reduction in material size, but also uses the milling energy to started chemical reactions between the milled raw substances, in which they usually involve two or more solid reactants. Sometimes, the starting substances are milled together in the presence of a huge amount of sacrificial salt, such as NaCl, which protects the accumulation of the purposed nanoscale particles. [31]

In addition, the high energy occurred during ball milling not only benefit to crystallize the HAp product without heat treatment, but also break the HAp product to the nanocrystalline HAp. [31] Some of simplified reactions are shown in equation (2.4-2.6) as follows: [32-33]

$$6CaHPO_4 + 4Ca(OH)_2 \longrightarrow Ca_{10}(PO_4)_6(OH)_2 + 6H_2O \quad (2.4)$$

$$10CaCO_3 + 6(NH_4)_2HPO_4 \longrightarrow Ca_{10}(PO_4)_6(OH)_2 + 2H_2O + 4CO_2 \quad (2.5)$$

$$6CaHPO_4{\cdot}2H_2O + 4CaO \longrightarrow Ca_{10}(PO_4)_6(OH)_2 + 14H_2O \quad (2.6)$$

2.2.1.3 Wet-chemical method

Liquid-phase syntheses are generally wet-chemical method, known as gentle solution procedure. An aqueous synthetic process becomes a remarkable method for synthesizing the ceramic powder, especially nanoscale-sized particles with an achievement of size control and morphology. The solution based chemical procedures have been generally recognized as an effective method to produce nanoscale crystalline particles using low temperature. Main benefits of liquid-phase procedure include: (1) The preparing procedure can be easily level up due to the nature of bulk-process; (2) The procedure has controlling ability because the preparation methods have been modified and developed for aqueous base chemical synthesis to produce the nanoscale particles; (3) Various procedures need only gentle conditions such as low temperature and atmospheric process; (4) The chemical constitutions of nanoparticles can be converted in an aqueous phase; (5) The addition of the surface-handily agents can be done in between and after nanoscale particle formation to control particle size and product the impurity of some substant accumulation in the liquid phase in order to control the size and prevent any unnecessary agglomeration; and (6) The process of a homogeneous nucleation, growth and aggregation mechanisms can be used to prepared monodispersed nanoscales in aqueous phase [31]

Reactions belonging to ideal ceramic nanoparticle formation include: (1) the oxidation-reduction reaction; (2) particle precipitated by poor solvent; (3) formation way of ions; (4) chelate formation ; (5) dissociation of compounds; (6) dissolvation in organic media, and (7) hydrolysis in liquid media. The particle forming process can be either by molecular diffusion/ addition to the nuclei surface or by a particle agglomerating mechanism. [31]

The aqueous based chemical syntheses are especially fitted to the syntheses of nanoscale particles (solid, core-shell, or hollow particles) with firmly controlled conditions, such as: size and shape, monodispersity, the chemical constitution and purity, bulk substructure, crystallinity (polycrystalline, single crystalline, or amorphous), functional group of surface, free energy of interface and density of surface charge, etc. [31] These methods can be mainly classified as chemical precipitation, sol-gel, sonochemical, microwave heating and hydrothermal methods. The simplified equations of commonly used chemical reactions modified for the aqueous based synthesis of HAp are shown in equation (2.7-2.11): [29, 32, 34]

$$10Ca(NO_3)_2+6(NH_4)_2HPO_4+8NH_4OH \longrightarrow Ca_{10}(PO_4)_6(OH)_2+20NH_4NO_3+6H_2O \quad (2.7)$$

$$10Ca(NO_3)_2+6(NH_4)_3PO_4+2H_2O \longrightarrow Ca_{10}(PO_4)_6(OH)_2+18NH_4NO_3+2HNO_3 \quad (2.8)$$

$$10CaCl_2+6K_2HPO_4+2H_2O \longrightarrow Ca_{10}(PO_4)_6(OH)_2+12KCl+8HCl \quad (2.9)$$

$$10Ca(OH)_2+6H_3PO_4 \longrightarrow Ca_{10}(PO_4)_6(OH)_2+18H_2O \quad (2.10)$$

$$10CaCO_3+6NH_4H_2PO_4+2H_2O \longrightarrow Ca_{10}(PO_4)_6(OH)_2+3(NH_4)_2CO_3+7H_2CO_3 \quad (2.11)$$

A. Chemical precipitation method

Precipitation of chemical process can be normally explained by the occurance of solid phase from the reactions of soluble reactive species in a solution (aqueous or nonaqueous). The the process of chemical precipitation consists of three steps; i.e. chemical reaction, nucleus formation, and crystal development. The chemical precipitation is naturally not a controlled process in terms of reaction kinetics and nucleus formation of solid phase and developing processes. Therefore, the solids achieved by chemical precipitation have a wide range of particle size distribution, uncontrolled particle morphology and accumulation. [31]

Moreover, the HAp manufactured from aqueous systems by precipitation or hydrolysis was frequently calcium-deficient and enriched HPO_4^- and the formation of a tri-calcium phosphate upon heating process above 800°C. [26] Moreover, the dicalcium phosphate anhydrous (DCPA) and dicalcium phosphate dihydrate (DCPD), the acidic phases of CaP, are thermodynamically lower stable under pH values larger than 6-7 and transform to the HAp phase, in which the transformation process depend on the temperature, pH value and illustration of other ions in the system. [32]

B. Sol-gel method

Metal in the form of alkoxides dissolved in the homogeneous alcohol-water solutions are significantly used in a sol-gel method. This process naturally relates to a stage of sol (solids suspended in a continuous liquid phase) formation and then a stage of gellation (liquid particles/ pockets suspended in a continuous solid phase). Science water and initial substance of alkoxide group are unmixable, thus, a common solvent such as alcohol is purposed Catalysts such as mineral acids (such as HCl) or bases (such as ammonia) are mostly used. [31]

Sol-gel process is related to the hydrolysis and condensation of initial molecules, in which it played an important role in glass and

ceramic coating applications. Through this process, the homogeneous oxide materials with sensible properties like hardness, optical transparency, chemical durability, customize porosity and thermal resistance can be produced at room (or low) temperatures. [31] Therefore, this process is one of the most popular method proposed for the wet chemical preparation of HAp and the HAp product can be calcined at lower temperature than that from the other wet chemical methods. [32]

In addition, a stoichiometric structure with huge surface area and little cluster size of powders was recieved by the typical sol–gel process. In the solution phase, the reaction between the Ca and P precursors with a long period of aging is frequently required for the formation of apatitic phase form. Furthermore, the heating process has been discovered to be critical in the generation of pure HAp. [32, 35] A general reaction is shown in equation (2.12) as follows:

$$10Ca(NO_3)_2{\cdot}4H_2O+6KH_2PO_4+20NH_4OH \rightarrow Ca_{10}(PO_4)_6(OH)_2+6KOH+20NH_4NO_3+5H_2O \quad (2.12)$$

However, the major disadvantages of this method include the high cost of alkoxide-based precursors and the generation of secondary phase, i.e. CaO. The CaO has been illustrated to be toxic to the biocompatibility of HAp. [32]

C. Sonochemical synthesis

Ultrasound has been utilized to particularly in materials synthesis for enhancing chemical reactivity. The chemical effect of ultrasound is primarily derived from acoustic cavitation. The breakdown of bubbles in liquid results a concentration of enormous power from the transformation of the kinetic energy of motion into heat liquid contents of the bubble, in which it occurs the rapid cooling from the high local temperature and pressure under extreme conditions. Additionally, the chemical reactants are activated to accelerate the heterogeneous reactions between liquid and solid substances, therefore; this method can increase the rate of reaction. [31] The general formation of HAp using sonochemical synthesis is shown in equation (2.13) as follows: [36]

$$6H_3PO_4 + 10Ca(OH)_2 \rightarrow Ca_{10}(PO_4)_6(OH)_2+18H_2O \quad (2.13)$$

D. Microwave heating synthesis

Microwave-assisted method for the manufacture of inorganic substances has been examined since 1986. As compared to tradiyional oven heating (with a low rate heating and heat transfer), the microwave "volumetric"

heating of liquids is an alternative heating approach with specific benefits The microwave heating of hydrothermal reactor was found in some cases to significantly reduce the time of reaction, to generate extraordinary uniformity size and to produce some new phases. [31]

In addition, the HAp-related bioceramics have been prepared by using microwave processing techniques under the optimum conditions in order to minimize the reaction time and product cost, and to increase the purity of biomaterials. This method offers several advantages over normal furnace heating corresponding to time and energy saving. [29]

E. Hydrothermal synthesis

Hydrothermal production methodology relates to the reaction of the starting solution at high temperature and high pressure atmosphere. This process able to prepare well phase of crystalline product with homogeneous composition. This synthetic method mention to liquid based process of metal salts or autoclaving of starting materials salts including gels at elevated temperatures (typically 100-300°C) and pressures above 1 atm. [29, 31]

In this purposed procedure, the sols of ceramics zre formed through chemical process in the aqueous solution under controlling of heat and pressure in the alkali or acid media having a pseudo catalytic effect following the reaction. In the laboratory, the synthetic process frequently used is hydrothermal method carried on in a batch-type autoclave, where moisture or liquid in solution are gentlely evaporated until reach the target temperature, and then spend several hours or days for aging. [31] It is also a useful technique for growth of single crystals; by arranging for a suitable temperature gradient to be present in the reaction vessel, dissolution of the starting material may occur at the hot end and reprecipitation at the cooler end. [37] In addition, the water in the hydrothermal synthesis acts as a reaction activator and occasionally as a component of solid phase in the synthesis. At the increased temperature and pressure, the requirements for the initiating materials used in the hydrothermal synthesis are the accurately known compositions that is as homogeneous, pure, and fine as possible. [38]

The conditions of the process including pH of solution, temperature and ion in solution, etc., can be used to identify what the phase of solid are formed. By changing the solution parameters (pH, surfactant concentrations, anion concentrations, cation concentrations and solvents) and processing parameters (temperature, duration and stirring), can effectively control the nanoparticle size and shape, and the extent of agglomeration. [31]

2.2.2 Template-assisted HAp preparation

In the present, templates have been used to develop the synthesis of high surface area materials with structure and size in the length scales between nanometer and micrometer for various applications. [25] Principles of the structure pattern through templating are based on two different procedures, i.e.

- Endotemplating; molecules or larger template are added to the mixture of precursors and are blocked in the growing solid. These templates are removed in the last step.
- Exotemplating; this approach is based on the infiltration of performed porous scaffold with a precursor mixture. After solidification, the porous scaffold or template is removed.

In addition, the removal of the template is the last step in the synthesis, in which it can generally be performed in different ways, e.g. [25]

- Extraction is performed by several washing steps.
- Organic solvents with dissolved acids, such as ethanol with HCl, are used to remove the template. However, the covalently bonded templates cannot be removed by this procedure.
- Calcination is typically performed between 400 and 600°C in various atmospheres such as nitrogen or air.

2.3 Polyelectrolytes

Polyelectrolytes are a class of macromolecular compounds or polymers that develop significant charges when dissociated or swollen in solvent having high polar such as water. These polymers are generally called *polyions* because their charges arise from various types of ionized functional groups located along the backbone (chain contour), resulting in the polymer chains with electrostatic charges. The force of electrostatic objects presents the interaction between the ionized groups on the backbone make the polyelectrolyte systems discrete from the neutral polymer systems, in which they show the prominent feature, i.e. stretching between the ionized groups on the chain due to the repulsive force. [39-42]

2.3.1 Types of Polyelectrolytes

McCormick *et al.* (1991) classified the types of polyelectrolytes based on their behaviors in aqueous electrolyte solutions as follows: [43]

- Univalent polyelectrolytes are polyelcetrolytes with same charges, either negative (anionic groups) or positive (cationic groups).

- Multivalent polyelectrolytes or polyampholytes are the polyelectrolytes contain both negative and positive groups.

The polyelectrolytes can also be classified into two categories, i.e. natural macromolecules (biopolymer) and synthetic macromolecules, in which some typical examples are given in Table 2.3. Furthermore, the polyelectrolytes exhibit various molecular architectures, e.g. globular polyelectrolytes, chainlike polyelectrolytes, etc. [41, 44-45]

Table 2.3 Typical Polyelectrolytes [46]

Natural Polyelectrolytes	Repeat Units
DNA (single stranded)	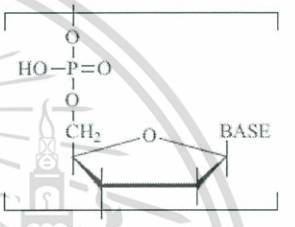
Chitosan	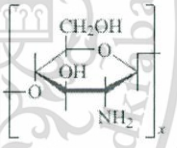
Hyaluronic acid	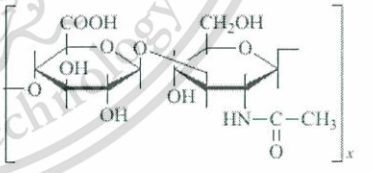
Synthetic Polyelectrolytes	**Repeat Units**
Poly(acrylic acid)	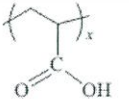
Poly(lysine)	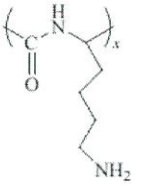

2.3.2 Properties of Polyelectrolytes

The solution properties of polyelectrolytes are described by Noda and Muroga (1996) [45] that the properties of polyelectrolytes are mainly related to the chain conformations, in which they are affected by short- range and wide gap electrostatic interactions. The narrow gap effects are the interactions between adjacent monomers charged groups, resulting in the chain stiffness. Whereas, the long-range effects are the interaction between the charged groups along the disconnected chains. Additionally, the behavior polyelectrolyte chains in solution can be determined by the solution conditions, such as ionic strength and temperature, in which these behaviors depended on the chain orientation and the electrostatic interactions between polyelectrolyte chains. [45] Considering the behavior polyelectrolyte chains in salt free solution, the electrostatic interaction is occurred between the charged groups along the polyelectrolyte backbone chains i.e. strong Coulombic repulsions resulting in the elongate chains. When a salt is added into the polyelectrolytes solution, the interaction of electrostatic force between the charged groups on the backbone is screened by the salt ions, therefore, the electrostatic interaction on the polyelectrolyte chains is collaped, creating the chain flexibility. [40]

Because of their specific properties, both natural and synthetic polyelectrolytes have been widely used in wide range of applications. Previously, they have been utilized as thickeners or gelling agents in foods, pharmaceutical and cosmetics. [41] Particularly, the polyelectrolytes are mostly used in biological functions, such as modification of solution rheology and controlling the agglomeration of colloidal particles. [42]

In this thesis, the sodium polystyrene sulfonate (PSS) was used as template for hydroxyapatite synthesis. The PSS is an anionic polyelectrolyte as shown in Fig. 2.2. The PSS is identified as a water-soluble substance generating strong multi-electrolyte, they possess the polyanions which can interact with the positive active sites.

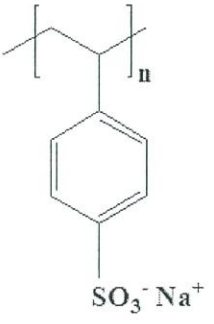

Figure 2.2 Chemical structure of sodium polystyrene sulfonate (PSS)

2.4 Biological Testing of Biomaterials

In the present, the biocompatible property of the biomaterials is important to utilize in the biomedical applications. Particularly, the consideration of this property is depended on two principles, i.e. biosafety and biofunctionality. The prominent properties of materials for biosafety and biofunctionality are these materials must not release any toxic substance into the system and relate to the efficiency of these materials for specific tissue applications, respectively. In order to determine the biocompatibility of biomaterials which will be used in the human body, they must be primarily *in vitro* tested by the standardized testing. [47]

2.4.1 Cytotoxicity Testing

Cytotoxicity relates to the effect of the toxic substances that affect the viability cells. The evaluation of cytotoxicity of biomaterials to cells by *in vitro* assays can be used for primary screening of biomaterials. The simplest *in vitro* cytotoxicity testing is the direct contact assays or the MTT assays. [48] The advantage of this study can provide the information about the response of a specific cell type to the biomaterials, therefore, the suitable materials can be selected for *in vivo* system. [22]

2.4.2 Anti-bacterial Testing

The study on the effect of the bacterial adhesion to the biomaterials surface is one of the necessary step for biomedical applications, particularly, the infection and the antibiotic sensitivity. This effect can be explained the interactions mechanisms between the bacterial and the biomaterials surface, in which it can provide the suitable surface properties of the biomaterials for the anti-adhesion bacterial applications. The simple method for screening the antibiotic sensitivity of biomaterials is the diffusion method using agar medium, in which it can be evaluated by the measuring of the diameter of the inhibition zone of bacterial growth. [49-50]

2.5 Literature Reviews

2.5.1 Preparation of Hydroxyapatite

The literature reviews involved the preparations of HAp are summarized as follows;

2.5.1.1 Solid state reaction

Hoa. *et al.* [51] studied on the synthesis of calcium phosphate bioceramic by solid state reaction. The solid state reactions were performed by using

calcium pyrophosphate ($Ca_2P_2O_7$) or dicalcium phosphate dihydrate ($CaHPO_4{\cdot}2H_2O$, DCPD) and eggshell powders. When the reaction between the eggshell powders and DCPD was heat-treated at 1150°C for 3 hrs, only a single HAp phase was achieved. By object in heat at 1100°C for 3 hrs, the fabricated product from raw eggshell powders ($CaCO_3$) and $Ca_2P_2O_7$ showed the XRD pattern β-tricalcium phosphate (β-TCP) with the trace quantity of HAp. The trace elements, i.e. Na, Mg and Sr, were also determined in calcium phosphate ceramics synthesized from eggshell powders.

Pramanik. *et al.* [52] studied on the synthesis of suitable bioceramic for hard tissue replacement. The HAp of hexagonal structure was done using reaction of solid state at temperature about 1250°C by using CaO and P_2O_5 as the reactants. The HAp samples were improved in the mechanical properties with increasing cold compaction pressures. The result indicated that it showed the high resistance to surface reaction with the simulated body fluid.

Guo. *et al.* [15] focused on the effect of calcination temperature on particle size of HAp. At room temperature, the HAp was manufactured by reaction of solid state, in which the initial materials were diammonium phosphate, calcium nitrate tetrahydrate and sodium bicarbonate. The size and shape of the HAp particles powerfully controlled by the calcination process. The morphologies of HAp particles were observed as irregular and aggregate particles when calcining at temperature lower than 600°C. The XRD patterns of products showed pure HAp crystalline phase when the products were calcined at temperature higher than 600°C. Therefore, the increase of calcinations temperature could promote the crystallization of HAp.

Monmaturapoj and Yatongchai [53] studied on the effect of sintering on microstructure and characteristics of nanosized HAp fine grains produced by aqueous based chemical precipitating and solid-state reaction using $Ca(NO_3)_2{\cdot}4H_2O$ and $(NH4)_2HPO_4$ as the reactants. The reactions were sintered at temperature ranging from 1200 to 1250°C. It was found that the increasing of sintered temperature could be effect to the increasing of the grain size, density and strength of the HAp powders. In addition, the morphologies and properties of the sintered HAp could be control by variation of particle size.

Pramanik. *et al.* [54] studied on the development of mechanical properties of HAp by reaction of solid state. The samples were generated by mixing the ingradients, i.e. CaO, P_2O_5 and SiO_2 and sintered these cold compacted pellets at wide range of temperature from 500 to 1250°C. The results showed that the monetite phase was obtained in the unsintered condition whereas the α-tricalcium phosphate was the final structural transformation of samples when increase the sintering temperature to 1250°C. In addition, the mechanical testing, i.e.

compressive, tensile and bending and were improved after resintering the pellets at 1250°C, where these pellets formerly refused at the similarity of temperature.

2.5.1.2 Mechanochemical Method

Nasiri-Tabrizi. *et al.* [13] purposed on the effect of milling conditions on the formation of nanocrystalline HAp using various kinds of initial materials. The milling parameters used in the synthesis of nanocrystalline HAp, i.e. milling time and atmosphere, in which the syntheses were performed under air or high purity Ar atmosphere at 800°C. The HAp products with high degree of crystallinity were obtained in both milling environments and were influenced by the chemical compositions of initial materials, i.e. $CaHPO_4$, $Ca(OH)_2$ and $CaCO_3$. In the air atmosphere, the average sizes of HAp were about 32 and 27 nm for products from 1-hr and 80-hrs milling, respectively. On the other hand, they were respectively about 32 and 34 nm for 1 hr and 80 hrs milling under Ar atmosphere. However, the milling under both atmospheres for 80 hrs could drastically decrease the crystalline phase of products.

Fahami. *et al.* [55] studied on the preparation of calcium phosphate-based composite nanopowders by mechanochemical method and heating process. After mechanochemical activation, the major phases, i.e. HAp, MgO and TiO_2 were obtained, in which the average HAp crystallite size for 10-hrs milling product was 21 nm. When thermal annealing at 700°C, the major crystalline phases were HAp, $MgTiO_3$ and MgO, in which the crystallite size of HAp was 34 nm. In addition, the decomposition of HAp to β-TCP was happened when heating step in between 900 to 1100°C and the morphological change from the cluster-like shape to the spheroidal crystals was observed.

Mandal. *et al.* [56] studied on the optimization of milling conditions of the mechanical synthesis of nanosize of crystals HAp using phosphorous pentoxide and calcium hydroxide as starting materials. The effects of milling process, i.e. ball size, milling time and milling speed, were studied. The result showed that the optimal grinding condition was the system using 4 nm diameter balls at 60% milling speed for 15 hrs, in which the milled HAp powder showed the spherical particles with size of around 100 nm.

Rhee [57] studied on the synthesis of HAp *via* mechanochemical method from calcium pyrophosphate ($Ca_2P_2O_7$) and calcium carbonate ($CaCO_3$) in acetone and water using milling time ranging from 2 to 8 hrs. The results showed that the single phase HAp was received when the fine grain was milled in water and followed by heating procedure at 1100°C for 1 hr without added water vapor. In addition, it was found that the hydroxyl group needed for the HAp

formation might be supplied from the mechanochemical reaction between the starting powders and water during milling.

Wu. *et al.* [58] prepared the HAp using oyster shell powders through ball milling and heat treatment. The raw materials were $CaCO_3$ (oyster shell) and calcium pyrophosphate ($Ca_2P_2O_7$) or dicalcium phosphate dihydrate ($CaHPO_4{\cdot}2H_2O$, DCPD). In the air atmosphere, the reaction between $CaCO_3$ and $Ca_2P_2O_7$ powders produced the major HAp phase with a small β-TCP by product. When the $CaCO_3$ and DCPD were mixed and milled for 5 hrs and followed with the heating process at 1000°C for 1 hr, the pure HAp phase was achieved.

Nasiri-Tabrizi. *et al.* [59] synthesized the nanosized single-crystal HAp through mechanochemical method using $Ca(OH)_2$, $CaHPO_4$ and $CaCO_3$ as the reactants. The nanorods and nanogranules of HAp crystals were synthesized when using the polymeric milling media. The average size of HAp powder was in the range of 20 to 23 nm. This proposed method was considered to be a facile method for synthesize the high quality single crystal HAp.

2.5.1.3 Chemical Precipitation Method

Monmaturapoj. [60] prepared the nanosized HAp powders by wet-chemical method using various concentrations of the starting solutions, i.e. $Ca(NO_3)_2{\cdot}4H_2O$ and $(NH_4)_2HPO_4$. The reactions were occurred under the reflux process at 100°C for 1hr followed by ageing for 24 hrs, in which their dried products were calcined at temperature ranging in between 800 to 1000°C. It was found that the optimized low concentration of the starting solution could be induced the nanosized HAp phase, but it obtained a small amount of β-tricalcium phosphate. In addition, the result of density and specific surface area of product were 4.05 g/ cm^3 and 89.58 m^2/ g, respectively.

Afshar. *et al.* [61] studied on the effects of many parameters in the wet precipitation process, i.e. pH, atmosphere and stirring speed on the HAp synthesis. In this process, the orthophosphoric acid solution was filled into the calcium hydroxide suspension. The high purity small rod-like particles of HAp precipitates were obtained.

Cengiz. *et al.* [62] studied on the preparation and characterization of HAp nanoscale particle by precipitation procedure in the presence of simulated body fluid (SBF) or calcium phosphor tris (CaPTris) solution. It was found that the HAp nanoparticles were obtained when the resulting precipitation in the CaPTris were sintered at 700°C for 2 hrs, whereas the HAp nanoparticles from SBF system need not to be sintered. The structured HAp crystallites from both CaPTris and SBF system were hexagonal structure. The SEM results showed that the needle-

shaped HAp from the SBF system had a width in the range of 10 to 50 nm and a length of 120 to 450 nm. Whereas the HAp desultory particles from the CaPTris system had the length and width lower than 500 and 100 nm, respectively.

Abidi and Murtaza [63] synthesized the HAp nano-powders *via* aqueous based chemical precipitation technique through $Ca(OH)_2$ and H_3PO_4 as precursors at different calcinations temperatures from 100 to 800°C. The deionized water and the ammonia were respectively used for diluting media and adjusting pH of the reaction. It was found that the optimum temperature was 600°C, in which the HAp powders were decomposed to CaO phase when the temperature was above this temperature. The calculated crystallite size of HAp was found in the range of 8.47 to 24.47 nm.

Zhu. *et al.* [64] studied on the manufacture of HAp by chemical precipitation method under atmospheric pressure. The mixtures of $Ca(NO_3)_2{\cdot}4H_2O$, $(NH_4)_2HPO_4$, $(NH_2)_2CO$ and HNO_3 were used as the starting solution, in which the molar ratio of Ca/P was strongly controlled at 1.67. The HAp particles were synthesized by heating the solution in the range from 60 to 80°C, followed by the heating process at 660°C for 8 hrs. The result showed that the increasing of the reaction temperature could increase the size of the particles. In addition, it was found that the various morphologies of HAp powders, such as sphere, rod, layered, dumbbell and fiber, were obtained by controlled conditions.

Rujitanapanich. *et al.* [34] synthesized the HAp from oyster shell *via* precipitation method. The Ca source was prepared by calcining the oyster shell to calcium oxide, and then the calcium oxide was reacted with nitric acid to calcium nitrate. The calcium nitrate was reacted with diammonium hydrogen phosphate at various pH, then the product was calcined at 900°C for 2 hrs. The XRD results showed that the HAp powder obtained at pH 10 had the crystallite size of about 89.5 nm.

Goloshchapov. *et al.* [65] synthesized the nanocrystalline HAp by precipitation method using hen's eggshell (the biological source) and orthophosphoric acid H_3PO_4 at pH 8.5 under the annealing temperature in between 400 to 900°C. The outcome illustrated that the single phase of globular HAp particles having size of 4 to 5 nm were obtained when the annealing temperature was below 900°C. While, the HAp particles decomposed to the calcium diphosphate at the annealing temperature of 900°C.

2.5.1.4 Sol-Gel Method

Bakan. *et al.* [14] synthesized the thermally stable of nanocrystalline HAp carried on by using $Ca(NO_3)_2{\cdot}4H_2O$ and $NH_4H_2PO_4$ through alcohol

based sol-gel pathway at room temperature. The samples were aged for 12, 24 and 48 hrs, followed by the calcinations at 750°C for 4 hrs. The results showed that this method could prepare the HAp nanoparticles with no catalyst and no grinding process uses in between the formation of gel. In addition, the SEM and TEM results showed that the nano-pin shape like HAp was a 12 nm of average particle diameter and 65 nm of average particle range.

Liu. *et al.* [66] studied on the aging effect of the HAp phase development in water-based sol–gel system. The aging time and aging temperature were varied in the range of 0.25 to 24 hrs and 35 to 80°C, respectively. It was found that the HAp phase was developed by aging of Ca and P molecular precursors. The monophasic HAp was obtained after the calcination at 400 or 500°C when using the higher aging temperature and shorter aging time. However, the contaminating phases, such as CaO, $Ca_2P_2O_7$, $Ca_3(PO_4)_2$ and $CaCO_3$, were detected in the system if the aging conditions were not perfectly controlled.

Fathi and Hanifi [67] prepared the HAp nanoparticles using $Ca(NO_3)_2{\cdot}4H_2O$ and P_2O_5 *via* the sol-gel method. It was found that the agglomerated single phase of HAp was achieved after heating process at 600°C, in which the particle size of HAp nanopowder was about 25-28 nm. Whereas the β-tricalcium phosphate and calcium oxide phases were detected due to the HAp decomposition when the sintering temperature were increased to 700°C.

Kumar and Kalainathan [68] synthesized the plate-like HAp nanocrystals using $Ca(NO_3)_2{\cdot}4H_2O$ and $(NH_4)_2HPO_4$ at 85°C in presence of polyethylene glycol as modifier by the sol-gel method. The samples were sintered at 400, 750 and 1100°C for 4 hrs. It was found that the single phase HAp was recieved after heating process at 1100°C. The SEM result showed that the polyethylene glycol molecules could force the start of HAp growth *via* the interaction between the ether bonds of polyethylene glycol and the HAp nanocrystallites, in which the average size of HAp was 50–70 nm.

Rajabi-Zamani. *et al.* [69] synthesized of the nanocrystalline HAp powder *via* nonalkoxide sol–gel process using $Ca(NO_3)_2{\cdot}4H_2O$ and P_2O_5. The samples were sintered at temperatures in the range of 300 to 750°C for 6 hrs. It was found that the nanocrystalline HAp was obtained at 450°C, but the presence of carbonated HAp was detected at 750°C. In addition, the crystallite sizes and the degree of crystallinity were increased with the increase of the calcining temperature.

Padmanabhan. *et al.* [35] synthesized the hexagonal HAp nanorods using calcium nitrate and potassium dihydrogenphosphate as reagents at different calcining temperatures in between 300 to 700°C. The results showed that the crystalline HAp nanorods were obtained with 70–90 nm in diameter and 400–500

nm in length. The particle size and the crystallinity of product increased with the increase of the calcination temperature. In addition, the forming ratio (length to diameter ratio) of HAp nanorods was in between 6 and 7.

2.5.1.5 Sonochemical Synthesis

Brundavanam. *et al.* [70] synthesized the nano HAp–gelatin (Gel-HAp) composites by a heating supported low-power ultrasonic irradiation process. The mixtures of $Ca(NO_3)_2$ and KH_2PO_4 in the presence of gelatin were used to prepare the Gel-HAp under the heat treatment between 100 and 400°C. The influence of the gelatine on the nucleation and growth of nano-HAp was examined. It was found that the gelatin could attach to the nano-HAp, resulting in the formation of normal spherical shaped crystals of Gel–HAp with the particle size of 29 nm ± 5%.

Cao. *et al.* [71] synthesized the nanocrystalline HAp using $Ca(NO_3)_2$ and $NH_4H_2PO_4$ as starting materials and carbamide (NH_2CONH_2) as precipitant by precipitation procedure with the assistantce of ultrasonic irradiation. The effects of Ca/P molar ratio, precipitation temperature, Ca^{2+}concentration and ultrasonic energy on the nano HAp powder were investigated. It was found that when the Ca^{2+} concentration was higher than 0.2 mol/L and the ultrasonic energy was lower than 300 W, the monophasic HAp powder could not be obtained. However, the spherical HAp nanoparticles could be obtained when using the reaction was performed at 80°C using 300 W of ultrasonic power and 2.0–2.5 of Ca/P molar ratio. Moreover, the crystallite size of HAp nanoparticles decreased with the decreasing of Ca^{2+} concentration in the system.

Han. *et al.* [72] prepared the HAp nanoparticles from $Ca(H_2PO_4)_2$ and saturated $Ca(OH)_2$ water based solution using glycosaminoglycans (GAGs) as additive by precipitation and ultrasound irradiation methods. The grain size and the size distribution of HAp depend on the GAGs concentration, but they were little sensitive to the ultrasound irradiation (UI) time. In addition, the GAGs could inhibit the HAp crystal growth and stabilized HAp nanoscale particles.

Poinern. *et al.* [73] prepared the nanostructured HAp using $Ca(NO_3)_2$ and KH_2PO_4 as starting materials with the Ca/P molar ratio at 1.67. The pH of reaction maintained at 9 under the ultrasonic irradiation, in which the heat treatment were performed in the range from 200 to 400°C for 2 hrs. The influences of the ultrasound and temperature conditions were investigated. The results showed that the spherical HAp particles with the size range of about 30 nm were obtained when using the ultrasonic power of 50 W and heat treatment at 400°C.

Giardina and Fanovich [36] synthesized the HAp powders by precipitation with ultrasonic irradiation (UI). The mixtures of $Ca(OH)_2$ and H_3PO_4 were

applied as the starting solution, in which the molar ratio of Ca/P was strongly controlled at 1.67. This method could produce the HAp powders with controlled crystal size between 31.7 and 70.6 nm. It was found that the thermal stability of HAp crystals was up to 1100°C.

Rouhani. *et al.* [74] prepared the HAp nanoparticles using ultrasonic irradiation at 24, 37 and 55°C for 6-40 min in the PBS solution. The result showed that the monophasic HAp crystals were obtained when using 15 min of the ultrasonic irradiation at 37°C. The ultrasonic could increase the HAp crystal development rate up to 5.5 times in comparison with that from non-sonication condition, however, the ultrasonic decreased the size of the HAp nanoparticles from 30 to 18 nm. In addition, the particles formed by ultrasonic were smaller and more spherical than those achieved without the ultrasonic treatment.

2.5.1.6 Microwave Heating Synthesis

Kumar. *et al.* [75] synthesized the flower-like HAp nanostructure from the conversion of eggshell by the fast microwave irradiation process with the ethylenediaminetetraacetic acid (EDTA) as chelating agent. The results showed that the transformation of eggshell into the HAp occurred through the production of Ca-EDTA complex, in which it subsequently reacted with the phosphate under microwave irradiation. It was found that the flower-like HAp nanostructure was composed of the leaf-like flakes having 100–200 nm width and 0.5–1μm length.

Kalita and Verma [76] synthesized the bioactive HAp powder utilizing calcium nitrate tetrahydrate and sodium phosphate dibasic anhydrous as the initiating materials. The ethylenediaminetetraacetic acid (EDTA) was used as the complex forming reagent at pH 9, in which the microwave power of 600 W was applied. It was found that the calculated average HAp crystallite size was about 12 nm after microwave synthesis. The TEM results indicated that the HAp powder possessed the rod-shaped crystals with ~5 nm in diameter and ~15 nm in length and the elliptical crystals with ~16 nm in diameter and ~27 nm.

Ramesh. *et al.* [77] studied on the influence of fast sintering by microwave heating on the properties of nanoscale crystalline HAp powder. The nano-HAp crystals were firstly synthesized by wet chemical precipitation procedure and sinter by microwave-heating at temperature in the range of 1000 to 1300°C. It was found that the microwave heating could prevent the grain growth of HAp when sintering at temperatures < 1200°C.

2.5.1.7 Hydrothermal Synthesis

Hao. *et al.* [78] synthesized the HAp fiber (fHA) by applying propionamide (PA) for pH adjusting. The concentrations of PA and calcium ion (Ca^{2+}) were varied from 0.05 $molL^{-1}$ to 5 $molL^{-1}$ and from 10 $mmolL^{-1}$ to 100 $mmolL^{-1}$, respectively. The results showed that the morphology of fHA moved from long fibers to flowers and thorn-like bundles when the concentrations of PA and Ca were increased. The higher temperature used in the synthesis, the higher crystallinity of fHA was obtained.

Zhang. *et al.* [79] prepared the plate-like HAp nanoparticles using calcium nitrate ($Ca(NO_3)_2$) and disodium hydrogen phosphate (Na_2HPO_4) as calcium and phosphorous initial substances, respectively, by the hydrothermal method. Sodium tripolyphosphate (STPP) was added into the synthesis system. It was found that the size of the HAp nanoparticles were increased with the increase of STPP concentration, whereas the particular ratios of HAp decreased with the increase of STPP concentration. When the concentration of STPP reached about 0.015 M, the average feature ratio of those nanoparticles was closed to 1, indicating that the STPP and its concentration affected on the morphology of the HAp crystals.

Zhao. *et al.* [80] synthesized the HAp nanorods using biomolecule pyridoxal-50-phosphate (PLP) as an organic phosphorus initial substances by hydrothermal method. The PLP biomolecules were hydrolyzed to generate phosphate ions, in which these phosphate ions further reacted with the pre-existing calcium ions to form hydroxyapatite nanorods. The result showed that the lower hydrothermal temperature (120°C) could not produce the HAp products. When the hydrothermal reaction was performed at 150°C or 180°C, the uniform HAp nanorods could be produced, in which the size of HAp increased with the increase of hydrothermal temperature.

Jokic. *et al.* [81] synthesized the HAp whiskers by hydrothermal method. Calcium nitrate tetrahydrate, sodium dihydrogen phosphate and urea were used as the starting agents. The HAp outcomes were flaky-like particles composed of HAp whiskers. TEM analysis of the HAp whiskers confirmed the formation of single crystal form of HAp with the *c*-axis orientation parallel to the long axis of the fibers. The result showed that the HAp and monetite crystals with different morphologies could be achieved when the different amounts of urea was added into the starting solution.

Yang. *et al.* [82] synthesized the HAp microspheres using calcium nitrate and ammonium dihydrogen by hydrothermal method. Trisodium citrate (TSC) was used as complexing agents. The influence of reaction times on the morphology of HAp crystals was investigated. When the hydrothermal reaction was

performed at 180°C for 24 hrs, the HAp dandelions were obtained due to the effect of the TSC-Ca^{2+} complex. The decomposition of the complex could release the Ca^{2+} into this system after the hydrothermal process, therefore, it could be produced the nanorod units of the dandelion HAp crystal growth. The results of drugs releasing showed that the ibuprofen could be stored in the HAp crystals with the uptake amount of 193 and 227 mg/g for dandelions and flowers structures, respectively.

Zhang and Darvell [83] synthesized the HAp whiskers by hydrothermal homogeneous precipitation using acetamide as the additive. The results showed that the low hydrolysis of the acetamide could raise the pH of reaction and increase the nucleus formation and development of HAp process. The HAp whiskers had an average length of about 60-116 μm when the Ca/P molar ratio was fixed at 1.67. The variation of acetamide concentration did not affect the HAp crystal growth.

Parthiban. *et al.* [84] focused on the effect of urea on the formation of HAp using beta-tricalcium phosphate (β-TCP) and dicalcium phosphate dihydrate (DCPD) as the precursors for double-steps hydrothermal processing, i.e. hydrothermal treatment in vapor condition and hydrothermal treatment in liquid condition. It was found that the application of urea in the double processes could effectively control the morphology of HAp compacts. However, the HAp crystal growth was inhibited from the CO_3^{2-} ions released from the urea during the hydrothermal treatment.

Jinawath. *et al.* [85] studied on the transformation of aragonite (calcium carbonate) to HAp *via* $CaHPO_4$ phase. The hydrothermal reactions were performed under vapor pressure of 1-2 MPa at 160-200°C for 8-14 hrs. It was found that the $CaCO_3$ in the phosphate solution transformed to the $CaHPO_4$, in which it could generate the plates and whiskers $CaHPO_4$ crystal. After hydrothermal treatment, the $CaHPO_4$ morphologies were transformed to the nanorods HAp by the dissolution – recrystallization mechanism.

Zhang and Vecchio [86] synthesized the HAp using dicalcium phosphate anhydrous ($CaHPO_4$, DCPA) by the hydrothermal reaction at temperature ranging from 120 to 180°C for 24 hrs with the two polymorphisms of the calcium carbonate, i.e. calcite and aragonite (cuttlebone). At the starting time of the reaction between DCPA and calcite, the nucleus formation and development of beta-tricalcium phosphate (β-TCP) particles on the calcite particles were found. The HAp rods were discovered to grow out of β-TCP particles. The size of synthesized HAp rods was about 200 nm in width and many microns in length. For the reaction of DCPA and aragonite, it was found that the nucleus formation and development of HAp occurred certainly on the DCPA particles.

Manafi and Rahimipour [87] synthesized of the HAp utilizing $Ca(NO_3)_2{\cdot}4H_2O$ and $(NH_4)_2HPO_4$ solutions as the beginning substances by hydrothermal method at temperature ranging from 120 to 200°C for 18 hrs. The results showed that the HAp crystals had size of 25-50 nm and lengths of 120±30 nm, in which the HRTEM showed the preferred rod-shaped orientation.

2.5.2 The template-assisted hydroxyapatite preparations

Xiao. *et al.* [17] prepared the spherical HAp crystals using $(NH_4)_3PO_4{\cdot}3H_2O$ and $Ca(NO_3)_2{\cdot}4H_2O$ with β-cyclodextrin (β-CD) as pattern by biomimetic process It was found that the morphology of HAp crystals were depended on the β-CD concentration, in which the spherical particles with the size of 1.0-3.0 μm were achieved in the finding of 1.5% β-CD.

He. *et al.* [88] synthesized the nanoflake HAp using $Ca(NO_3)_2.4H_2O$ and $(NH_4)_3PO_4.3H_2O$ as reagents with chondroitin sulfate (ChS) as a pattern by a biomimetic method according to the biomineralization theory. It was found that the nucleus formation and development of the HAp crystals took place in chemical interactions between HAp crystals and the ChS pattern. The concentration of ChS influented to the morphology of HAp crystals. The elemental analysis indicated that a small amount of the ChS was detected in the HAp crystal. In addition, the staple-fiber-like and the flake-like HAp crystals were respectively obtained when using the low and high concentration of ChS in the synthesis.

Garcia. *et al.* [89] synthesized the HAp nanoparticles by applying calcium nitrate tetrahydrate and diammonium hydrogen phosphate as initiating substances in a reverse microemulsion system containing cetyltrimethylammonium bromide (CTAB)/toluene/n-butanol/water by hydrothermal method. It was found that the monophasic HAp could be obtained by adjusting the pH between 10 and 11. The corresponded size distribution of the HAp particles was varied in the in between 60 and 105 nm by varying microemulsion conditions, i.e. the molar ratios of water to surfactant and cosurfactant to surfactant. In addition, the probable mechanism for the crystallization of HAp was considered to occur from the interaction between the ionized groups of CTAB and the reactant ions.

Zhu. *et al.* [90] produced the rod-like HAp nanoparticles with a N-[(2-hydroxy-3-trimethylammonium) propyl]chitosan chloride (HTCC) as pattern by hydrothermal procedure with low heating level of temperature. The results showed that the size and morphology could be customized by moving synthesis conditions, i.e. pH, hydrothermal temperature and the mole ratio of PO_4^{3-} to quaternary ammonium in the HTCC. The cationic macromolecule of HTCC pattern affected to the nucleus formation and development of HAp crystals.

Tsetsekou. *et al.* [16] synthesized the HAp nanoplates using H_3PO_4, $Ca(OH)_2$ and L-arginine as precursor solutions in the presence of collagen or chitosan by sol-gel method. The reaction was investigated by using two molar ratios of Ca/P, i.e. 1/1 and 10/6 under basic conditions at the biomimetic temperature 40°C. The mean size of the HAp crystals ranging from 5 nm to 20 nm depended on the precursor concentration. In addition, the best homogeneity of HAp nanoplates was obtained when the molar ratio of Ca/P was 10/6.

Ramedani. *et al.* [91] prepared the nano-HAp using calcium nitrate tetrahydrate ($Ca(NO_3)_2{\cdot}4H_2O$) and diammonium hydrogen phosphate ($(NH_4)_2HPO_4$) precursors with nanoliposomes template. It was found that the nanoliposomes could in chart as carriers for the crystal development of nano-HAp particles. The nano-HAp from liposome encapsulation contained hexagonal bipyramidal structure with spherical form of about 60 nm.

Verma. *et al.* [92] synthesized the porous HAp nanorods using cationic cetyltrimethylammonium bromide (CTAB) and anionic hydrotrope sodium salicylate (SS) as templates. The results showed that the formation of rod-like HAp crystals having length of 100–500 nm and size of~50 nm were obtained in the mediated surfactant condition, whereas, the irregular shaped nanoaggregates of HAp crystals were obtained in the absence of surfactant.

Gopi. *et al.* [93] synthesized the HAp nanoparticles using calcium nitrate tetrahydrate ($(CaNO_3)_2{\cdot}4H_2O$) and diammonium hydrogen orthophosphate ($(NH_4)_2HPO_4$) as starting materials with glycine–acrylic acid (GLY–AA) hollow sphere organic pattern by ultrasonic assisted method. When the ultrasonic irradiation time was increased, the crystallinity and size of HAp particles would be declined. The stable HAp nanoparticles at higher temperature were obtained by using an ultrasonic irradiation time for 3 hrs.

Li. *et al.* [94] synthesized the nanoporous HAp from $K_2HPO_4{\cdot}3H_2O$ and $CaCl_2$ with cetyltrimethylammonium bromide (CTAB) template. It was found that the nanoporous HAp with pore size of about 1-5 nm were obtained, in which the porous HAp structure was thermally stable up to 700°C.

Amer. *et al.* [95] manufactured the mesoporous nano-HAp (mn-HAP) using calcium nitrate tetrahydrate ($Ca(NO_3)_2{\cdot}4H_2O$) and diammonium hydrogen phosphate ($(NH_4)_2HPO_4$ as calcium and phosphorous sources, respectively, by micelle-templating process with a lauryl dimethylaminoacetic acid as zwitterionic surfactant. When the combination between microwave energy and the surfactant were used in the system, the HAp with controlled pore size in a narrow-size distribution range of about 36 nm was obtained. The results showed that the specific surfaces area of dried and calcined HAp products were 87 m^2g^{-1} and 55 m^2g^{-1},

respectively, in which they were the basic role of zwitterionic surfactant in the preparation of mn-HAp.

Liu. *et al.* [96] synthesized the extremely ordered lamellar HAp (Lα-HAp) powder by surfactant templating process using sodium dodecyl sulphonate (SDS, $C_{12}H_{25}SO_3Na$) as a pattern. $Ca(NO_3)_2$ and $(NH_4)_2HPO_4$ were applied as calcium and phosphorus initial substance, respectively. The results showed that the HAp was the only phase in the Lα-HAp with the crystal size of about 3.6 nm. The surfactant template might affect to the formation mechanism of Lα-HAp.

2.5.3 The biomedical applications of hydroxyapatite

Kawakita. *et al.* [97] studied on the controlled protein adsorption by dextran on the surface of HAp. The results showed that the dextransucrase was immobilized to the HAp surface when the HAp was immersed in the 0.3 U/mL at pH 5.5 dextransucrase solution. The immobilized dextransucrase reacted with a sucrose, in which it could transfer to the dextran and generated the adsorption sites of HAp. When the bovine serum albumin (BSA) and c-globulin were bound to the surfaces of both HAp and dextrangenerated HAp, the quantity of protein adsorption declined with the enhancing quantity of dextran manufactured. It was found that the protein did not reach the adsorption sites of HAp due to the steric effect of dextran.

Zhang. *et al.* [98] studied on the controlled bovine serum albumin (BSA) delivery of mesoporous HAp (MHAp) at different pH environment, i.e. 4.7, 7.4 and 8.4. The adsorption behavior showed that the adsorbed amount of BSA on the MHAp depended on the pH of protein solution. It was found that the loading amounts of the BSA on the MHAp decreased when the pH was increased. In addition, the MHAp adsorbed BSA showed a different release kinetic at the basic pH 8.4 when comparing with those in acid and neutral conditions, indicating that the release of protein could be controlled by pH conditions.

Matsumoto. *et al.* [99] studied on the possibility of utilizing HAp particles as a controlled release carrier of protein. The HAp was synthesized in wet chemical system at low temperature, having little crystallinity, high solubility and huge specific surface area. The basic proteins were used as the growth factors for bone regeneration in the protein adsorption, i.e. BMP, bFGF and TGF-b. It was found that the protein binding on the HAp particles changed depending on its specific surface area, in which it could be controlled by temperature and the concentration of protein solution used in the synthesis system. When the particles of HAp bound the protein (HAp-pro) at pH 4.0, it was found that the quantity of outcoming protein depended on the time goes by.

Tomoda. *et al.* [100] studied on the protein adsorption of the HAp particles synthesized by three methods, i.e. solvent diffusion, sintering and homogeneous precipitation, in which they possessed spiky crystals, spherical amorphous agglomerates and spherical particles, respectively. The shape and size of the synthesized HAp depended on the temperature and duration time use in the synthesis and the amount of additives, i.e. urea and Na_2EDTA. The adsorptions of bovine serum albumin (BSA) or lysozyme hydrochloride (LSZ) on the HAp particles were investigated. The surface area ratio of *a* plane against total surface area of the HAp crystals became smaller by decreasing Na_2EDTA concentration. The HAp surface charges of *a* plane and *c* plane were positive and negative charged, respectively. The amounts of BSA and LSZ adsorbed on the HAp particle surfaces were different since the BSA was negatively charged but LSZ was positively charged in the solution.

Yin. *et al.* [101] studied on the binding of bovine serum albumin (BSA) on HAp by investigation on ζ-potential of the HAp. When considering the binding of BSA buffed at pH 6.80 with different phosphate concentrations, it was found that the increase of the phosphate concentration could be generated more PO_4^{3-} ions at the HAp surface, corresponding to the high negative ζ-potential value and enhancing the electrostatic repulsion force between the HAp and the BSA. Therefore, it could be reduced the adsorption of the BSA on the HAp surface.

Chapter 3
Research methodology

3.1 Materials

- Calcium nitrate tetrahydrate ($Ca(NO_3)_2{\cdot}4H_2O$), Ajax Finechem, Analytical grade
- Diammonium Hydrogen Phosphate ($(NH_4)_2HPO_4$), Fisher Scientific, Analytical grade
- Sodium poly(4-styrene sulfonate) (PSS), Sigma Aldrich, Analytical grade
- Sodium hydroxide (NaOH), Calro Erba, Analytical grade
- Ethanol (C_2H_5OH), Calro Erba, Analytical grade
- Phosphate buffer saline (PBS), Sigma Aldrich, Analytical grade
- L-aspartic acid, Acros, Analytical grade
- L-arginine, Acros, Analytical grade

3.2 Apparatus

- X-ray diffractometer (XRD), Bruker AG, D8 Advance
- Transmission electron microscope (TEM), JEOL, JEM 1220 and 2010
- Fourier transform infrared spectrometer (FT-IR), Bruker AG, IFS28
- Zeta potential analyzer, Beckman Coulter, Delsa™ Nano C particle analyzer
- pH meter, Mettler Toledo FiveEasy™, FE20/ FG2
- Oven, Lab Companion
- Sonic bath, Cole-Parmer, 8892
- Refluxing set (Figure 3.1)
- Teflon-lined stainless steel autoclave, PARR INSTRUMENT COMPANY, 302AC T304 040511 (Figure 3.2)
- Mortar and Pestle

Figure 3.1 Refluxing set

Figure 3.2 Teflon-lined stainless steel autoclave

3.3 Studied Factors

In this thesis, the experiment could be divided into 3 main sections as follow;

1. Preparation of HAp by refluxing method

   Various preparation parameters are carried out, i.e.

   1.1 PSS concentration in the synthesized reaction; i.e. 0.00, 0.05, 0.20 and 0.30 w/v%

   1.2 pH of reaction; i.e. 8.5, 9.5, 10.5, 11.5 and 12.5

   1.3 Refluxing times; i.e. 0, 1, 3 and 6 hrs

2. Preparation of HAp by hydrothermal method
   Various preparation conditions are carried out, i.e.
   2.1 Hydrothermal times; i.e. 0, 0.5, 1, 2 and 3 hrs
   2.2 PSS concentration in the synthesized reaction; i.e. 0.00 and 0.20 w/v%
   2.3 pH of hydrothermal reaction; i.e. 8.5, 9.5 and 10.5
3. Characterization and testing of the synthesized HAp
   The synthesized HAp are characterized and tested by various techniques as follows:
   3.1 Crystalline phase and crystallite size of HAp by XRD
   3.2 Purity and functional groups of HAp by FT-IR
   3.3 Morphology and selected area of electron diffraction (SAED) pattern of HAp by TEM
   3.4 Surface charge of HAp and modified HAp by zeta potential analyzer in phosphate buffer saline
   3.5 *In vitro* MTT cytotoxicity testing
   3.6 Anti-bacterial testing

3.4 Experiment

3.4.1 Preparation of HAp without PSS template by refluxing method

The concentrations of $Ca(NO_3)_2{\cdot}4H_2O$ and $(NH_4)_2HPO_4$ were respectively fixed at 0.2 mol/L and 0.12 mol/L, corresponding to the stoichiometric concentration of HAp (Ca/P molar ratio = 1.67). Firstly, the $(NH_4)_2HPO_4$ water based solution was dropwisely added into the $Ca(NO_3)_2{\cdot}4H_2O$ aqueous solution under powerful stirring for 30 min. The pH values of the mixing solutions were adjusted to 8.5, 9.5, 10.5, 11.5 or 12.5 by adding 0.5 mol/L of NaOH solution. After that, the mixtures were refluxed at 100°C for 1, 3 and 6 hrs with continuous stirring. The white precipitates were separated from the starting solutions by centrifugation, washed with distilled water and ethanol for many times and leave until dry in oven at 45°C for 24 hrs. Finally, the products were characterized by XRD, FT-IR and zeta potential analyzer. Figure 3.3 shows the preparation procedure of HAp without PSS template by refluxing method.

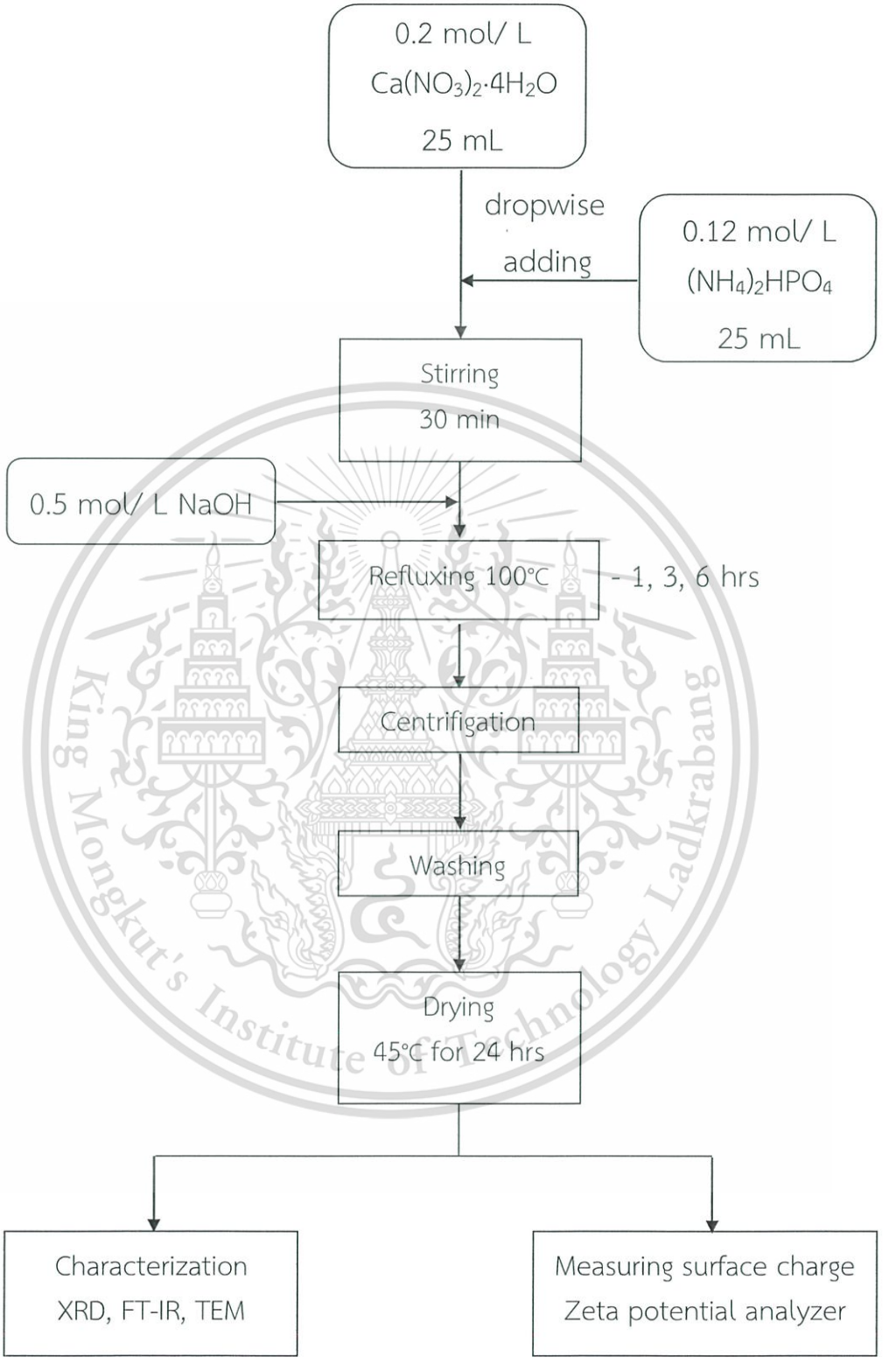

Figure 3.3 Preparation of HAp without PSS template by refluxing method

3.4.2 Preparation of HAp with PSS template by refluxing method

The concentrations of $Ca(NO_3)_2{\cdot}4H_2O$ and $(NH_4)_2HPO_4$ were respectively used at 0.2 mol/L and 0.12 mol/L, corresponding to the stoichiometric concentration of HAp (Ca/P molar ratio = 1.67). The PSS water based solution was diluted to achieve 3 different concentrations, i.e. 0.05, 0.20 and 0.30 w/v%. Firstly, the diluted PSS solution was added $Ca(NO_3)_2{\cdot}4H_2O$ water based solution and stirred for 10 min. Subsequently, the $(NH_4)_2HPO_4$ aqueous solution was dropwisely added into the previous mixture under powerful stirring for 30 min. The pH levels of the mixtures were adjusted to 8.5, 9.5, 10.5 or 11.5 by adding 0.5 mol/L of NaOH solution. After that, the mixing solution were evaporated by refluxing process at 100°C for 1, 3 and 6 hrs with continuous stirring. The white precipitates were removed from the starting solutions by centrifugation, washed with distilled water and ethanol for many times and leave until dry in oven at 45°C for 24 hrs. Finally, the products were characterized by XRD, FT-IR and zeta potential analyzer. Figure 3.4 shows the preparation procedure of HAp with PSS template by refluxing method.

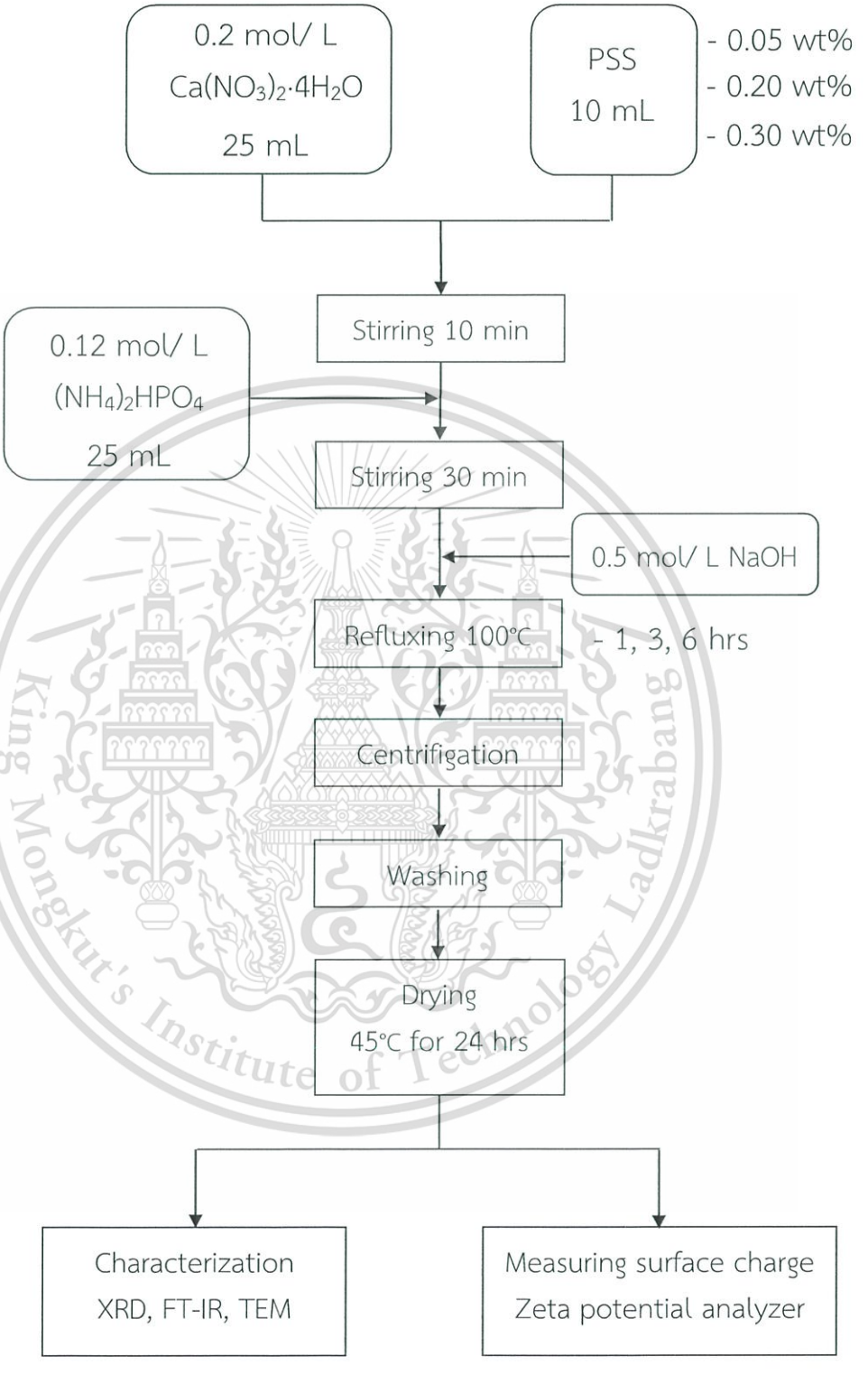

Figure 3.4 Preparation of HAp with PSS template by refluxing method

Table 3.1 Synthesis of HAp: refluxing conditions

Sample	[PSS] (w/v%)	pH value	Refluxing time (hr)
P0.0R6-12.5	0.00	12.5	6
P0.0R6-11.5	0.00	11.5	6
P0.0R6-10.5	0.00	10.5	6
P0.0R3-10.5			3
P0.0R1-10.5			1
P0.0R0-10.5			0
P0.0R6-9.5	0.00	9.5	6
P0.0R3-9.5			3
P0.0R0-9.5			0
P0.0R6-8.5	0.00	8.5	6
P0.0R3-8.5			3
P0.0R0-8.5			0
P0.2R6-12.5	0.20	12.5	6
P0.2R6-11.5	0.20	11.5	
P0.3R6-10.5	0.30	10.5	
P0.2R6-10.5	0.20	10.5	
P0.05R6-10.5	0.05	10.5	
P0.2R3-10.5	0.20	10.5	3
P0.2R1-10.5			1
P0.2R0-10.5			0
P0.2R6-9.5	0.20	9.5	6
P0.2R3-9.5			3
P0.2R0-9.5			0
P0.2R6-8.5	0.20	8.5	6
P0.2R3-8.5			3
P0.2R0-8.5			0

3.4.3 Preparation of HAp without PSS template by hydrothermal method

The mixing solution of $Ca(NO_3)_2 \cdot 4H_2O$ and $(NH_4)_2HPO_4$ were set at 0.2 mol/L and 0.12 mol/L, respectively, corresponding to the stoichiometric concentration of HAp (Ca/P molar ratio = 1.67). Firstly, the $(NH_4)_2HPO_4$ water based solution was dropwisely transferred into the $Ca(NO_3)_2 \cdot 4H_2O$ aqueous solution under high energy stirring for 30 min. The pH values of the mixing solution were leveled at 8.5, 9.5, or 10.5 by adding 0.5 mol/L of NaOH solution. After that, the mixing solution were transferred to Teflon-lined stainless steel autoclave of 50 mL capacity and heated in an oven at 100°C for 0.5, 1, 2 and 3 hrs. After hydrothermal treatment, the products were removed from the starting solutions by centrifugation, washed with distilled water and ethanol for many times, and then leave until dry in oven at 45°C for 24 hrs. Finally, the products were characterized by XRD, FT-IR and zeta potential analyzer. Figure 3.5 shows the preparation procedure of HAp without PSS template by hydrothermal method.

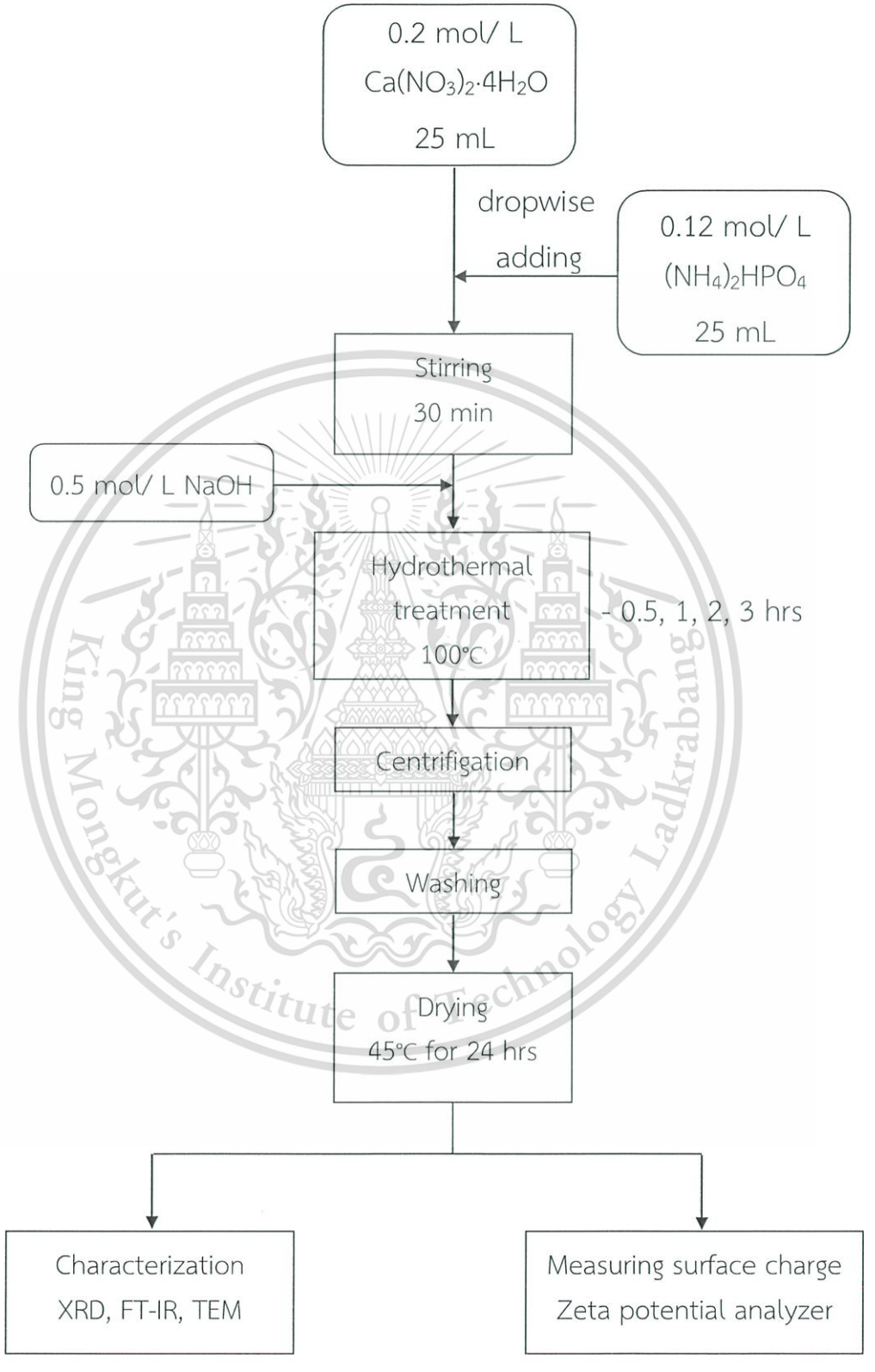

Figure 3.5 Preparation of HAp without PSS template by hydrothermal method

3.4.4 Preparation of HAp with PSS template by hydrothermal method

The $Ca(NO_3)_2{\cdot}4H_2O$ and $(NH_4)_2HPO_4$ were mixed and fixed the concentration at 0.2 mol/L and 0.12 mol/L, respectively, corresponding to stoichiometry of HAp (Ca/P ratio = 1.67). The PSS water based solution was diluted to 0.20 w/v%. Firstly, the 10 mL of PSS diluted solution was conveyed into the $Ca(NO_3)_2{\cdot}4H_2O$ water based solution and stirred for 10 min. Subsequently, the $(NH_4)_2HPO_4$ aqueous solution was dropwisely tranferred into the previous mixing solution under powerful stirring for 30 min. The pH levels of the mixing solution were leveled at 8.5, 9.5, or 10.5 by adding 0.5 mol/L of NaOH solution. After that, the mixing solution were transferred to Teflon-lined stainless steel autoclave of 50 mL capacity and heated in an oven at 100°C for 0.5, 1, 2 and 3 hrs. After hydrothermal treatment, the resulting products were removed from the starting solutions by centrifugation, washed with distilled water and ethanol for many times, and then leave until dry in an oven at 45°C for 24 hrs. Finally, the products were characterized by XRD, FT-IR and zeta potential analyzer. Figure 3.6 shows the preparation procedure of HAp with PSS template by hydrothermal method.

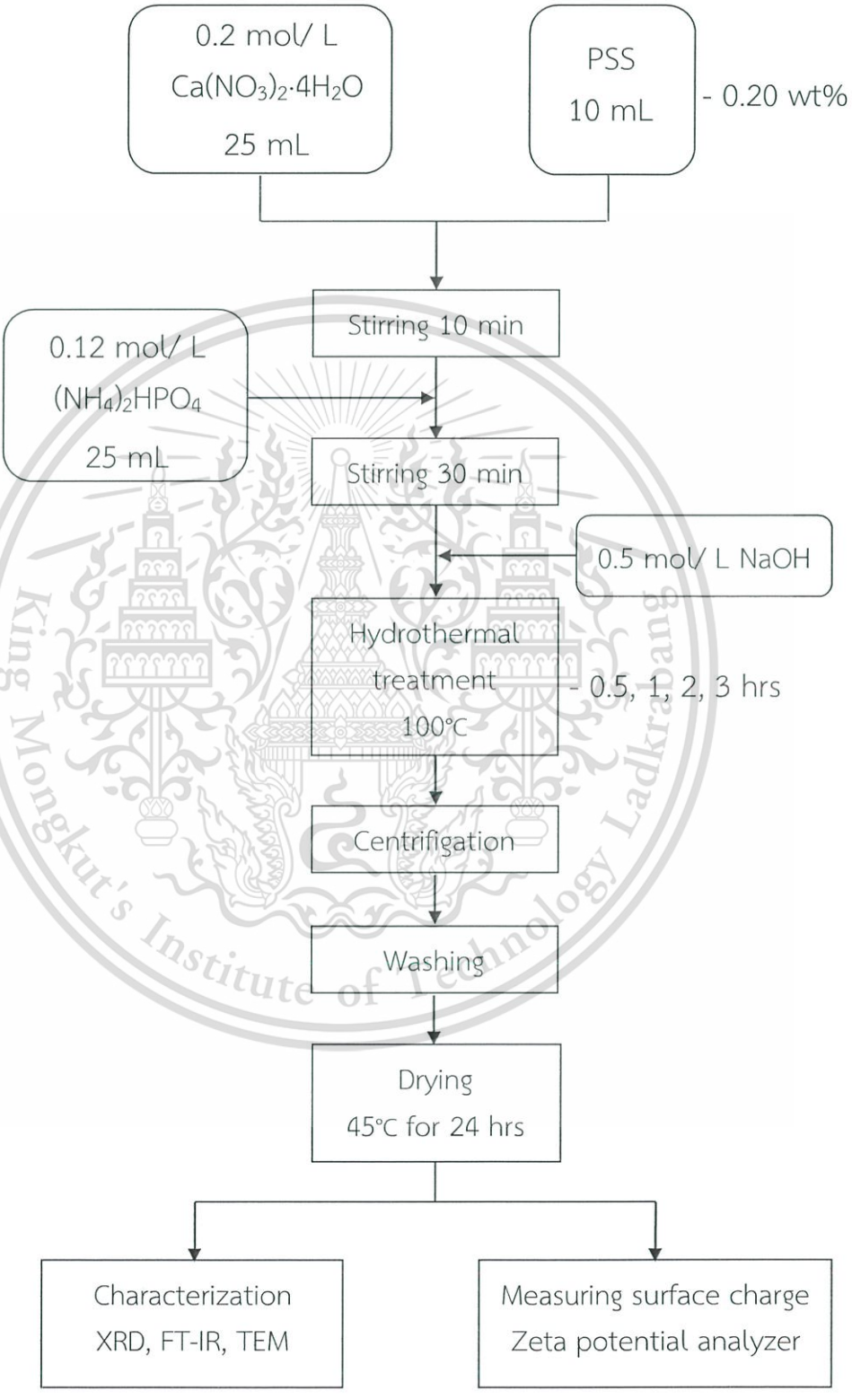

Figure 3.6 Preparation of HAp with PSS template by hydrothermal method

Table 3.2 Hydrothermal conditions for synthesis of HAp

Sample	[PSS] (w/v%)	pH value	Hydrothermal time (hr)
P0.0H3-10.5	0.00	10.5	3
P0.0H2-10.5			2
P0.0H1-10.5			1
P0.0H0.5-10.5			0.5
P0.0H0-10.5			0
P0.0H3-9.5	0.00	9.5	3
P0.0H3-8.5		8.5	
P0.2H3-10.5	0.20	10.5	3
P0.2H2-10.5			2
P0.2H1-10.5			1
P0.2H0.5-10.5			0.5
P0.2H0-10.5			0
P0.2H3-9.5	0.20	9.5	3
P0.2H3-8.5		8.5	

3.4.5 Surface modification and surface charge measuring of the synthesized HAp

The as-prepared HAp samples were developed with the amino acids, i.e. 0.25 mol/L L-aspartic acid (Asp) and 0.25 mol/L L-arginine (Arg). Firstly, 0.2 g of HAp was blended with 40 mL of amino acid solution at pH 7 with stirring for 2 hrs. The mixing solution were centrifuged in order to separate the modified HAp. The surface charges of the developed HAp were examined by using zeta potential analyzer. All zeta potential (ζ) measurements were measured in phosphate buffered saline (PBS) at pH 7.4. Each sample was analyzed in triplicate and the mean of three ζ values was reported.

3.4.6 Characterization of the synthesized HAp

- XRD

All powder samples were analyzed by XRD to analyze crystalline structures using CuKα radition (λ= 1.54 Å) with step size of 0.04°/step, scanning speed of 1°/sec and scanning range (2θ) of 20°-60°. Full width at half-maximum (FWHM) of the peak of crystalline phase at 2θ =25.8° was applied to identify the size of crystal as-synthesized HAp through Scherrer's equation as shown in equation (3.1)

$$\tau = \frac{k\lambda}{\beta cos\theta} \quad (3.1)$$

; in which τ is the crystallite size (Å)

k is the shape constant (~ 0.9)

λ is the wavelength (Å)

θ is the Bragg's angle (degree)

β is the resulted FWHM of peak at 2θ =25.8° (Radian)

- FT-IR

Chemical functional groups of the as-prepared HAp and the surface modified HAp were analyzed by FT-IR. The small amount of sample was mixed with potassium bromide (KBr) and made in the form of pellet. The spectra were collected in the range of 400 to 4000 cm^{-1}.

- TEM

Morphologies of the synthesized HAp samples were investigated by TEM. The morphology and the corresponding selected area of electron diffraction (SAED) patterns of the produced HAp samples were analyzed 200 keV of TEM (JEM 2010, JEOL), in which the d spacing of the *002* plane can be calculated by using formula as shown in equation (3.2)

$$R * d = \lambda * L \quad (3.2)$$

; where d is the spacing of lattice planes *(002)*

L is the camera length (30 cm)

λ is the wavelength of the electrons (200 keV)

R is the physical spacing measured on the picture

3.4.7 Biological properties testing of the synthesized HAp

- *In vitro* cytotoxicity testing

An investigation of cytotoxicity *in vitro* of the produced nHAp against Affrican green monkey kidney fibroblasts (Vero cells) was carried out by MTT assays for preliminary observing. The examining process was done pursuant to ISO 10993-5. [102]

- Antibacterial testing

The nHAp synthesized in this work was applied to test an antibacterial activity against *Staphylococcus aureus* ATCC®25923 *(S.aureus)* and *Escherichia coli* ATCC®25922 *(E.coli)*. The antibacterial testing were done by disc diffusion process in agar medium and performed according to the Performance Standards for Antimicrobial Susceptibility Testing, M100-21 [103].

Chapter 4

Main results and Discussions

4.1 Preparation of HAp by refluxing method

4.1.1 Effect of PSS template

Figure 4.1 and Table 4.1 illustrate the XRD patterns and the zeta potential (ζ) values of the starting precursors and the nHAp synthesized without and with PSS template by refluxing process at pH 10.5 for 6 hrs. It can be observed that the crystalline peaks of both initial precursors before refluxing in the systems without and with PSS template, i.e. P0.0R0-10.5 and P0.2R0-10.5, respectively, were predominantly composed of the diffraction peaks at 2θ = 20.9°, 29.3°, 30.5° and 34.2° that related to the crystalline phase of dicalcium phosphate dihydrate ($CaHPO_4 \cdot 2H_2O$ or DCPD) in JCPDS 09-0077. The DCPD precursor was formed from the reaction between Ca^{2+} from $Ca(NO_3)_2 \cdot 4H_2O$ and HPO_4^{-} from $(NH_4)_2HPO_4$ in the aqueous media as presented in the chemical equation (4.1) as follows [104]:

$$Ca^{2+} + HPO_4^{2-} + 2H_2O \longrightarrow CaHPO_4 \cdot 2H_2O \quad (4.1)$$

In addition, these DCPD precursors obtained in both systems were evaluated their ζ values (not adjusted pH condition) in order to determine their surface properties, in which they were respectively designated as P0.0R0 and P0.2R0 in the absence template system and in the presence template system, as shown in Table 4.1. Despite the initial precursors in both systems were DCPD, their ζ values were entirely different, designating their variation in surface charge. The ζ value of the P0.0R0 without PSS template was positive, but that of P0.2R with PSS template was largely negative. These results indicated that the existence of anionic PSS template brought about the negative charged particles.

After refluxing treatment for 6 hrs, it was found that the both P0.0R0-10.5 and P0.2R0-10.5 precursors conversed to HAp crystalline phase in the P0.0R6-10.5 and P0.2R6-10.5 samples using the chemical process as shown in equation (4.2). [105] The XRD patterns of the P0.0R6-10.5 and P0.2R6-10.5 in Fig. 4.1(a) and Fig. 4.1(b), respectively, could be indexed as a monophasic hydroxyapatite phase, having the diffraction peaks at 2θ = 25.8°, 31.7°, 32.2°, 34.1°, 39.8° and 49.5° (JCPDS 09-0432). There are no characteristic peaks of the DCPD precursor observed in the XRD patterns.

$$10CaHPO_4 \cdot 2H_2O \longrightarrow Ca_{10}(PO_4)_6(OH)_2 + 4PO_4^{3-} + 18H_2O + 12H^+ \quad (4.2)$$

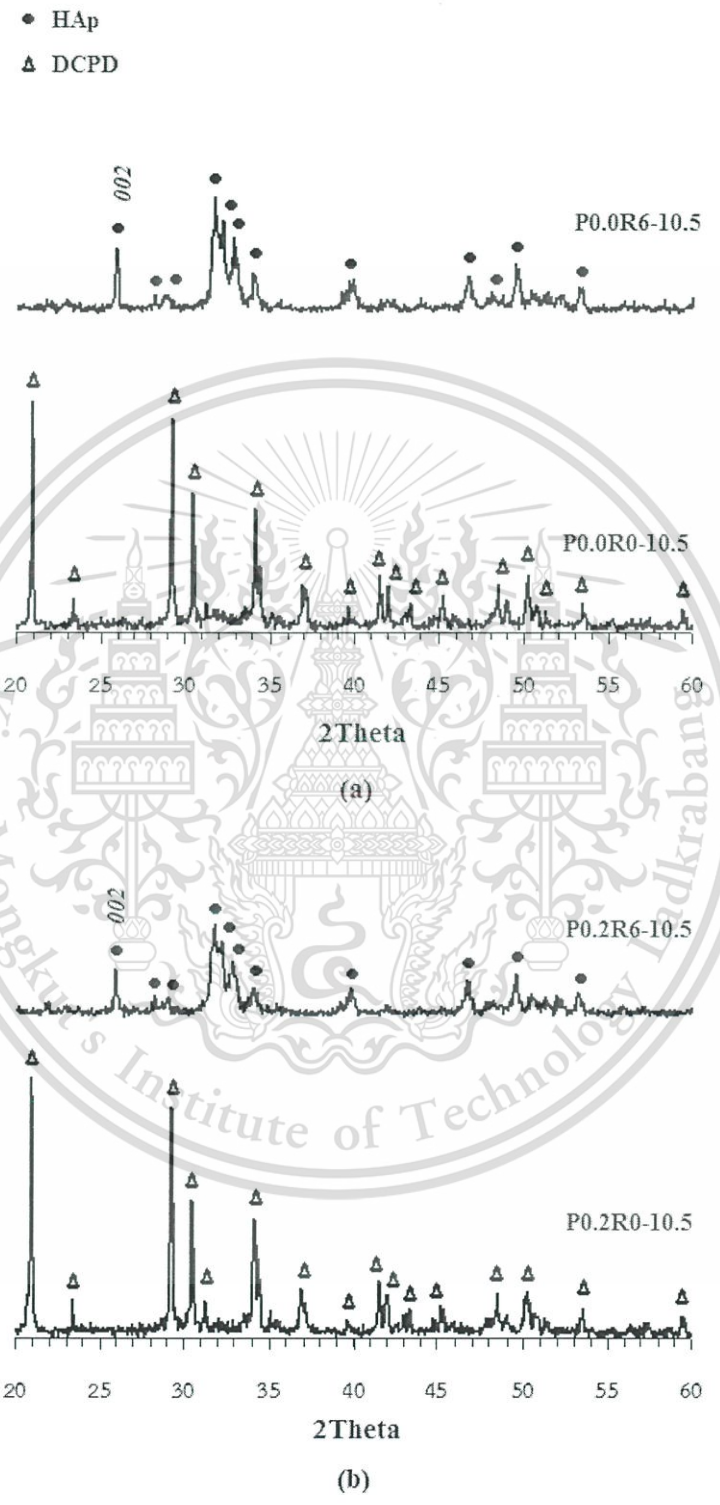

Fig.4.1 XRD patterns of the synthesized nHAp by refluxing for 6 hrs at pH 10.5; (a) without PSS template and (b) with PSS template

The crystallite sizes of the synthesized nHAp along *002*-plane were deliberated by Scherrer's equation as shown in equation (4.3) [107] and summarized in Table 4.1.

$$\tau = \frac{k\lambda}{\beta cos\theta} \quad (4.3)$$

where τ is the crystallite size (Å), k is the shape constant (~ 0.9), λ is the CuK_α wavelength used in the XRD measurement (1.54 Å), θ is the Bragg's angle (Degree) and β is the resulted full width at half maximum of peak at 2θ =25.8° (Radian). When the HAp crystals were produced in the PSS template free (P0.0R6-10.5), the synthesized sample illustrated a strong and sharp crystalline HAp diffraction peak of *002*-plane, with corresponding calculated large crystallite size of 52.6 nm. On the other hand, the P0.2R6-10.5 sample presented a broader *(002)* diffraction peak when compared with that of the P0.0R6-10.5 sample, in which it was concomitant with smaller crystallite size of 41.4 nm. It can be observed that the crystalline particle size along *002*-plane of P0.2R6-10.5 was less than that of P0.0R6-10.5, indicating the effect of PSS template on the crystal growth along *c*-axis.

Table 4.1 Phase composition, zeta potential of the starting precursor and crystallite sizes of the synthesized nHAp without and with 0.20 w/v% PSS template by refluxing method at pH 10.5

System	Refluxing for 0 hr			Refluxing for 6 hrs			Zeta potential (mV)
	Sample	Phase composition	Crystallite size (τ_{002}:nm)	Sample	Phase composition	Crystallite size (τ_{002}:nm)	
Without PSS template	P0.0R0-10.5	DCPD	n/a	P0.0R6-10.5	HAp	52.6	+6.04
With PSS template	P0.2R0-10.5	DCPD	n/a	P0.2R6-10.5	HAp	41.4	-20.63

In the PSS-free process, the P0.0R0-10.5 initial substance has comparatively low positive ζ value that might lead to the accumulation of precursor particles as illustrated in Fig. 4.2, influencing on the confinement of hydroxyapatite crystal growth during refluxing procedure. It was, however, the hydroxyapatite crystals could freely grow along their preferred *c*-axis direction due to the intrinsic crystal habit in the solution, promoting the larger crystallite size in the P0.0R6-10.5 sample.

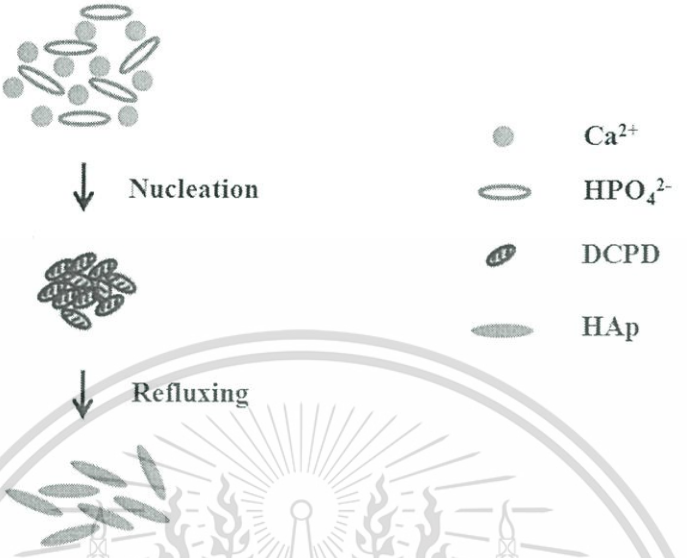

Fig.4.2 Schematic representation of refluxing synthesis of nHAp in the absence of PSS template

On the other hand, the P0.2R0-10.5 precursor with the PSS template has largely negative ζ value, in which this highly charged surface could prevent the agglomeration of precursor particles as shown in Fig. 4.3. In addition, the PSS template dissociated in aqueous solution possessed the negatively charged sulfonic groups that would promote the formation of PSS-Ca intermediate, in which it functioned as the heterogeneous nucleus forming site. Therefore, this led to the decrease of the concentration of free Ca^{2+} ions in the system, resulting in the limitation of HAp growth along the *c*-axis direction.

The influence of the PSS template on the mechanism of phase conversion and the HAp crystals development are schematically explained in Fig. 4.3. The stretched network conformation of PSS template was achieved in the aqueous solution due to the firmly Coulombic repulsive force between the negative charged sulfonic groups ($-SO_3^-$) on the backbone of PSS networks. In step I, the Ca^{2+} ions combined with the negatively charged $-SO_3^-$ groups on the PSS chain and formed as the PSS-Ca intermediate. The intermediate would interact with HPO_4^{2-} from the initiating solution and OH^- ions from base reagent used for pH adjusting in step II, outcoming in creation of DCPD precursor on the rigid-rod PSS chains. The crystalline DCPD was achieved in the XRD pattern of precursor before evaporating in reflux treatment as shown in Fig. 4.1(b). The DCPD phase conversion to HAp after refluxing

treatment in step III. Finally, the produced HAp nanoparticles were washed with distilled water and ethanol in order to clearify the PSS template in step IV.

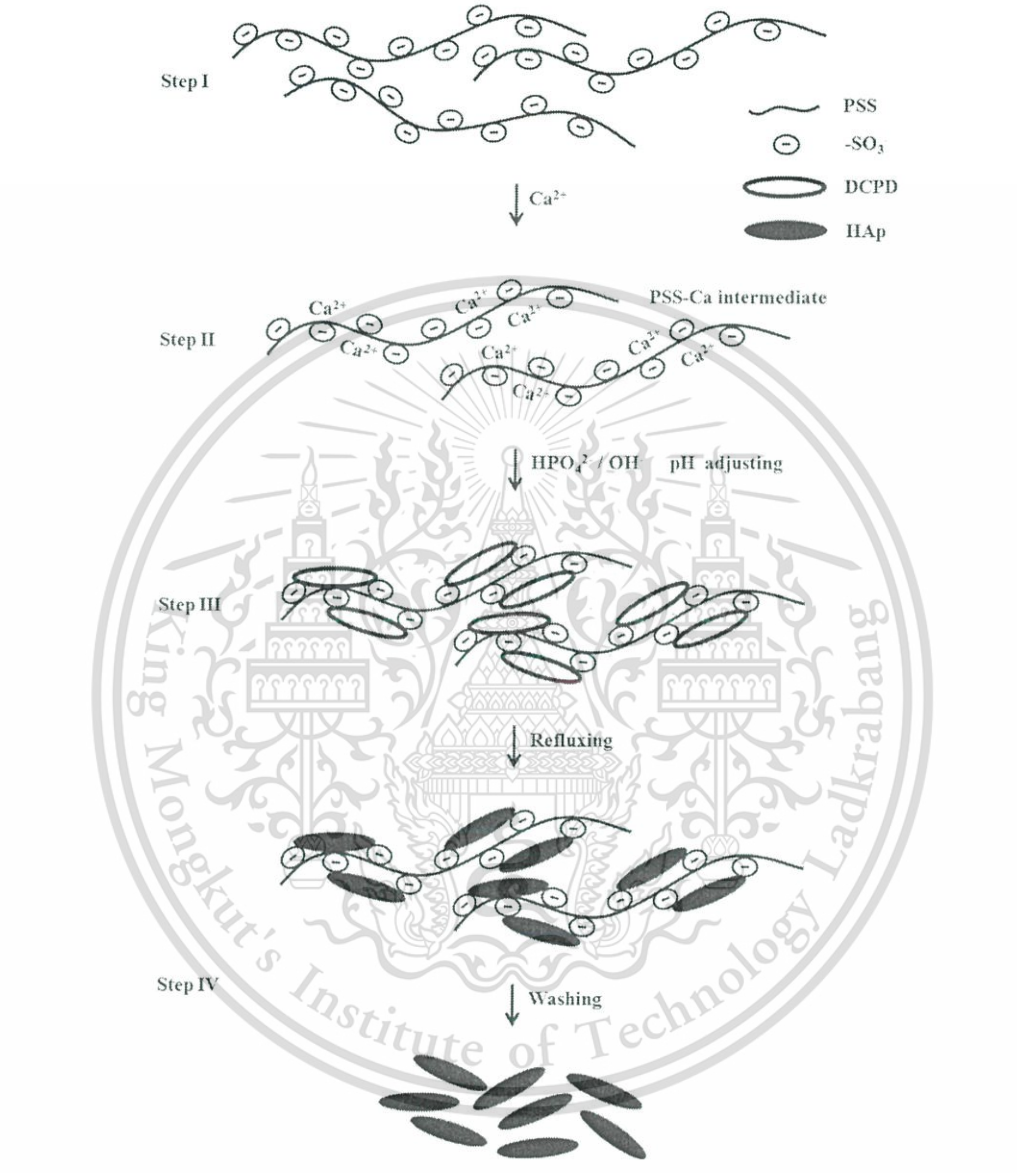

Fig.4.3 Schematic representation of refluxing synthesis of nHAp in the presence of PSS template

From previous mentioned, size of crystalline particle and ζ values of nHAp achieved from the refluxing synthesis. It can be concluded that the existence of PSS template influenced on the decrease in crystallite size along the *002*-plane of HAp nanoparticles. Furthermore, the monophasic HAp was found without forming any by-products, indicating that the PSS template had no effect on purity of HAp resulting products.

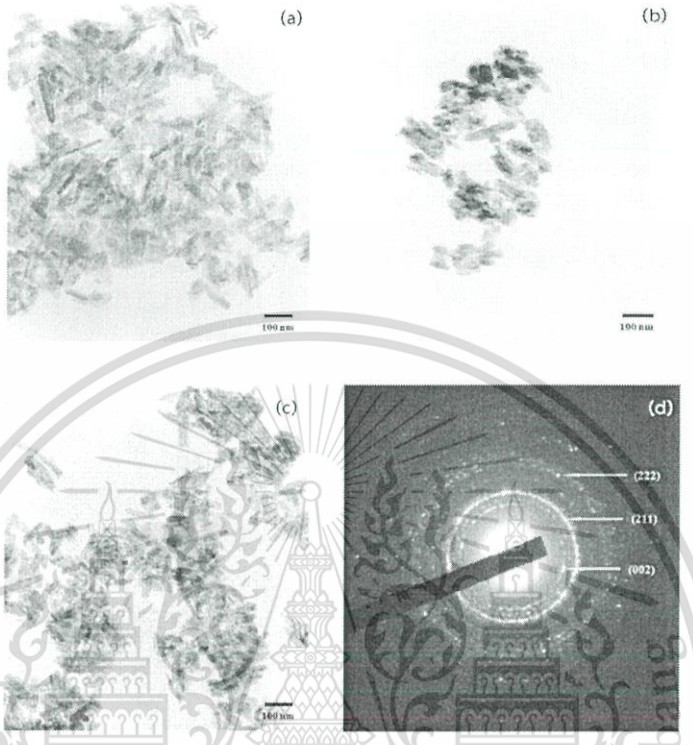

Fig.4.4 TEM images of the synthesized nHAp by refluxing for 6 hrs at pH 10.5 with varying PSS concentrations; (a) P0.0R6-10.5, (b) P0.05R6-10.5, (c) P0.2R6-10.5 and (d) SAED pattern of P0.2R6-10.5

Figure 4.4 (a) and 4.4 (c) respectively illustrate the TEM images of the P0.0R6-10.5 and P0.2R6-10.5 samples. The long rod-formed hydroxyapatite crystals in the absence of PSS template that was in agreement with the extreme high crystallinity in the XRD pattern as shown in Fig. 4.1 (a), while the shorter rod-formed crystals were recieved in the P0.2R6-10.5 sample, corresponding to the XRD pattern in Fig. 4.1 (b). These results were in agreement with the calculated crystallite size along *002*-plane as previously mentioned. Figure 4.4 (d) presents the selected area electron diffraction (SAED) pattern of the rod-formed HAp crystals in the P0.2R6-10.5 sample. The characteristic polycrystalline rings of hydroxyapatite are in agreement with the XRD pattern in Fig. 4.1 (b). Moreover, the imperfect *(002)* ring was discovered, identifying the development of HAp crystals with favored orientation in *002*-plane.

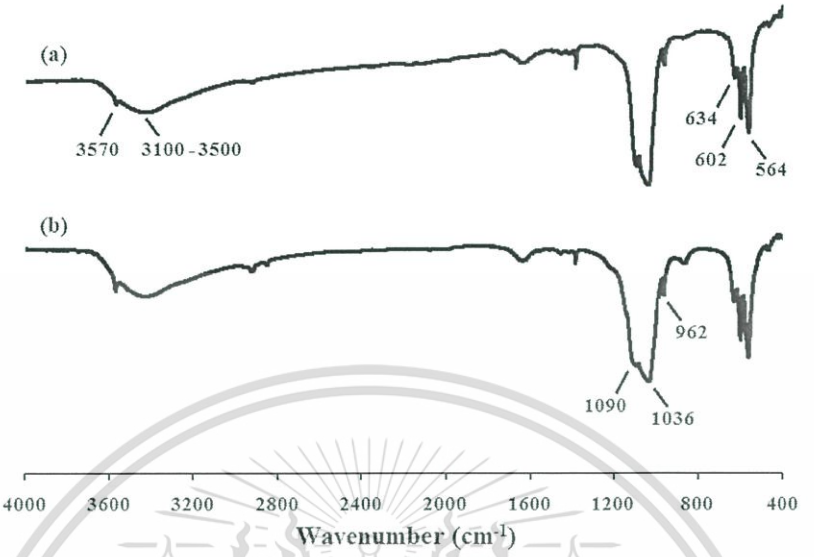

Fig.4.5 FT-IR spectra of the produced nHAp by refluxing for 6 hrs at pH 10.5; (a) P0.2R6-10.5 and (b) P0.0R6-10.5

Figure 4.5 presents the FT-IR spectra of the HAp nanoscale particles prepared with and without PSS template. All HAp samples displayed a set of characteristic bands of PO_4^{3-} group at 564 and 602 cm^{-1} of bending vibration and 962, 1036 and 1090 cm^{-1} of stretching vibration. In addition, the FT-IR bands of OH^- vibration of HAp were achieved at 634 and 3570 cm^{-1} together with the wide range band at 3100-3500 $cm^{-1}$of bound water. It was, however, the signal of PSS template at 1540 and 2925 cm^{-1} corresponded to the C-H stretching vibration of methylene and phenyl groups [106] were not observed in the P0.2R6-10.5 sample (Fig. 4.5(a)), identifying that the PSS template could be effectively removed from the HAp particles.

In addition, the chemical functional groups of the synthesized nHAp were confirmed their chemical structures by FT-IR. This research also studied the elemental composition of the P0.2R6-10.5 sample by scanning electron microscopy (SEM) and energy-dispersive x-ray (EDX) spectroscopy as shown in Fig. 4.6.

Fig. 4.6(a) shows the EDX spectrum of the P0.2R6-10.5 sample, the high amounts of Ca and P elements were observed, i.e. 64.38 and 34.29 atomic%, respectively, corresponding to the predominant phase of hydroxyapatite. However, it can be seen that the trace amounts of S element was detected in this spectrum, in which it could be identified as the PSS template. Fig. 4.6(b) shows the SEM micrographs of the P0.2R6-10.5 surfaces with their Ca, P and S mapping images.

From the above mentioned FT-IR and SEM-EDX results of the P0.2R6-10.5, it can be summarized that the trace amount of PSS template might be remained on the sample. Therefore, the cytotoxicity of this sample was analyzed in order to confirm its probability for biomedical applications.

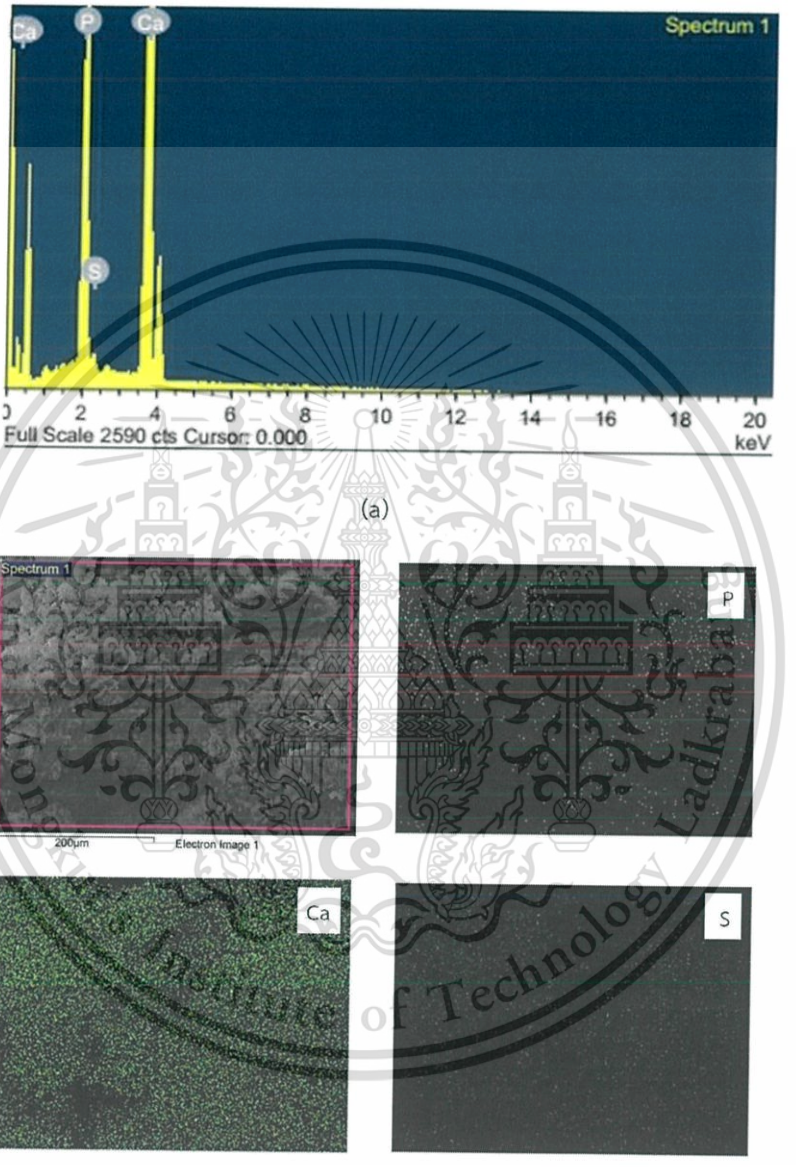

Fig.4.6 SEM-EDX micrograph images of P0.2R6-10.5; (a) EDX spectrum and (b) elemental mapping images of Ca, P and S elements

In comparison between the HAp synthesized without and with PSS template, it can be summarized that the existence of PSS template caused the decline of the HAp crystallite size along the *002*-plane under the refluxing for 6 hrs at pH 10.5 by using 0.20 w/v% PSS.

In the next section of this work was to investigate the influence of PSS concentration on the synthesized HAp under the refluxing synthesis at pH 10.5 for 6 hrs by using various PSS concentrations, i.e. 0.00, 0.05, 0.20 and 0.30 w/v%, in which they were respectively designated as P0.0R6-10.5, P0.05R6-10.5, P0.2R6-10.5 and P0.3R6-10.5.

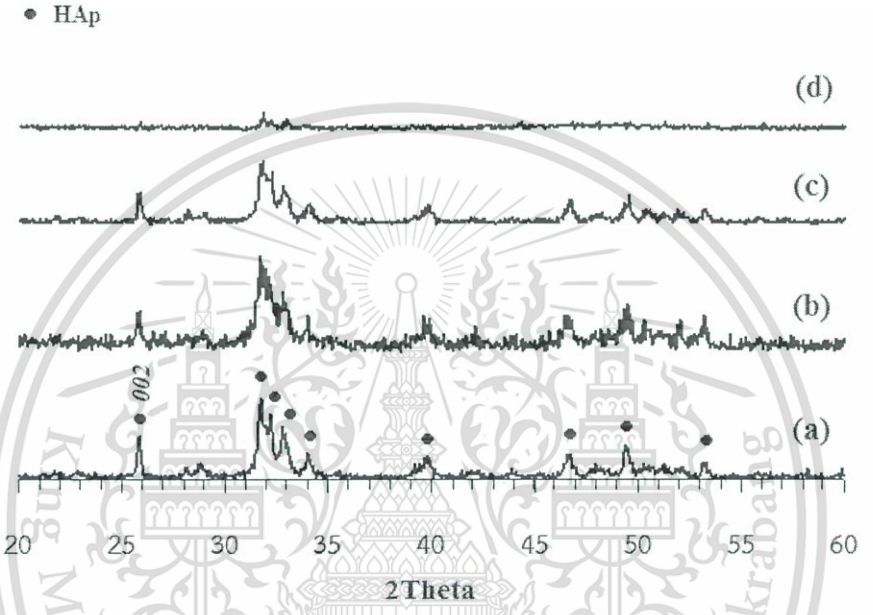

Fig.4.7 XRD patterns of the synthesized nHAp by refluxing for 6 hrs at pH 10.5 with varying PSS concentrations; (a) P0.0R6-10.5, (b) P0.05R6-10.5, (c) P0.2R6-10.5 and (d) P0.3R6-10.5

Table 4.2 Crystallite size of the synthesized nHAp by refluxing for 6 hrs at pH 10.5 using various PSS concentrations

Sample	PSS concentration (w/v%)	Crystallite size (τ_{002}:nm)
P0.0R6-10.5	0.00	52.6
P0.05R6-10.5	0.05	43.4
P0.2R6-10.5	0.20	41.4
P0.3R6-10.5	0.30	n/a

Figure 4.7 and Table 4.2 show the XRD patterns and the crystallite sizes of the HAp crystalline particles synthesized by refluxing for 6 hrs at pH 10.5 in the absence and presence of PSS template. All samples, i.e. P0.0R6-10.5, P0.05R6-10.5, P0.2R6-10.5 and P0.3R6-10.5, were certainly composed of the crystalline

hydroxyapatite. When the HAp crystalline particles were produced in the absence of the PSS template (P0.0R6-10.5) shown in Fig. 4.7 (a), the resulting sample presented a strong and sharp crystalline HAp *(002)* diffraction peak, corresponding to the calculated large crystallite size of 52.6 nm.

On the other hand, the P0.05R6-10.5, P0.2R6-10.5 and P0.3R6-10.5 samples in Fig. 4.7 (b), 4.7 (c) and 4.7 (d), respectively, illustrated the broader HAp crystalline *(002)* diffraction peak when compared with that of the P0.0R6-10.5 sample. The calculated crystallite sizes of P0.05R6-10.5 and P0.2R6-10.5 samples were less than that of P0.0R6-10.5. Moreover, the XRD pattern of P0.3R6-10.5 sample in Fig. 4.7 (d) revealed the poorly crystalline HAp was achieved; its crystallite size could not be investigated by Scherrer's equation. It can be seen that the crystallite size along the *002*-plane of HAp declines with the increase in the PSS concentration. These results explained that the production of good crystallinity HAp nanocrystals under using various PSS conditions could be obtained when the PSS concentration was 0.20 w/v%.

To investigate the effect of PSS template, the images of the HAp nanoparticles synthesized in the existence of PSS template (P0.05R6-10.5 and P0.2R6-10.5) in Fig. 4.4 (b) and 4.4 (c) were compared with those produced in the absence of PSS template (P0.0R6-10.5) in Fig. 4.4 (a). The P0.0R6-10.5 exhibited the long rod-formed HAp crystals that were in agreement with extremely high crystallinity in the XRD pattern as shown in Fig. 4.7 (a).

Nevertheless, Fig. 4.4 (b) and 4.4 (c) showed the formation of shorter rod-formed HAp crystals when using the 0.05 and 0.20 w/v% PSS as templates in the P0.05R6-10.5 and P0.2R6-10.5 samples, respectively. These results indicated that the PSS template performed a notable role in the size and morphology of the synthesized nHAp. It can be summarized that the size and morphology of the synthesized nHAp were dependent on the presence of PSS template.

From all results above mentioned, when the 0.20 w/v% PSS template was used in the synthesized nHAp by refluxing system, it could control the shorter size along *002*-plane and still could preserve a good crystallinity of the synthesized nHAp. Therefore, the 0.20 w/v% PSS was used as template by refluxing synthesis for further study about the effect of reaction pH and reaction time on the synthesis of nHAp.

4.1.2 Effect of reaction pH

Figure 4.8 shows the XRD patterns of the synthesized nHAp by refluxing for 6 hrs without and with 0.20 w/v% PSS template with varying reaction pH of 8.5, 9.5 10.5, 11.5 and 12.5 as shown in Fig. 4.8. It can be observed that the

synthesized samples using reaction pH of 8.5, 9.5 and 10.5, i.e. P0.0R6-8.5, P0.0R6-9.5 and P0.0R6-10.5 in Fig. 4.8 (a), could be identified as a monophasic hydroxyapatite phase, corresponding to JCPDS 09-0432. Meanwhile using reaction pH of 11.5 and 12.5, the results showed that the formation of calcium hydroxide ($Ca(OH)_2$) was observed, having the diffraction peaks at 2θ = 28.7° and 34.1° (JCPDS 04-0733) in the P0.0R6-11.5 and P0.0R6-12.5 samples. Therefore, it can be suggested that the suitable reaction pH for synthesized monophasic HAp were 8.5, 9.5 and 10.5.

Table 4.3 Crystallite size of synthesized nHAp by refluxing for 3 hrs and 6 hrs without and with 0.20 w/v% PSS template using various reaction pH

Reaction pH	Refluxing for 3 hrs				Refluxing for 6 hrs			
	Without PSS		With PSS		Without PSS		With PSS	
	Sample	τ_{002} (nm)*	Sample	τ_{002} (nm)*	Sample	τ_{002} (nm)*	Sample	τ_{002} (nm)*
8.5	P0.0R3-8.5	38.8	P0.2R3-8.5	55.8	P0.0R6-8.5	34.4	P0.2R6-8.5	n/a
9.5	P0.0R3-9.5	31.2	P0.2R3-9.5	37.0	P0.0R6-9.5	37.0	P0.2R6-9.5	51.6
10.5	P0.0R3-10.5	30.9	P0.2R3-10.5	28.3	P0.0R6-10.5	52.6	P0.2R6-10.5	41.4
11.5	P0.0R3-11.5	-	P0.2R3-11.5	-	P0.0R6-11.5	n/a	P0.2R6-11.5	n/a
12.5	P0.0R3-12.5	-	P0.2R3-12.5	-	P0.0R6-12.5	n/a	P0.2R6-12.5	n/a

*Crystallite size calculated by Scherrer's equation

In addition, Table 4.3 shows the crystallite sizes of nHAp synthesized by refluxing without and with 0.20 w/v% PSS template with varying reaction pH. In the absence of PSS template, the crystallite sizes of synthesized nHAp according to the *002*-plane at 2θ = 25.8° would increased when the reaction pH of refluxing synthesis was increased from 8.5 to 10.5, in agreement with the XRD patterns in Fig. 4.8(a). These results were attributed to hydroxyapatite crystalline particles the unconstrained growth of along their preferred *c*-axis direction due to the intrinsic crystal habit in the solution.

On the other hand, Fig. 4.8(b) shows the XRD patterns of the synthesized nHAp in the presence of PSS template. The XRD pattern of P0.2R6-8.5 sample illustrated the unwell crystalline HAp was achieved, in which its size of crystalline particle could not be calculated by Scherrer's equation. The XRD patterns of P0.2R6-9.5 and P0.2R6-10.5 samples displayed the sharp crystalline peaks of HAp especially at 2θ = 25.8° (*002*-plane), indicated that the well-crystallized HAp

was obtained in both conditions. The crystallite size belonged to the *002*-plane would decreased from 51.6 nm to 41.4 nm when the pH of reaction was increased from 9.5 to 10.5. These outcomes adviced that the production of high cyrstallinity HAp crystals would be achieved when the pH of reaction was high enough.

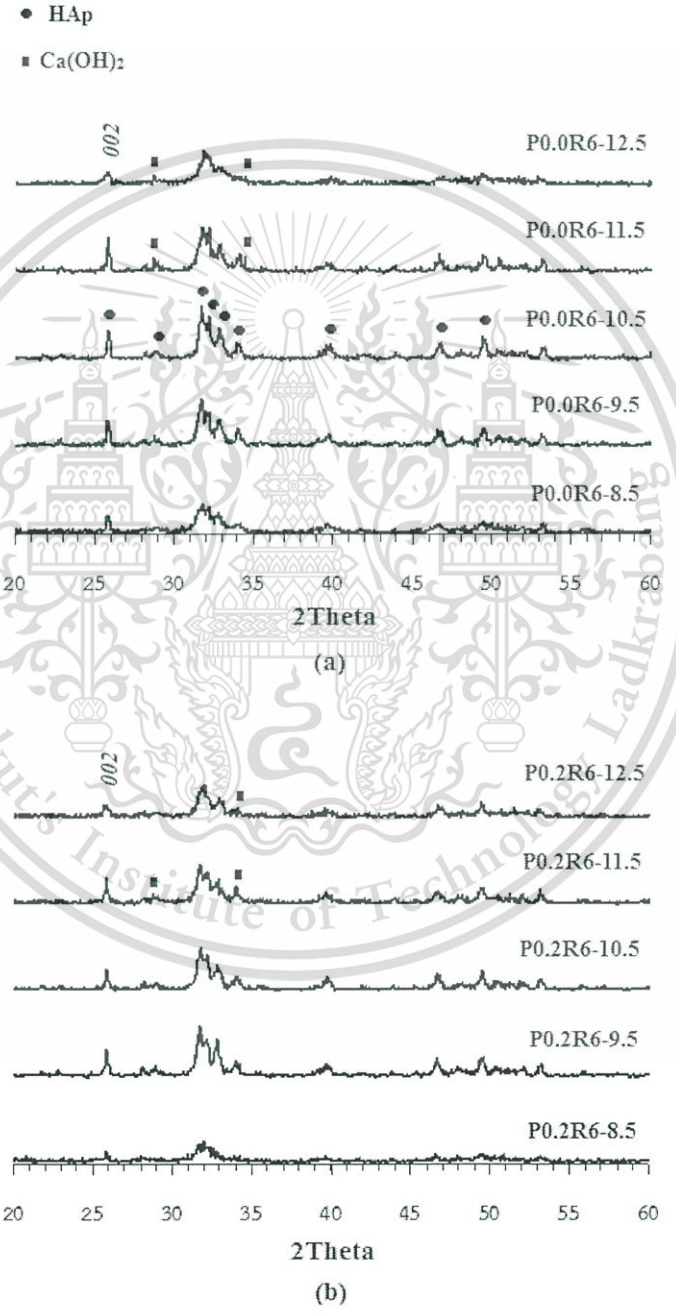

Fig.4.8 XRD patterns of synthesized nHAp by refluxing for 6 hrs using various reaction pH; (a) without PSS template and (b) with PSS template

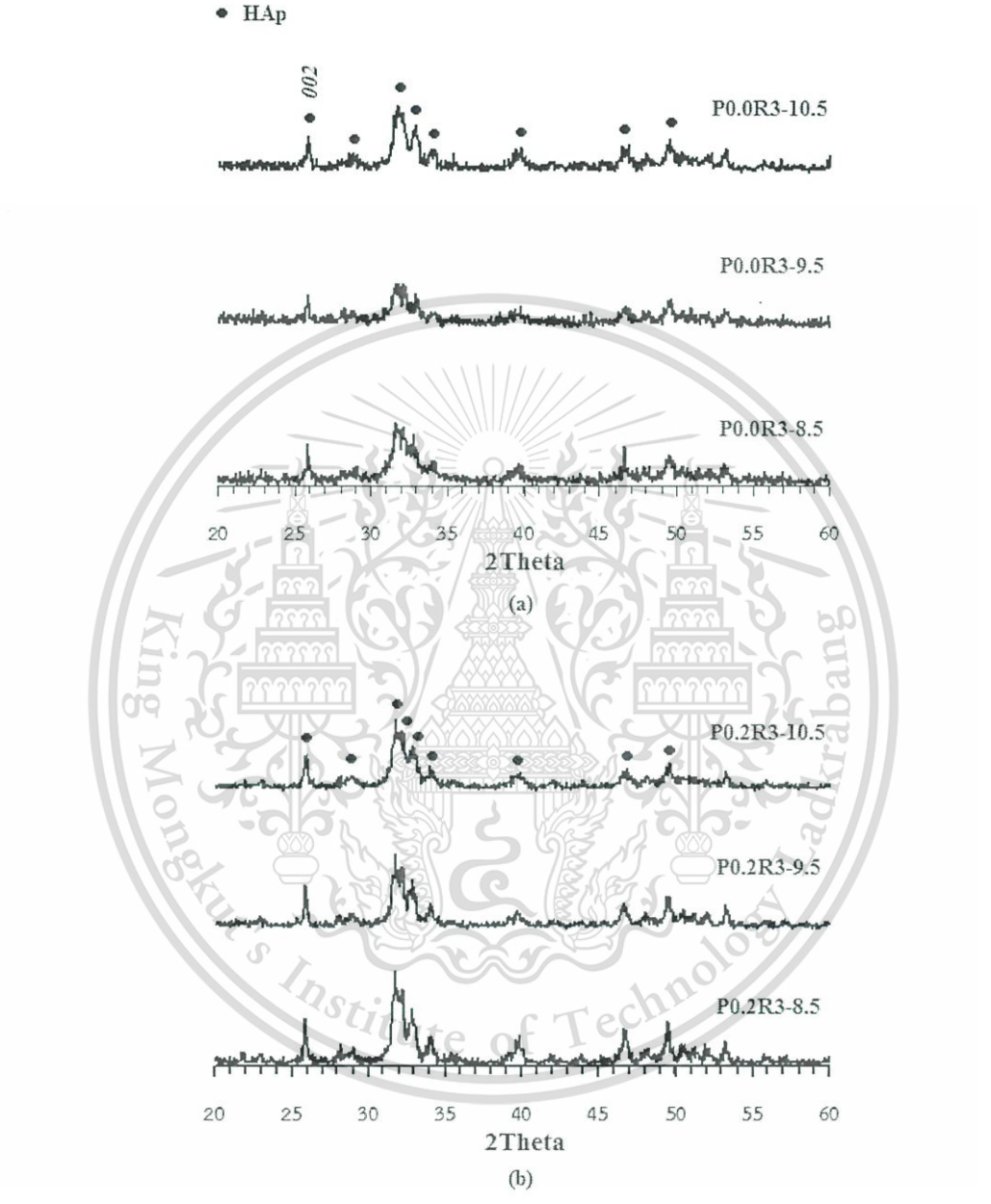

Fig.4.9 XRD patterns of the synthesized nHAp by refluxing for 3 hrs with varying reaction pH; (a) without PSS template and (b) with PSS template

When reducing reaction time to 3 hrs with varying the reaction pH of 8.5, 9.5 and 10.5 under the absence and presence of PSS systems. The XRD patterns of all samples in Fig. 4.9 (a) and 4.9 (b) in the absence and presence of PSS template, respectively, show the monophasic hydroxyapatite phase in agreement with JCPDS 09-0432. It can be seen that the broadened HAp crystalline *(002)* diffraction peak at

2θ = 25.8° was observed when the reaction pH was increased, representing smaller crystallite size. Table 4.3 shows the crystallite sizes of nHAp synthesized by refluxing for 3 hrs, corresponding to the XRD patterns in Fig. 4.9.

In the absence of PSS template, the calculated crystallite size of nHAp synthesized at the reaction pH of 8.5, 9.5 and 10.5 were 38.8 nm, 31.2 nm and 30.9 nm whereas their crystallite sizes were 55.8 nm, 37.0 nm and 28.3 nm in the presence of PSS template, respectively. From these results, in both systems of 3 hrs and 6 hrs refluxing, it can be seen that the increase of reaction pH could reduce the nHAp crystal growth along *002*-plane, but it was inconsistent with the absence of PSS template by refluxing for 6 hrs. This result might be due to the predominant HAp crystals growth along their preferred *c*-axis direction for the longer reaction time.

Considering between two different pH systems, the effect of the reaction pH on the nHAp crystal growth was shown schematically in Figure 4.10. This figure presents the HAp hexagonal form and its rhombic cross-section. There are two binding sites that called the C-site and P-site. The C-sites are on the *(a,c)* or *(b,c)* crystal faces that are full of positive charges, i.e. Ca^{2+} cations. Nevertheless, the P-sites are on the *(a,b)* crystal face having negative charges on their surfaces [108]. Comparing between two different pH systems, the OH^- concentration in the solution system with pH 9.5 was lower than that with 10.5, influencing on the HAp crystallites preferentially grew onto P-site. On the other hand, the system with pH 10.5 having high OH^- concentration brought about the binding of OH^- ions on the C-site of HAp nuclei, supporting the development of HAp crystallites along C-sites, then, the length of HAp crystals was declined.

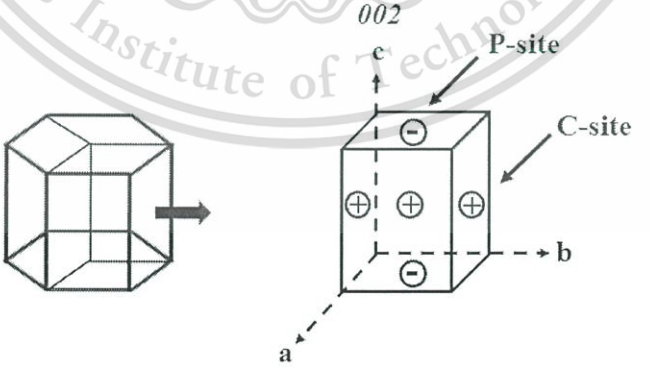

Fig.4.10 HAp hexagonal structure and its rhombic cross section

From the effect of reaction pH, it can be concluded that this effect has significantly resulted in the reduction of the HAp crystallite size along *002*-plane in the presence of PSS template by refluxing for 3 hrs. Therefore, the next section, this research also studied the effect of pH on the PSS template by evaluating surface

charge of the precursor before refluxing treatment with varying pH of 8.5, 9.5 and 10.5.

Since the PSS template is a strong anionic polyelectrolyte, the negatively charged sulfonic group ($-SO_3^-$) on its backbone can fully dissociate in aqueous solution. Therefore, the reaction of pH did not affect the charged ionization of this template in the aqueous system. By considering the starting ionic strength in the system i.e. $Ca(NO_3)_2{\cdot}4H_2O$ and $(NH_4)_2HPO_4$ concentrations were constant and the pH values at 8.5, 9.5 and 10.5 were studied before refluxing treatment.

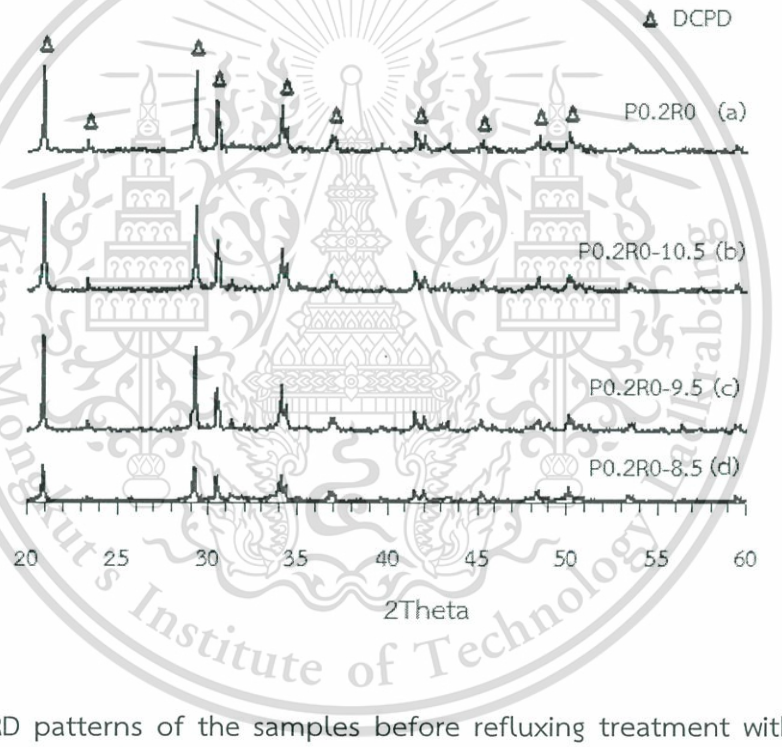

Fig.4.11 XRD patterns of the samples before refluxing treatment with varying reaction pH; (a) as-mixed sample, (b) 10.5, (c) 9.5 and (d) 8.5

Figure 4.11 displays the XRD patterns of the samples before refluxing treatment with varying adjusted pH and as-mixed P0.2R0 sample (not adjusted pH). It can be noticed that the crystalline peaks of all samples were attributed to dicalcium phosphate dihydrate ($CaHPO_4{\cdot}2H_2O$ or DCPD) in JCPDS No.09-0077, in which it was the precursor of the nHAp formation.

Table 4.4 Zeta potential values of the as-mixed DCPD precursor and precursors with varying adjusted pH at 8.5, 9.5 and 10.5

Sample	Reaction pH	Zeta potential (mV)
P0.2R0 (as-mixed precursor)	5.5	-20.63
P0.2R0-8.5	8.5	+9.76
P0.2R0-9.5	9.5	-9.90
P0.2R0-10.5	10.5	-2.94

Table 4.4 shows the ζ values of the DCPD precursors at pH 8.5, 9.5 and 10.5 were +9.76 mV (P0.2R0-8.5), -9.90 mV (P0.2R0-9.5) and -2.94 mV (P0.2R0-10.5), respectively. Whereas the P0.2R0 sample possessed higher ζ value. When the pH of synthesized system was adjusted to be higher basicity before refluxing treatment, the ζ values of the DCPD precursor samples would decreased. These results described that the higher amount of OH^- concentration in the system (higher ionic environment) could be affected to the screening of the electrostatic repulsions between the $-SO_3^-$ groups along the PSS backbone, allowing for the conformation to fold up. So, the lower ζ values, the higher agglomeration of the DCPD particles was obtained, limiting the HAp crystal growth along preferred *c*-axis direction (*002*-plane) after refluxing treatment. This result was in agreement with the calculated HAp crystallite sizes in Table 4.3.

On the other hand, the high ζ value of the as-mixed P0.2R0 precursor represented the PSS chains in the free system, having strong Coulombic repulsions between the $-SO_3^-$ groups along the backbone, therefore, the extended conformation of the PSS chains was obtained. The stretched PSS backbone could minimize the agglomeration of nHAp crystals.

From the above mentioned results, it can be concluded that the adjusted pH before refluxing treatment clearly influenced on the chain conformation of PSS template, in which it subsequently effected to the DCPD precursor agglomeration before transforming to the HAp crystals. Therefore, the presence of the PSS template with the adjusted reaction pH, it could predominantly control the HAp crystal growth along *002*-plane better than that of the absence PSS template.

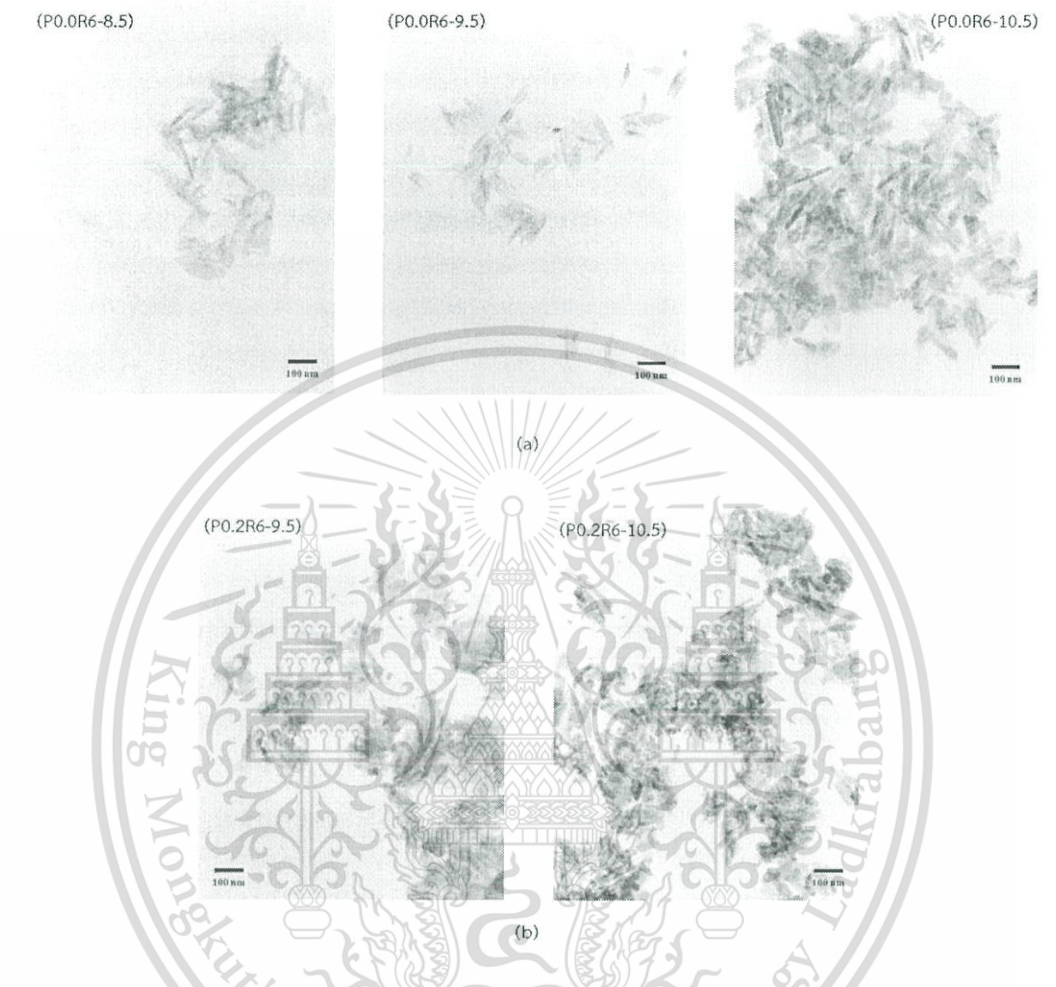

Fig.4.12 TEM images of the synthesized nHAp by refluxing for 6 hrs with varying reaction pH; (a) without PSS template and (b) with PSS template

Figure 4.12 shows the TEM images of the synthesized nHAp by refluxing for 6 hrs with varying reaction pH. Fig. 4.12(a) shows the morphologies of the HAp nanoscale particles produced in the system without PSS template at reaction pH of 8.5 (P0.0R6-8.5), 9.5 (P0.0R6-9.5) and 10.5 (P0.0R6-10.5). It can be recognized that the prolonged rod-formed HAp nanocrystals were obtained when the pH of reaction were increased to higher basicity, as consistent with the higher relative intensity of the (*002*) peak in the XRD patterns (Fig. 4.8(a)). Conversely, Fig. 4.12(b) shows the morphologies of the HAp nanoparticles produced in the system with the PSS template adding at reaction pH of 9.5 (P0.2R6-9.5) and 10.5 (P0.2R6-10.5). It can be seen that the shorter rod-shaped HAp crystals would be obtained

when the pH of reaction were increased, corresponding to the (*002*) peak of the XRD patterns in Fig. 4.8(b) and the calculated HAp crystallite sizes in Table 4.3. These results advocated that the pH of synthesis reaction would effect on the morphology and crystals size of synthesized HAp.

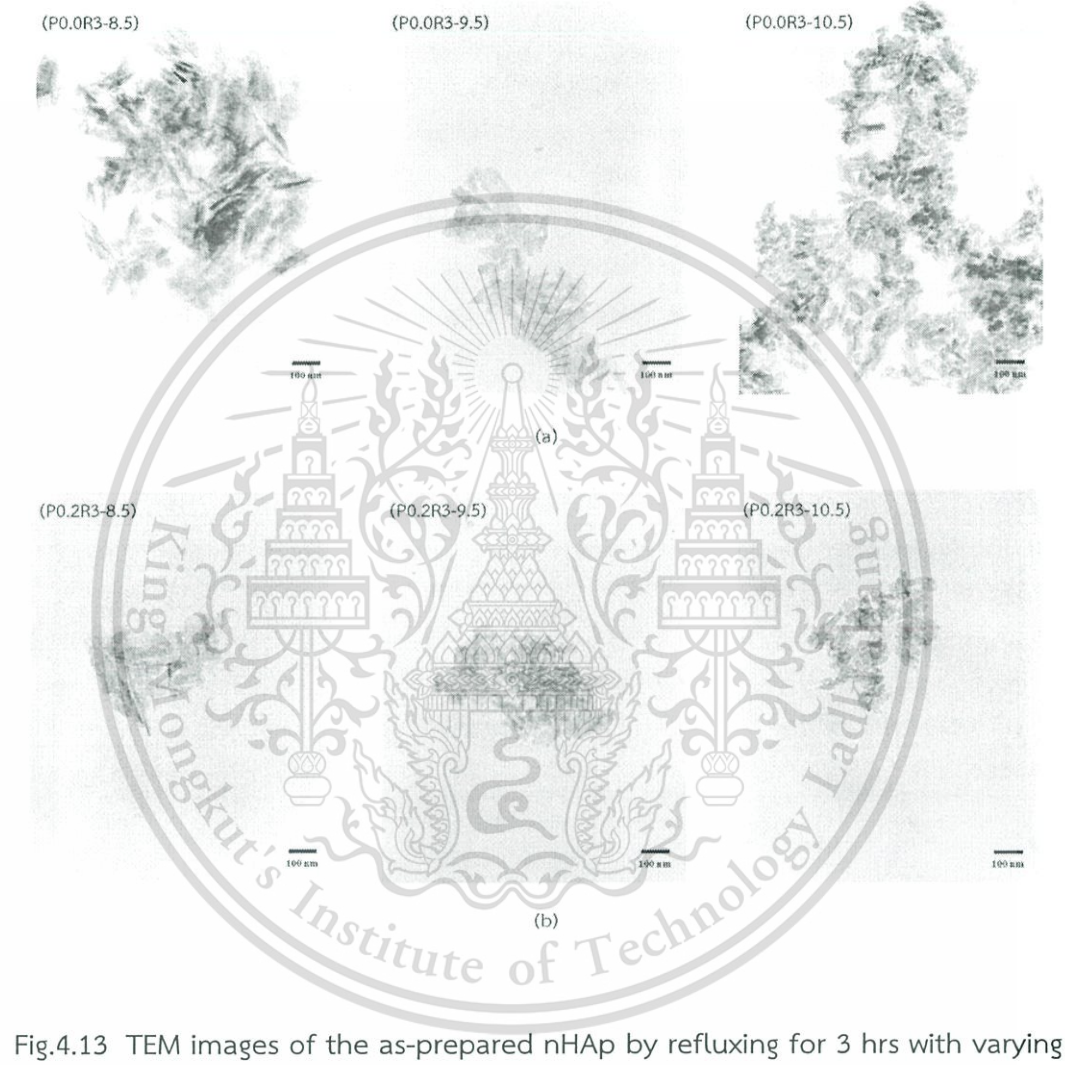

Fig.4.13 TEM images of the as-prepared nHAp by refluxing for 3 hrs with varying reaction pH; (a) without PSS template and (b) with PSS template

Figure 4.13 (a) and (b) respectively demonstrates the TEM images of the nHAp particles synthesized by refluxing for 3 hrs in the nonexistence of the PSS template and in the existence of the PSS template with varying reaction pH. It can be noticed that the shorter rod-shaped HAp crystals were obtained in the both systems when the pH of reaction were increased, supporting the calculated HAp crystallite sizes in Table 4.3. However, the obvious reductions in the HAp crystals size were observed in the system with the addition of PSS template system. From the above mentioned results, it can be concluded that the pH of reaction exhibited

a remarkable role in the size and morphology of the nHAp products in the presence of the PSS template system.

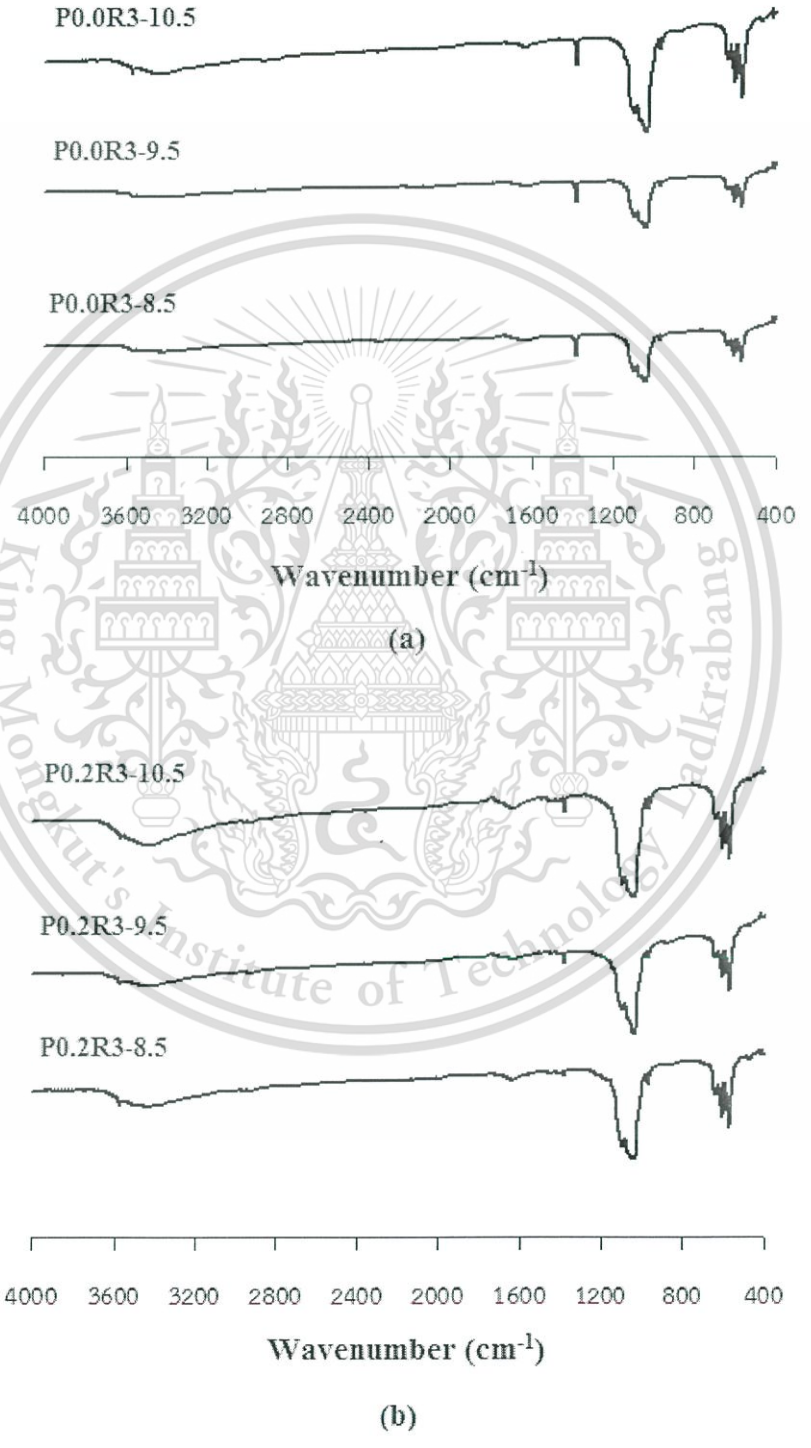

Fig.4.14 FT-IR spectra of the prepared nHAp by refluxing for 3 hrs with varying reaction pH; (a) without PSS template and (b) with PSS template

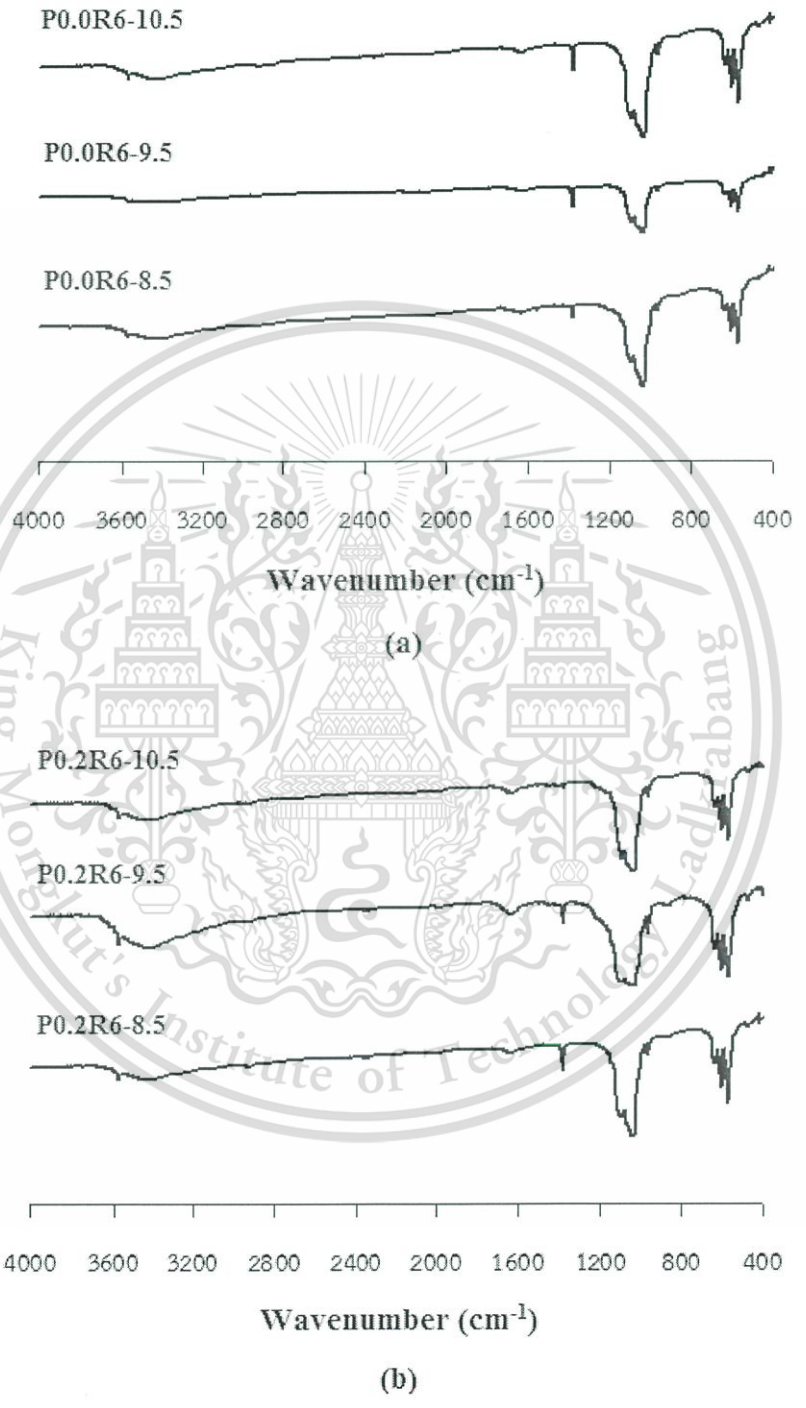

Fig.4.15 FT-IR spectra of the prepared nHAp by refluxing for 6 hrs with varying reaction pH; (a) without PSS template and (b) with PSS template

Table 4.5 Functional groups of the nHAp synthesized without and with 0.20 w/v% PSS template (refluxing for 3 and 6 hrs with varying reaction pH at 8.5, 9.5 and 10.5)

Functional group	Wavenumber (cm^{-1})											
	Refluxing time for 3 hrs						Refluxing time for 6 hrs					
	Without PSS template			With PSS template			Without PSS template			With PSS template		
	pH 8.5	pH 9.5	pH 10.5	pH 8.5	pH 9.5	pH 10.5	pH 8.5	pH 9.5	pH 10.5	pH 8.5	pH 9.5	pH 10.5
OH^-	622	627	628	627	627	623	627	620	629	628	630	634
	3561	3564	3562	3564	3558	3558	3564	3570	3558	3565	3567	3570
PO_4^{3-}	561	562	562	563	562	563	562	561	562	563	561	564
	600	599	601	600	599	601	600	601	600	601	600	602
	956	959	960	958	957	956	958	953	960	960	959	962
	1029	1022	1025	1028	1028	1034	1031	1029	1028	1027	1023	1036
	1090	1090	1084	1087	1085	1092	1085	1092	1087	1093	1093	1090

To characterize the chemical functional groups to justify the chemical structure of the produced nHAp, the FT-IR spectra with varying reaction pH by refluxing for 3 and 6 hrs were presented in Fig. 4.14 and Fig. 4.15, respectively. Two main functional groups of the synthesized nHAp, i.e. OH^- and PO_4^{3-} were identified as shown in Table 4.5. All HAp samples displayed a set of characteristic bands of PO_4^{3-} group at 564 and 602 cm^{-1} of bending vibration and 962, 1036 and 1090 cm^{-1} of stretching vibration. Furthermore, the FT-IR bands of OH^- vibration of HAp were achieved at 634 and 3570 cm^{-1} together with the wide range band at 3100-3500 $cm^{-1}$of adsorbed water. However, it can be seen that the band observed about 1457 cm^{-1} corresponding to the stretching vibration of the CO_3^{2-}, in which it was structured by the adsorption of CO_2 during the preparation of samples.

From the above mentioned results, it can be concluded that all synthesized samples by refluxing for 3 and 6 hrs with varying reaction pH were mainly composed of nHAp products. Moreover, the signals of main functional groups of PSS template, i.e. methylene and phenyl groups, were not observed in the FT-IR spectra, indicating that the PSS template could be effectively removed from the nHAp products.

4.1.3 Effect of refluxing times

Figure 4.16 illustrates the XRD patterns of the synthesized nHAp at pH 10.5 by varying refluxing times; the crystallite sizes along the *002*-plane were determined by Scherrer's equation and presented in Table 4.6. The phases of crystalline particle of the HAp nanoscale particle synthesized at pH 10.5 by varying refluxing times, i.e. 0, 1, 3 and 6 hrs in the PSS free and in the presence of 0.20 w/v% PSS template were illustrated in Fig. 4.16(a) and Fig. 4.16(b), respectively. In both systems, it can be noted that the initial precursor before refluxing, i.e. P0.0R0-10.5 (Fig. 4.16(a)) and P0.2R0-10.5 (Fig. 4.16(b)) were principally composed of the diffraction peaks at 2θ = 20.9°, 29.3°, 30.5° and 34.2° that coincide with the crystalline phase of dicalcium phosphate dihydrate ($CaHPO_4 \cdot 2H_2O$ or DCPD) in JCPDS 09-0077.

After the refluxing treatment for 1 hr, it was notified that the DCPD precursor in both P0.0R0-10.5 and the P0.2R0-10.5 samples transformed to HAp crystalline phase (JCPDS No. 09-0432) in the P0.0R1-10.5 (Fig. 4.16 (a)) and the P0.2R1-10.5 (Fig. 4.16 (b)) samples through the chemical reaction as shown in equation (4.2). There are no characteristic peaks of the DCPD precursor and the calcium hydroxide ($Ca(OH)_2$) by product existed in the XRD patterns. Additionally, the XRD patterns of the P0.0R1-10.5 and the P0.2R1-10.5 samples presented the low crystallinity of HAp

products; therefore, its crystallite size could not be determined by Scherrer's equation.

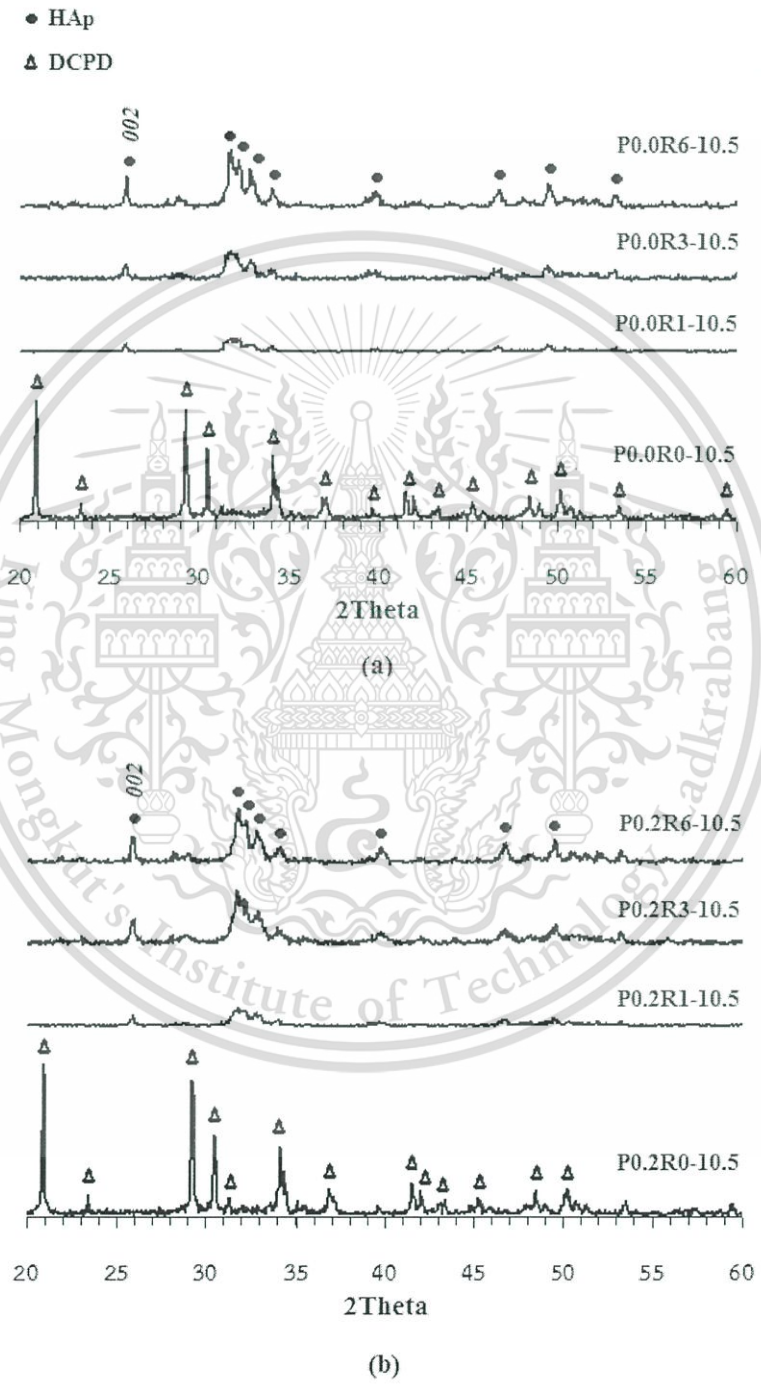

Fig.4.16 XRD patterns of the synthesized nHAp at pH 10.5 by variation of refluxing times; (a) without PSS template and (b) with PSS template

When using the longer refluxing times from 3 to 6 hrs, the XRD patterns of the P0.0R3-10.5 and P0.0R6-10.5 samples in Fig. 4.16(a) and the P0.2R3-10.5 and P0.2R6-10.5 samples in Fig. 4.16(b) illustrated the sharp crystalline peaks of HAp especially at 2θ = 25.8° (*002*-plane), indicating that the well-crystallized HAp were obtained in both systems. In Table 4.6, the crystallite sizes calculated from the *002* preferred-oriented plane increased from 30.9 nm to 52.6 nm in the absence of the PSS template system when the refluxing time was increased from 3 to 6 hrs. Similarly, the crystallite sizes of nHAp increased from 28.3 nm to 41.4 nm in the presence of the PSS template system. These outcomes suggested that the formation of the large nHAp crystals could be achieved when prolonging the refluxing times, supporting the preferred *c*-axis direction of the HAp crystal growth.

Table 4.6 Phase composition and crystallite size of the synthesized nHAp without and with 0.20 w/v% PSS template at pH 10.5 by varying refluxing times for 0, 1, 3 and 6 hrs

Refluxing time	Without PSS template			With PSS template		
	Sample	Phase composition	Crystallite size (τ_{002}:nm)	Sample	Phase composition	Crystallite size (τ_{002}:nm)
0 hr	P0.0R0-10.5	DCPD	n/a	P0.2R0-10.5	DCPD	n/a
1 hr	P0.0R1-10.5	HAp	n/a	P0.2R1-10.5	HAp	n/a
3 hrs	P0.0R3-10.5	HAp	30.9	P0.2R3-10.5	HAp	28.3
6 hrs	P0.0R6-10.5	HAp	52.6	P0.2R6-10.5	HAp	41.4

Figure 4.17 shows the TEM micrographs of DCPD precursor and synthesized nHAp products using pH of 10.5 with variation of the reaction time of refluxing process. The morphologies of DCPD precursor in the PSS-free (P0.0R0-10.5) and in the presence of the PSS template (P0.2R0-10.5) as demonstrated in Fig. 4.17 (a) and Fig. 4.17 (b), respectively. It can be seen that the large DCPD crystallite size with non-uniform morphologies were obtained. Additionally, it was found that on the surfaces of the P0.2R0-10.5 particles (Fig. 4.17 (b)) were covered by the PSS chains.

Fig.4.17 TEM micrographs of the DCPD precursor and the synthesized nHAp at pH 10.5 by varying refluxing times; (a) without PSS template and (b) with PSS template

After the refluxing treatment for 1 hr, the morphologies of the P0.0R1-10.5 (Fig. 4.17(a)) and the P0.2R1-10.5 (Fig. 4.17(b)) revealed the non-uniform of HAp crystals, in which it corresponded to the low crystalline peak of HAp in the XRD patterns as illustrated in Fig. 4.16(a) and Fig. 4.16(b). When using the longer refluxing times for 3 hrs and 6 hrs, it can be seen that all samples, i.e. the PSS-free synthesized products pattern (P0.0R3-10.5 and P0.0R6-10.5) and the PSS-adding synthesized products pattern (P0.2R3-10.5 and P0.2R6-10.5) presented the production of rod-formed nHAp crystals, in which the different in their calculated crystallite sizes were described in the previous section (4.1.3).

From all study results mentioned above in this refluxing section, it can be concluded that the size and morphology of the prepared HAp nanoscale particles were clearly effected by the existence of PSS template, the reaction pH and the refluxing time. In addition, the suggested conditions for synthesis of small HAp crystal size were performed at pH 10.5 with the addition of 0.20 w/v% PSS template and refluxing for 3 hrs. Therefore, these conditions were selected for further study in the synthesis of HAp by hydrothermal reaction as discussed in the next section.

4.2 Preparation of HAp by hydrothermal method

4.2.1 Effect of hydrothermal times

Figure 4.18 illustrates the XRD patterns of the synthesized nHAp at pH 10.5 for various hydrothermal periods. The crystallite sizes along the *002*-plane were determined by Scherrer's equation [106] and presented in Table 4.7. The phase of crystalline product of the HAp nanoparticles synthesized by varying hydrothermal period, i.e. 0, 0.5, 1, 2 and 3 hrs in the absence of the PSS template and in the presence of 0.20 w/v% PSS template at pH 10.5 were shown in Fig. 4.18 (a) and Fig. 4.18 (b), respectively. In the both systems, it can be noted that the starting chemical substance before hydrothermal treatment, i.e. P0.0H0-10.5 (Fig. 4.18 (a)) and P0.2H0-10.5 (Fig. 4.18 (b)), were mainly composed of the diffraction peaks at 2θ = 20.9°, 29.3°, 30.5° and 34.2°, in which they were correlated with the crystalline phase of dicalcium phosphate dihydrate ($CaHPO_4 \cdot 2H_2O$ or DCPD) in JCPDS 09-0077.

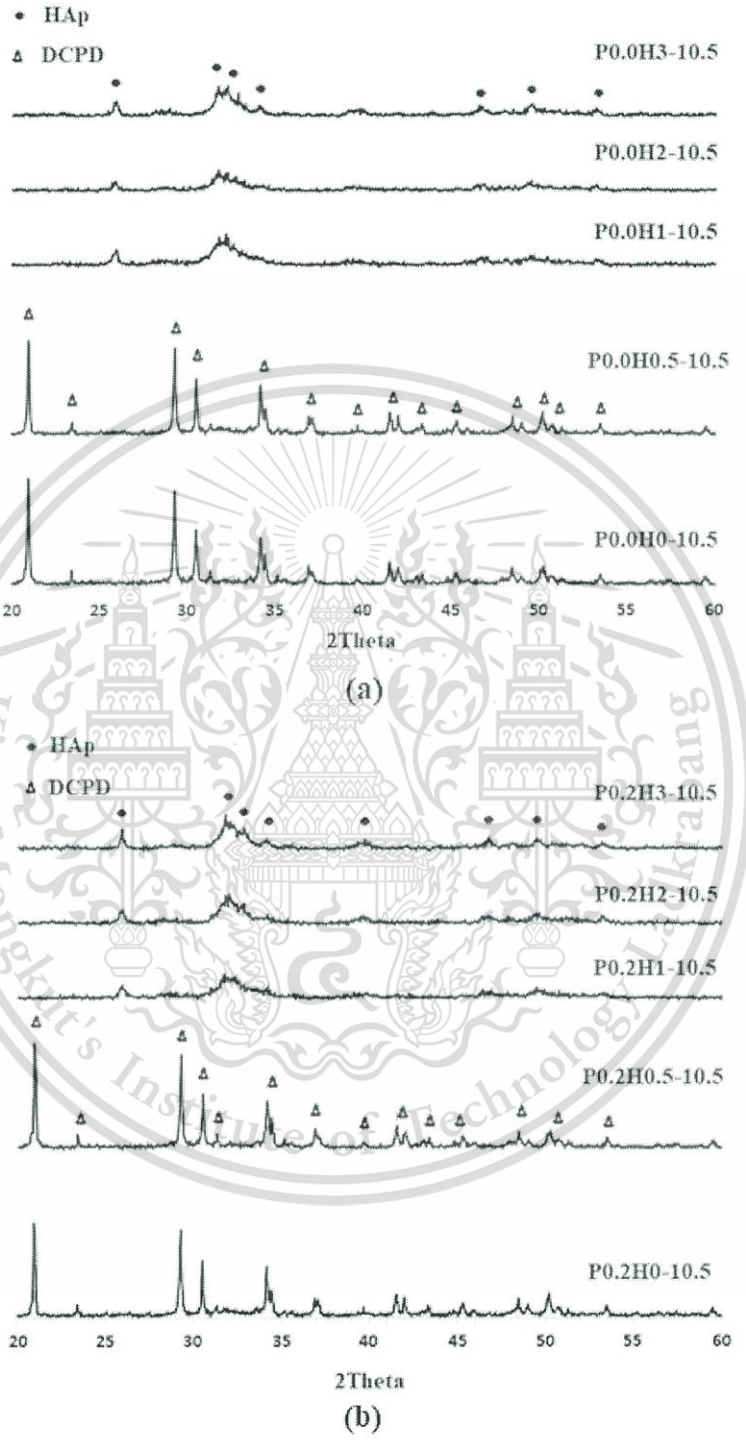

Fig.4.18 XRD patterns of the synthesized nHAp at pH 10.5 for various hydrothermal periods; (a) without PSS template and (b) with PSS template

Table 4.7 Chemical composition of crystalline phase and size of crystal for synthesized nHAp without and with 0.20 w/v% PSS template at pH 10.5 by varying hydrothermal times for 0 hr, 30 min (0.5 hr), 1 hr, 2 hrs and 3 hrs

Hydrothermal times	Without PSS template			With PSS template		
	Sample	Phase composition	Crystallite size (τ_{002}:nm)	Sample	Phase composition	Crystallite size (τ_{002}:nm)
0 hr	P0.0H0-10.5	DCPD	n/a	P0.2H0-10.5	DCPD	n/a
30 min (0.5 hr)	P0.0H0.5-10.5	DCPD	n/a	P0.2H0.5-10.5	DCPD	n/a
1 hr	P0.0H1-10.5	HAp	25.9	P0.2H1-10.5	HAp	23.6
2 hrs	P0.0H2-10.5	HAp	35.4	P0.2H2-10.5	HAp	28.0
3 hrs	P0.0H3-10.5	HAp	29.5	P0.2H3-10.5	HAp	47.1

Figure 4.19 (a) and 4.19 (b) respectively display the TEM images of the P0.0H3-10.5 and P0.2H3-10.5 samples. The irregular rod-liked crystalline hydroxyapatite were achieved in the P0.0H3 sample. These outcomes were in agreement with the calculated size of crystal along *002*-plane as formerly mentioned. The selected area electron diffraction (SAED) of the P0.2H3-10.5 sample shown in Fig.4.19 (c) presents the characteristic ring form of multi-crystalline hydroxyapatite. It can be noticed the wide range scattered ring coinciding to (112), (211) and (300) reflection together with, where it was in concession with the extended peaks of crystal at $2\theta \sim 31^\circ - 34^\circ$ in the XRD pattern. Moreover, an incomplete ring reciprocating to (002) reflection was also achieved, insisting the preferential growth of hydroxyapatite along *c*-axis.

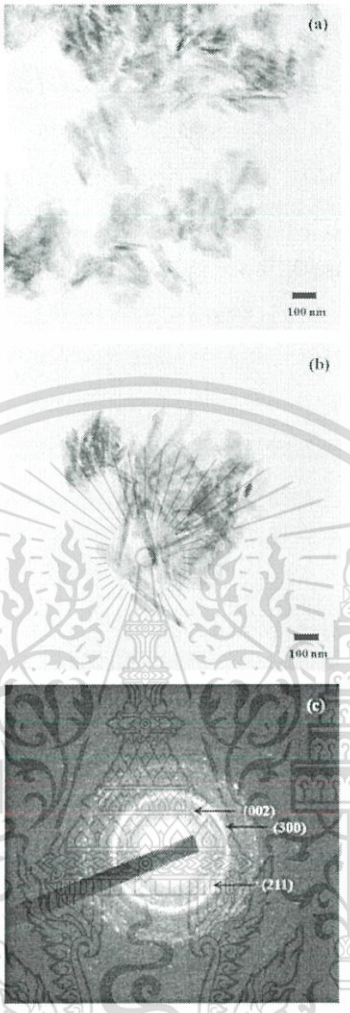

Fig.4.19 TEM micrograph of the purposed nHAp at pH 10.5 by hydrothermal treatment for 3 hrs; (a) without PSS template, (b) with PSS template and (c) SAED pattern of the P0.2H3-10.5

Figure 4.20 illustrates the XRD patterns of the nHAp synthesized by using 0.2 % w/v PSS pattern at pH 10.5 and hydrothermal treatment for 1, 2 and 3 hrs. It can be identified that all diffraction peaks of nHAp products shown in Fig. 4.20 (a) – 4.20 (c) coincided with the phase of hydroxyapatite (JCPDS No.09-0432). There are neither peaks of DCPD precursor nor other by products observed in the XRD patterns of the hydrothermal nHAp products. These results indicated that the DCPD phase in the P0.2H0-10.5 precursor converted to hydroxyapatite phase after hydrothermal process for 1 hr. The size of HAp crystal along *002*-plane of P0.2H1-10.5, P0.2H2-10.5 and P0.2H3-10.5 calculated from the Scherrer's equation were 23.6

nm, 28.0 nm and 47.1 nm, respectively. The longer period of hydrothermal process, the larger size of nHAp crystal was achieved.

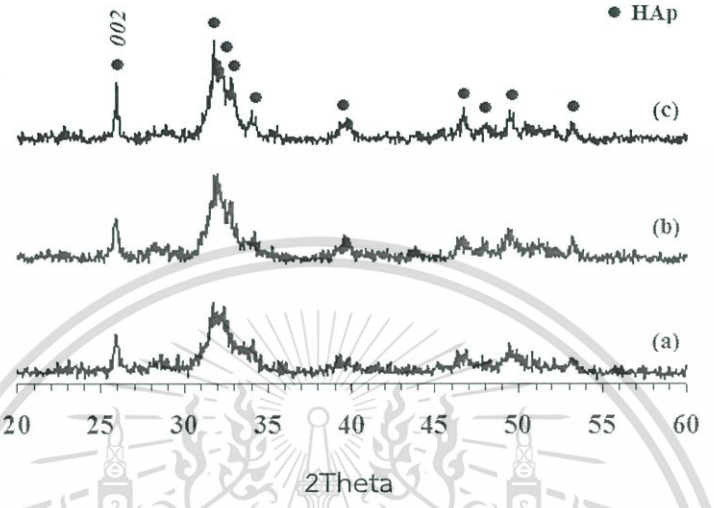

Fig.4.20 XRD patterns of the synthesized nHAp at pH 10.5 for various hydrothermal periods; (a) 1 hr, (b) 2 hrs and (c) 3 hrs

Figure 4.21 presents the morphologies of P0.2H1-10.5, P0.2H2-10.5 and P0.2H3-10.5 samples. In Fig. 4.21 (a), the P0.2H1-10.5 sample was consisted of the accumulated bundles of rod-liked hydroxyapatite nanoscale crystals. After prolonged hydrothermal treatment, the enlarged rod-liked hydroxyapatite nanoscale crystals were achieved and displayed in Fig. 4.21 (b) and 4.21 (c). These outcomes implied that the prolonged hydrothermal process could enhance the exquisite development of hydroxyapatite along *c*-axis.

Fig.4.21 TEM images of the synthesized nHAp at pH 10.5 for various hydrothermal periods; (a) 1 hr, (b) 2 hrs and (c) 3 hrs

4.2.2 Effect of reaction pH

Figure 4.22 illustrates the XRD patterns of the synthesized nHAp by hydrothermal process for 3 hrs at varying reaction pH of 8.5, 9.5 and 10.5 without and with 0.20 w/v% PSS template as presented in Fig. 4.22(a) and 4.22(b), respectively. It can be seen that the crystalline peaks of both synthesized samples using reaction pH at 8.5, 9.5 and 10.5 could be indexed to the monophasic hydroxyapatite phase, correlating to JCPDS No.09-0432.

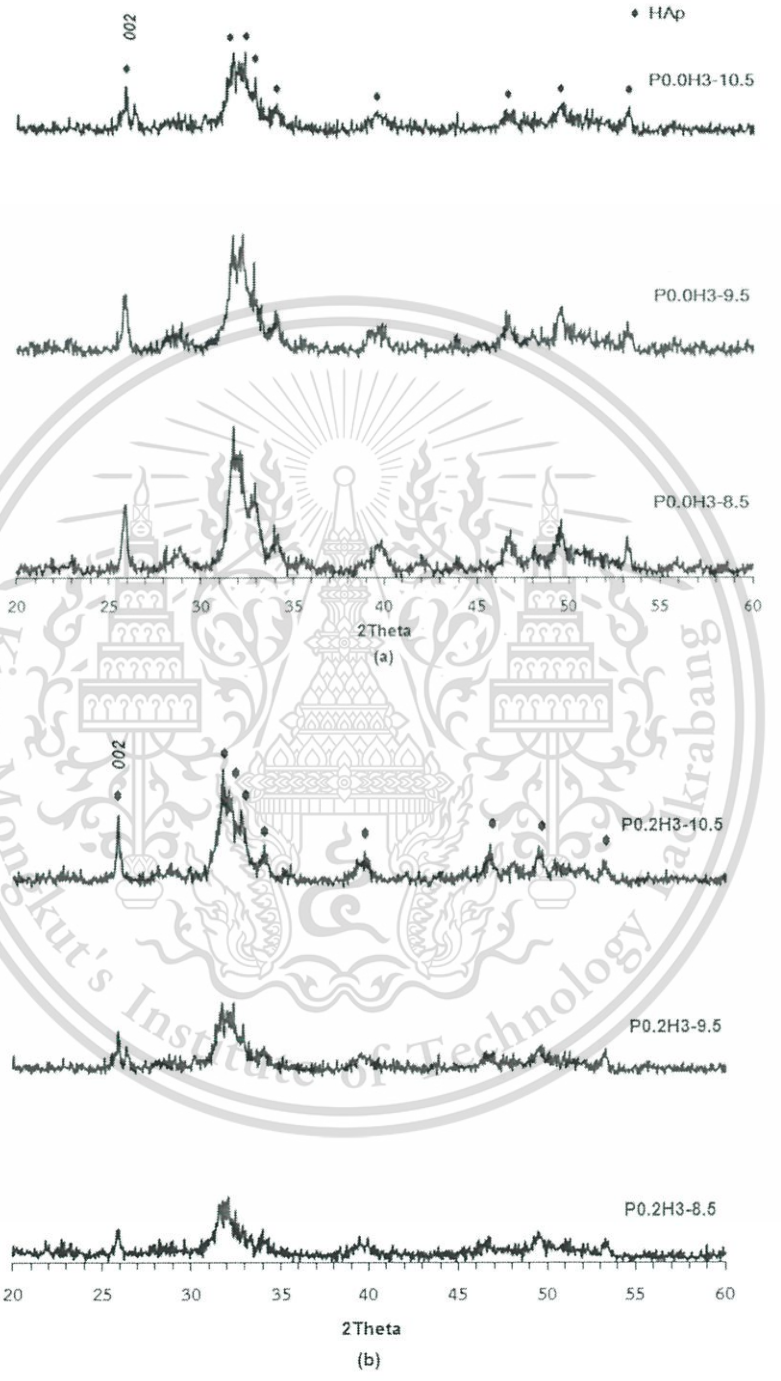

Fig.4.22 XRD patterns of the nHAp synthesized by hydrothermal process for 3 hrs using various reaction pH; (a) without PSS template and (b) with PSS template

Table 4.8 Crystallite size of the synthesized nHAp by hydrothermal for 3 hrs without and with 0.20 w/v% PSS template with varying reaction pH of 8.5, 9.5, and 10.5

pH	Without PSS template		With PSS template	
	Sample	Crystallite size $\tau_{(002)}$ (nm)	Sample	Crystallite size $\tau_{(002)}$ (nm)
8.5	P0.0H3-8.5	79.9	P0.2H3-8.5	33.9
9.5	P0.0H3-9.5	30.4	P0.2H3-9.5	35.4
10.5	P0.0H3-10.5	29.5	P0.2H3-10.5	47.1

Table 4.8 shows the crystallite sizes of the nHAp products synthesized by hydrothermal treatment for 3 hrs without and with 0.20 w/v% PSS template at varying reaction pH. In the absence of PSS template, the calculated size of HAp crystal corresponded to the *002*-plane at 2θ = 25.8° would decreased from 79.9 nm, 30.4 nm to 29.5 nm when the reaction pH were respectively increased from 8.5, 9.5 to 10.5, in agreement with the XRD patterns in Fig. 4.22 (a).

Furthermore, Fig. 4.22 (b) presents the XRD patterns of the synthesized nHAp in the presence of PSS template. The XRD patterns of P0.2H3-8.5, P0.2H3-9.5 and P0.2H3-10.5 samples displayed the peaks of HAp crystal especially at 2θ = 25.8° (*002*-plane). The size of crystal belonged to the *002* preferred-oriented plane increased from 33.9 nm to 35.4 and 47.1 nm when the pH of hydrothermal reaction was increased from 8.5 to 9.5 and 10.5, respectively. These results noticed that the production of large HAp crystals would be achieved when the pH of reaction was high enough.

From the effect of reaction pH experiments, it can be concluded that this effect has significantly resulted in the increasing of the HAp crystallite size along *002*-plane in the existence of PSS template by hydrothermal for 3 hrs. Therefore, the next section, the effect of pH on the synthesis of HAp in the system with the PSS template in comparison between the refluxing and hydrothermal methods, in which 0.20 w/v% PSS template was added and the reaction was performed for 3 hrs at pH 10.5.

Table 4.9 Crystallite size of the synthesized nHAp by refluxing and hydrothermal methods varying reaction pH of 8.5, 9.5, and 10.5 with 0.20 w/v% PSS template for 3 hrs

pH	Refluxing method		Hydrothermal method	
	Sample	Crystallite size $\tau_{(002)}$ (nm)	Sample	Crystallite size $\tau_{(002)}$ (nm)
8.5	P0.2R3-8.5	55.8	P0.2H3-8.5	33.9
9.5	P0.2R3-9.5	37.0	P0.2H3-9.5	35.4
10.5	P0.2R3-10.5	28.3	P0.2H3-10.5	47.1

Table 4.9 shows the crystallite sizes of the nHAp products synthesized under varying pH in the presence PSS template in comparison between the refluxing and hydrothermal methods. It can be seen that the increase of refluxing reaction pH could reduce the nHAp crystallite sizes. On the other hand, these results showed that the longer nHAp crystals would be obtained when the higher pH was used in the hydrothermal reaction.

Therefore, it can be concluded that the adjusted reaction pH might be influenced on the crystallite sizes of nHAp products. From the different prominent of crystallite size values between two methods; therefore, these conditions were selected for further study about the properties of synthesized HAp, i.e. surface charge, cytotoxicity and antibacterial activity.

4.3 Biological activity of synthesized nHAp

4.3.1 Surface testing of synthesized nHAp

In this section, the surface properties of the as-produced nHAp were evaluated by adsorption tests using two different types of amino acids, i.e. L-aspartic acid (Asp, negative charge) and L-arginine (Arg, positive charge) as displayed in Fig. 4.23.

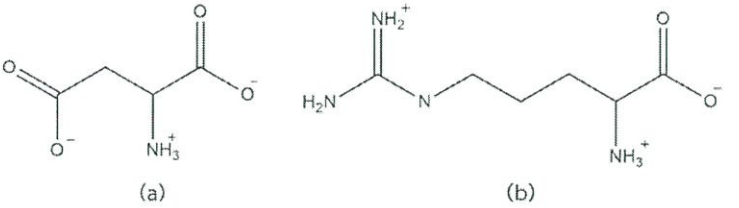

(a) (b)

Fig.4.23 Structures of amino acids used in adsorption testing: (a) Aspartic acid (Asp) and (b) Arginine (Arg)

Table 4.10 Surface charge of the synthesized nHAp surface after modification with amino acids (Arg and Asp)

Refluxing method		Hydrothermal method	
Sample	Zeta potential (mV)	Sample	Zeta potential (mV)
P0.2R3-10.5*	+5.46	P0.2H3-10.5*	-19.52
Arg-HAp-R	+4.72	Arg-HAp-H	+0.41
Asp-HAp-R	-24.70	Asp-HAp-H	-22.38

*The nHAp synthesized by refluxing and hydrothermal methods at pH 10.5 for 3 hrs with 0.20 w/v% PSS

Table 4.10 shows the surface charges of the modified HAp nanoparticles were analyzed in comparison with the as-prepared nHAp. It was found that the nHAp prepared by refluxing (P0.2R3-10.5) showed a positive ζ value of +5.46 mV due to the rod-shaped morphology that possessed high quantities of the C-sites on the HAp faces as discussed in the previous section (4.1.2). After modification with Asp, the ζ value of nHAp surface was drastically changed from the positive ζ value of the as-prepared nHAp to -24.70 mV of the Asp modified HAp (Asp-HAp-R). This negatively charged surface of Asp-HAp-R was because the Asp possesses two acidic $-COO^-$ groups, whereby one $-COO^-$ could bond to the Ca^{2+} on the C-sites of HAp surface as schematically shown in Fig. 4.24(a). The other acidic $-COO^-$ group of Asp was then exposed to the outer surface of nHAp particles, leading to the negative ζ value of Asp-HAp-R. On the other hand, the ζ value of Arg-modified nHAp (Arg-HAp-R) was +4.72 mV, which was comparable with that of the as-prepared HAp nanoparticles (i.e. +5.46 mV). This result was considered to be because the nHAp with rod-shaped morphology possessed low quantities of the negative P-sites [108]. Therefore, the bonding between the positive charge of the guanidyl group ($-(CH_2)_3NHC(NH_2)^+$) in Arg and the PO_4^{3-} on the P-sites of nHAp as shown in Fig. 4.24(b) rarely occurred.

In the case of hydrothermal method, it was found that the as-prepared HAp (P0.2H3-10.5) showed the high negative ζ value of -19.52 mV, in which it was quite different from that of the refluxed product. After modification with Arg, the ζ value of nHAp surface was drastically changed from the negative ζ value of P0.2H3-10.5 to +0.41 mV of the Arg modified nHAp (Arg-HAp-H). This result could be explained that the guanidyl group ($-(CH_2)_3NHC(NH_2)^+$) of Arg bond to the PO_4^{3-} on the P-sites of nHAp, exposing its positively charged NH_3^+ groups on the Arg-HAp-H surface. On the other hand, the ζ value of Asp-modified nHAp (Asp-HAp-H) was -22.38 mV, which was comparable with that of P0.2H3-10.5 (i.e. -19.52 mV). This result was because Asp could bond to the Ca^{2+} on the C-sites of nHAp surface with the $-COO^-$ group, whereby the other acidic $-COO^-$ group of Asp was then exposed to the outer

surface of nHAp particles, leading to the negative ζ value of Asp-HAp-H as shown in Fig.4.24 (a).

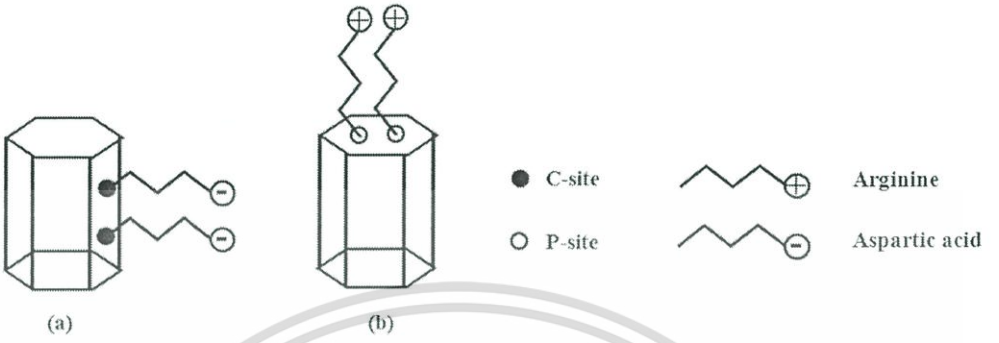

Fig.4.24 Schematic representation of nHAp surface modified with: (a) Asp-HAp and (b) Arg-HAp

Fig. 4.25 displays the FT-IR spectra of amino acid modified HAp nanoparticles. The Asp-HAp and Arg-HAp samples possessed the characteristic bands of amino acid, i.e. 1408 cm^{-1} of $-NH_2$ vibration and 1441 cm^{-1} of $-COO^-$ stretching. The FT-IR bands of C–H stretching of amino acid were achieved at 2848 and 2917 cm^{-1}. Furthermore, the noticeable signals of HAp at 3570 cm^{-1} were ascribed to the typical OH vibration and the stretching vibration at 962, 1036, and 1090 cm^{-1} corresponded to the PO_4^{3-} group of HAp [108]. These results indicated that the amino acids could bound onto the surface of nHAp.

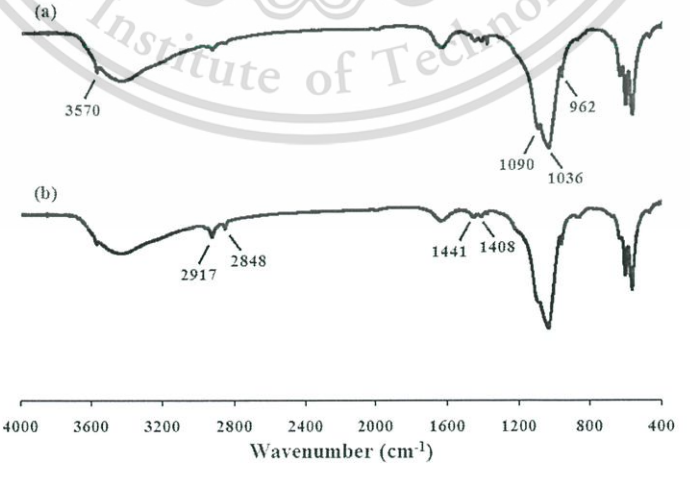

Fig.4.25 FT-IR spectra of the modified nHAp particles: (a) Arg-HAp and (b) Asp-HAp

From the above mentioned results, it can be summarized that the negatively charged (Asp) and positively charged (Arg) amino acids were exceptionally bound onto the as-prepared HAp nanoparticles through their electrostatic interaction. Moreover, the different surface charge properties of the modified as-prepared and amino acid HAp nanoparticles could be used in some medical purposes, such as a transporter for acidic protein including bovine serum albumin and glutamic acid, etc.

4.3.2 *In vitro* cytotoxicity testing

From the previous study, the as-prepared nHAp from the refluxing and hydrothermal methods which the different ζ values, i.e. +5.46 mV and -19.52 mV, respectively, were selected for cytotoxicity testing. In addition, the nHAp modified with the opposite charged amino acids, i.e. Asp-HAp and Arg-HAp were chosen for cytotoxicity testing in comparison with the as-prepared nHAp.

Table 4.11 shows the *in vitro* cytotoxicity of the as-prepared HAp by refluxing and hydrothermal samples against Vero cells was assessed by MTT assay for principle screening using cell concentration of 1,000 μg/mL. It was noticed that the percentage developing inhibition were 5.32% and 13.78% of the as-prepared HAp by refluxing and hydrothermal samples, respectively. When considering the Asp-HAp sample from refluxing method, it showed the lower percentage of cytotoxicity than the as-prepared nHAp. Whereas the Arg-HAp sample from hydrothermal presented the higher percentage of cytotoxicity than the as-prepared nHAp. It was, however, the % cytotoxicities of all samples still in the range of low cytotoxicity against the Vero cells [109]. Therefore, the modified nHAp samples from refluxing and hydrothermal methods were considered to be biocompatible materials for biomedical applications.

Table 4.11 *In vitro* cytotoxicity testing of the synthesized nHAp and the modified nHAp by Refluxing and hydrothermal methods at pH 10.5 for 3 hrs with 0.20% PSS template

Method	Cytotoxicity (%)		
	as-prepared HAp	Arg-HAp	Asp-HAp
Refluxing	5.32	-	2.75
Hydrothermal	13.78	29.55	-

4.3.3 Antibacterial activity

The antibacterial activity of all samples were examined by agar disc diffusion procedure using *Staphylococcus aureus* ATCC®25923 *(S.aureus)* and *Escherichia coli* ATCC®25922 *(E.coli)* as model organisms. Table 4.12 shows the inhibition zone of all samples for *S.aureus*. Nevertherless, there were no inhibition zone around all samples for *E.coli*. These results were belonged to the influence of negative –OH group on the nHAp surface of all samples, in which it could effectively interact with the gram-positive *S.aureus*, but not the gram-negative *E.coli*.

Table 4.12 Surface charge and antibacterial activity for *S.aureus* of the nHAp synthesized by refluxing and hydrothermal methods for 3hrs with varying pH of 8.5, 9.5 and 10.5 and 0.20 w/v% PSS template

Refluxing Method		Hydrothermal Method	
Sample	Clear zone (mm)	Sample	Clear zone (mm)
P0.2R3-10.5	7	P0.2H3-10.5	9.5
P0.2R3-9.5	16	P0.2H3-9.5	10
P0.2R3-8.5	10	P0.2H3-8.5	16
P0.0R3-10.5	8	P0.0H3-10.5	6.5
P0.0R3-9.5	9	P0.0H3-9.5	7
P0.0R3-8.5	12	P0.0H3-8.5	8

Chapter 5

Conclusions and Suggestions

5.1 Conclusions

In this study, hydroxyapatite nanoparticles (nHAp) were successfully synthesized at low reaction temperature by facile eco-friendly refluxing and hydrothermal method. In the proposed low temperature conditions, the nHAp synthesis was achieved through the formation of dicalcium phosphate dehydrate (DCPD) precursor.

In the refluxing system, the DCPD precursor obtained in the polyelectrolyte free system has low ζ value, leading to the accumulation of precursor particles, therefore, the growth of nHAp crystals during refluxing was confined. However, the nHAp crystals could freely grow along their preferred *c*-axis direction due to the intrinsic crystal habit in the solution, promoting the larger crystallite size nHAp products. On the other hand, the presence of PSS template induced the formation of DCPD precursor with higher ζ value, preventing the agglomeration of precursor particles. In addition, the PSS template dissociated to the $-SO_3^-$ groups on the backbone, promoting the formation of PSS-Ca intermediate in the system. This led to the decreased of free Ca^{2+} ions, resulting in the limitation of nHAp growth along the c-axis direction. Therefore, it can be concluded that the existence of PSS template influenced on the reduction of crystallite size along the *002*-plane of nHAp products, resulting in the shorter rod-liked nHAp crystals. Besides, the long rod-liked nHAp crystals was obtained in the refluxing without PSS template.

The effect of reaction pH on the refluxing products can be concluded that the higher pH in the presence of PSS template has significantly resulted in the shorter rod-liked nHAp crystallite size along *002*-plane. This result corresponded the adjusted pH to higher basicity before refluxing treatment, in which the higher agglomeration of DCPD precursor was obtained, limiting the nHAp crystals growth after refluxing treatment.

Considering the effect of refluxing times between the absence and the presence of PSS template, the formation of the long rod-liked nHAp crystals were obtained in the both system when prolonging the refluxing times. It can be concluded that the size and morphology of the nHAp products were clearly effected by the existence of PSS template, the reaction pH and the refluxing time.

For synthesized nHAp crystals without and with PSS template by hydrothermal method, the DCPD precursor was transformed to the long rod-liked nHAp crystals in the both system when prolonging the hydrothermal treatment times. The shorter rod-liked nHAp crystals would be obtained when the reaction pH was increased in the absence PSS template. On the other hand, the longer rod-liked nHAp crystals

would be obtained when the reaction pH were increased to higher basicity in the PSS system.

The surface charge of the synthesized nHAp from refluxing method showed the positive ζ value, preferably bonding with the negatively charged aspartic acid than the positively charged arginine. On the other hand, the surface of nHAp particles synthesized by hydrothermal process possessed the negative ζ value, therefore, they preferably bond with the negatively charged arginine. Besides, the nHAp synthesized by refluxing and hydrothermal methods with and without PSS template showed the low percentage of cytotoxicity against Vero cells and effective inhibition of *S.aureus* microorganism.

5.2 Suggestions

5.2.1 In this work, it should be investigated the other properties of the synthesized nHAp products such as mechanical property, adsorption ability, cell viability testing, etc., in which it can be used of information for the variety of biomedical applications.

5.2.2 It should be investigated the effect of the cationic polyelectrolyte as template, in which it might obtaine the nHAp with different morphology and properties which are suitable for other applications.

References

1. Jarcho, M. Bolen, C.H. Thomas, M.B. Bobick, J. Kay, J.F. and Doremus R.H. 1976. "Hydroxyapatite Synthesis and Characterization in Sense Polycrystalline Forms." *Journal of Materials Science.* 11(11) : 2027-2035.
2. Dewith, G. Vandijk, H.J.A. Hattu, N. and Prijs, K. 1981. "Preparation, Microstructure and Mechanochemical Properties of Dense Polycrystalline Hydroxyapatite." *Journal of Materials Science.* 16(6) : 1592-1598.
3. Cai, Y. Liu, Y. Yan, W. Hu, Q. Tao, J. Zhang, M. Shi, Z. and Tang, R. 2007. "Role of Hydroxyapatite Nanoparticle Size in Bone Cell Proliferation." *Journal of Materials Chemistry*. 17 : 3780-3787.
4. Tiselius, A. Hjerten, S. and Levin, O. 1956. "Protein Chromatography on Calcium Phosphate Columns." *Archives of Biochemistry and Biophysics.* 65 : 132- 155.
5. Cheng, K. Han, G. Weng, W. Qu, H. Du, P. Shen, G. Yang, J. and Ferreira, J.M.F. 2003. "Sol-Gel Derived Fluoridated Hydroxyapatite Films." Materials Research Bulletin. 38(1) : 89-97.
6. Cheng, K. Shen, G. Weng, W. Han, G. and Ferreira, J.M.F. 2001. "Synthesis of Hydroxyapatite/Fluoroapatite Solid Solution by a Sol-Gel Method." *Materials Lettrs.* 51(1) : 37-41.
7. Perla, V. and Webster, T.J. 2006. "Nano-Hydroxyapatite-Thermally Denatured Small Intestine Sub-Mucosa Composites for Entheses Applications." *Interna-tional Journal of Nanomedicine*. 1(3) : 351-359.
8. Roy, M. Bandyopadhyay, A. and Bose, S. 2011. "Induction Plasma Sprayed Nano Hydroxyapatite Coatings on Titanium for orthopaedic and Dental Implants." *Surface and Coating Technology.* 205(8-9) : 2785-2792.
9. Stupp, S.I. and Ciegler, G.W. 1992. "Organoapatites: Materials for Artificial Bone. I. synthesis and Microstructure." *Journal of Biomedical Materials Research.* 26(2) : 169-183.
10. Intapong, S. and Raksudjarit, A. 2013. "Treatment of Agricultural Wastewater Using Porous Ceramics Composite of Hydroxyapatite and Silica." *Advanced Materials Research.* 622-623 : 915-918.
11. Mahabole, M.P. Aiyer, R.C. Ramakrishna, C.V. Sreedhar, B. and Khairnar, R.S. 2005 "Synthesis, Characterization and Gas Sensing Property of Hydroxyapatite Ceramic." *Bulletin of Materials Science.* 28(6) : 535–545.
12. Smith, G.P. and Gingrich, T.R. 2005. "Hydroxyapatite Chromatography of Phage-Display Virions." *BioTechniques.* 39(6) : 879-884.

13. Nasiri-Tabrizi, B. Fahami, A. and Ebrahimi-Kahrizsangi, R. 2013. "Effect of Milling Parameters on the Formation of Nanocrystalline Hydroxyapatite Using Different Raw Materials." *Ceramics International.* 39 : 5751–5763.
14. Bakan, F. Laçin, O. and Sarac, H. 2013. "A Novel Low Temperature Sol–Gel Synthesis Process for Thermally Stable Nanocrystalline Hydroxyapatite." *Powder Technology.* 233 : 295–302.
15. Guo, X. Yan, H. Zhao, S. Zhang, L. Li, Y. and Liang, X. 2013. "Effect of Calcining Temperature on Particle Size of Hydroxyapatite Synthesized by Solid-state Reaction at Room Temperature." *Advanced Powder Technology.* 24 : 1034–1038.
16. Tsetsekou, A. Brasinika, D. Vaou, V. and Chatzitheodoridis, E. 2014. "On the Synthesis of Tailored Biomimetic Hydroxyapatite Nanoplates through a Bioinspired Approach in the Presence of Collagen or Chitosan and L-arginine." *Materials Science and Engineering C.* 43 : 555–565.
17. Xiao, X. Liu, R. Qiu, C. Zhu, D. and Liu, F. 2009. "Biomimetic Synthesis of Micrometer Spherical Hydroxyapatite with β-Cyclodextrin as Template." *Materials Science and Engineering C.* 29 : 785–790.
18. Seo, D.S. and Lee, J.K. 2008. "Synthesis of Hydroxyapatite Whiskers through Dissolution–Reprecipitation Process Using EDTA." *Journal of Crystal Growth.* 310(7-9) : 2162–2167.
19. Xu, S. Shi, J. Feng, D. Yang, L. and Cao, S. 2014. "Hollow Hierarchical hydroxylapatite/Au/Polyelectrolyte Hybrid Microparticles for Multi-Responsive Drug Delivery." *Journal of Materials Chemistry B.* 2 : 6500-6507.
20. Sato, K. and Anzai, J.I. 2013. "Dendrimers in Layer-by-Layer Assemblies: Synthesis and Applications." *Molecules.* 18 : 8440-8460.
21. He´lary, G. Noircle`re, F. Mayingi, J. and Migonney, V. 2009. "A New Approach to Graft Bioactive Polymer on Titanium Implants: Improvement of MG 63 cell Differentiation onto This Coating." *Acta Biomaterialia.* 5 : 124–133.
22. Temnoff, J.S. and Mikos, A.G. 2008. **Biomaterials the Intersection of Biology and Materials Science.** London : Pearson Education.
23. Williams, D.F. 1999. **Williams Dictionary of Biomaterials.** New York : Liverpool University Press.
24. Bizios, R. Dee, K.C. and Puleo, D.A. 2003. **An Introduction to Tissue-Biomaterial Interactions.** New Jersey : John Wiley & Sons.
25. Schubert, U. and Hüsing, N. 2012. **Synthesis of Inorganic Materials.** 3rd, rev.ed. Weinheim : Wiley-VCH Verlag GmbH & Co. KGaA.
26. Hench, L.L., editor. 2013. **An Introduction to Bioceramics.** 2nd ed. Florida : Imperial College Press.

27. Wong, J.Y. and Bronzino, J.D., editor. 2007. **Biomaterials.** London : CRC Press.
28. Nalwa, H.S., editor. 2004. **Encyclopedia of Nanoscience and Nanotechnology.** Vol. 7. California : American Science Publisher.
29. Nalwa, H.S., editor. 2005. Handbook of Nanostructured Biomaterials and Their Applications in Nanobiotechnology Vol. 2. California : American Science Publisher.
30. Dorozhkin, S.V. 2012. "Nanodimensional and Nanocrystalline Calcium Orthophosphates." *American Journal of Biomedical Engineering.* 2(3) : 48-97.
31. Nalwa, H.S., editor. 2004. **Encyclopedia of Nanoscience and Nanotechnology Vol. 1.** California : American Science Publisher.
32. Sadat-Shojai, M. Khorasani, M.T. Dinpanah-Khoshdargi, E. and Jamshidi, A. 2013. "Synthesis Methods for Nanosized Hydroxyapatite with Diverse Structures." *Acta Biomaterialia.* 9 : 7591–7621.
33. Nasiri-Tabrizi, B. Honarmandi, P. and Ebrahimi-Kahrizsangi, R. 2009. "Synthesis of Nanosize Single-Crystal Hydroxyapatite via Mechanochemical Method." *Materials Lettrs.* 63 : 543-546.
34. Rujitanapanich, S. Kumpapan, P. and Wanjanoi, P. 2014. "Synthesis of Hydroxyapatite from Oyster Shell via Precipitation." *Energy Procedia.* 56 : 112–117.
35. Padmanabhan, S.K. Balakrishnan, A. Chu, M.C. Lee, Y.J. Kim, T.N. and Cho, S.J. 2009. "Sol–Gel Synthesis and Characterization of Hydroxyapatite Nanorods." *Particuology.* 7 : 466–470.
36. Giardina, M.A. and Fanovich, M.A. 2010. "Synthesis of Nanocrystalline Hydroxyapatite from $Ca(OH)_2$ and H_3PO_4 Assisted by Ultrasonic Irradiation." *Ceramics International.* 36 : 1961–1969.
37. West, A.N. 1984. **Solid State Chemistry and Its Applications.** New York : John Wiley & Sons.
38. Somiya, S. Roy, R. and Komarneni, S. 2002. "Hydrothermal Synthesis of Ceramic Oxide Powders." *Bull.Mat.Sci.* 23 : 453-460.
39. Kötz, J. Kosmella, S. and Beitz, T. 2001. "Self-Assemble Polyelectrolyte Systems." *Progress in Polymer Science.* 26 : 1199-1232.
40. Wyatt, N.B. Gunther, C.M. and Liberatore, M.W. 2011. "Increasing Viscosity in Enlangled Polyelectrolyte Solutions by the Addition of Salt." *Polymer.* 52 : 2437-2444.
41. Kroschwitz, J.I., editor. 1990. **Consice Encyclopedia of Polymer Science and Engineering.** New York : John Wiley & Sons.
42. Mark, H.F., editor. 2007. Encyclopedia of Polymer Science and Technology. 3rd ed. New Jersey : John Wiley & Sons.

43. Israelachrili, J.N. 2011. **Intermolecular and Surface Forces.** 3rd ed. Amsterdam Academic Press.
44. Fuoss, R.M. 1948. "Polyelectrolytes." *Science.* 19(108) : 545-550.
45. Salamone, J.C., editor. 1996. **Polymeric Materials Encyclopedia.** Vol. 8. Boca Raton: CRC Press.
46. Mark, H.F., editor, 2003. **Encyclopedia of Polymer Science and Technology** Vol.7. 3rd ed. New Jersey : CRC Press.
47. Xian, W. 2009. **A Laboratory Course in biomaterials.** Boca Raton : CRC Press.
48. Khademhosseini, A. and Jabbari, E., editors. 2010. Biologically-Responsive Hybrid Biomaterials. London : World Scientific Pubishing.
49. Sawan, S.P. and Manivannam, G., editor. 2000. **Antimicrobrial/Anti-Infective Materials : Principles, Applications and Devices.** Pennylvania : Technomic Publishing Company.
50. Greenwood, D.,editor. 2000. **Antimicrobial Chemotherapy.** 4th ed. New York : Oxford University Press.
51. Hoa, W.F. Hsu, H.C. Hsu, S.K. Hung, C.W. and Wu, S.C. 2013. "Calcium Phosphate Bioceramics Synthesized from Eggshell Powders through a Solid State Reaction." *Ceramics International.* 39 : 6467–6473.
52. Pramanik, S. Agarwal, A.K. and Rai, K.N. 2005. "Development of High Strength Hydroxyapatite for Hard Tissue Replacement." *Trends Biomater. Artif. Organs.* 19(1) : 46-51.
53. Monmaturapoj, N. and Yatongchai, C. 2010. "Effect of Sintering on Microstructure and Properties of Hydroxyapatite Produced by Different Synthesizing Methods." *Journal of Metals, Materials and Minerals.* 20(2) :53-61.
54. Pramanik, S. Agarwal, A.Kumar. Rai, K.N. and Garg, A. 2007. "Development of High Strength Hydroxyapatite by Solid-State-Sintering Process." *Ceramics International.* 33 : 419–426.
55. Fahami, A. Nasiri-Tabrizi, B. Ebrahimi-Kahrizsangi, R. 2012. "Synthesis of Calcium Phosphate-Based Composite Nanopowders by Mechanochemical Process and Subsequent Thermal Treatment." *Ceramics International.* 38 : 6729–6738.
56. Mandal, T. Mishra, B.K. Garg, A. and Chaira, D. 2014. "Optimization of Milling Parameters for the Mechanosynthesis on Nanocrystalline Hydroxyapatite." *Powder Technology.* 253 : 650–656.
57. Rhee, S.H. 2002. "Synthesis of Hydroxyapatite via Mechanochemical Treatment." *Biomaterials.* 23 : 1147–1152.

58. Wu, S.C. Hsu, H.C. Wu, Y.N. and Ho, W.F. 2011. "Hydroxyapatite Synthesized from Oyster Shell Powders by Ball Milling and Heat Treatment." *Materials Characterization.* 62 : 1180–1187.

59. Nasiri-Tabrizi, B. Honarmandi, P. Ebrahimi-Kahrizsangi, R. and Honarmandi, P. 2009. "Synthesis of Nanosize Single-Crystal Hydroxyapatite via Mechanochemical Method." *Materials Letters.* 63 : 543–546.

60. Monmaturapoj, N. 2008. "Nano-Size Hydroxyapatite Powders Preparation by Wet-Chemical Precipitation Route." *Journal of Metals, Materials and Minerals.* 18(1) : 15-20.

61. Afshar, A. Ghorbani, M. Ehsani, N. Saeri, M.R. and Sorrell, C.C. 2003. "Some Important Factors in the Wet Precipitation Process of Hydroxyapatite." *Materials and Design.* 24 : 197–202.

62. Cengiz, B. Gokce, Y. Yildiz, N. Aktas, Z. and Calimli, A. 2008. "Synthesis and Characterization of Hydroxyapatite Nanoparticles." *Colloids and Surfaces A: Physicochemical and Engineering Aspects.* 322 : 29–33.

63. Abidi, S.S.A. and Murtaza, Q. 2014. "Synthesis and Characterization of Nano-Hydroxyapatite Powder Using Wet Chemical Precipitation Reaction." *Journal of Materials Science & Technology.* 30(4) : 307-310.

64. Zhu, J. Kong, D. Zhang, Y. Yao, N. Tao, Y. and Qiu, T. 2011. "The Influence of Conditions on Synthesis Hydroxyapatite By Chemical Precipitation Method." *Materials Science and Engineering.* 18 : 1-4.

65. Goloshchapov, D.L. Kashkarov, V.M. Rumyantseva, N.A. Seredin, P.V. Lenshin, A.S. Agapov, B.L. and Domashevskaya, E.P. 2013. "Synthesis of Nanocrystalline Hydroxyapatite by Precipitation Using Hen's Eggshell." *Ceramics International.* 39 : 4539–4549.

66. Liu, D.M. Troczynski, T. Tseng, W.J. 2002. "Aging Effect on the Phase Evolution of Water-Based Sol–Gel Hydroxyapatite." *Biomaterials.* 23 : 1227–1236.

67. Fathi, M.H. and Hanifi, A. 2007. "Evaluation and Characterization of Nanostructure Hydroxyapatite Powder Prepared by Simple Sol–Gel Method." *Materials Letters.* 61 : 3978–3983.

68. Kumar, A.R. and Kalainathan, S. 2010. "Sol–Gel Synthesis of Nanostructured Hydroxyapatite Powder in Presence of Polyethylene Glycol." *Physical B: Condensed Matter.* 405 : 2799–2802.

69. Rajabi-Zamani, A.H. Behnamghader, A. and Kazemzadeh, A. 2008. "Synthesis of Nanocrystalline Carbonated Hydroxyapatite Powder via Nonalkoxide Sol–Gel Method." *Materials Science and Engineering C.* 28 : 1326–1329.

70. Brundavanam, R.K. Jiang, Z.T. Chapman, P. Le, X.T. Mondinos, N. Fawcett, D. and Poinern, G.E.J. 2011. "Effect of Dilute Gelatine on the Ultrasonic Thermally

Assisted Synthesis of Nano Hydroxyapatite." *Ultrasonics Sonochemistry.* 18 : 697–703.

71. Li-yun, C. Chuan-bo, Z. and Jian-feng, H. 2005. "Influence of Temperature, [Ca^{2+}], Ca/P Ratio and Ultrasonic Power on the Crystallinity and Morphology of Hydroxyapatite Nanoparticles Prepared with a Novel Ultrasonic Precipitation Method." *Materials Letters.* 59 : 1902 – 1906.
72. Han, Y. Li, S. Wang, X. Bauer, I. and Yin, M. 2007. "Sonochemical Preparation of Hydroxyapatite Nanoparticles Stabilized by Glycosaminoglycans." *Ultrasonics Sonochemistry.* 14 : 286–290.
73. Poinern, G.E. Brundavanam, R.K. Mondinos, N. and Jiang, Z.T. 2009. "Synthesis and Characterisation of Nanohydroxyapatite Using an Ultrasound Assisted Method." *Ultrasonics Sonochemistry.* 16 : 469–474.
74. Rouhani, P. Taghavinia, N. and Rouhani, S. 2010. "Rapid Growth of Hydroxyapatite Nanoparticles Using Ultrasonic Irradiation." *Ultrasonics Sonochemistry.* 17 : 853–856.
75. Kumar, G.S. Thamizhavel, A. and Girija, E.K. 2012. "Microwave Conversion of Eggshells into Flower-like Hydroxyapatite Nanostructure for Biomedical Applications." *Materials Letters.* 76 : 198–200.
76. Kalita, S.J. and Verma, S. 2010. "Nanocrystalline Hydroxyapatite Bioceramic Using Microwave Radiation: Synthesis and Characterization." *Materials Science and Engineering C.* 30 : 295–303.
77. Ramesh, S. Tan, C.Y. Bhaduri, S.B. and Teng, W.D. 2007. "Rapid Densification of Nanocrystalline Hydroxyapatite for biomedical Applications." *Ceramics International.* 33 : 1363–1367.
78. Hao, L. Yang, H. Zhao, N. Du, C. and Wang, Y. 2014. "Controlled Growth of Hydroxyapatite Fibers Precipitated by Propionamide through Hydrothermal Synthesis." *Powder Technology.* 253 : 172–177.
79. Zhang, H.B. Zhou, K.C. Li, Z.Y. and Huang, S.P. 2009. "Plate-like Hydroxyapatite Nanoparticles Synthesized by the Hydrothermal Method." *Journal of Physics and Chemistry of Solids.* 70 : 243–248.
80. Zhao, X.Y. Zhu, Y.J. Lu, B.Q. Chen, F. Qi, C. Zhao, J. and Wu, J. 2014. "Hydrothermal Synthesis of Hydroxyapatite Nanorods Using Pyridoxal-5′-Phosphate as a Phosphorus Source." *Materials Research Bulletin.* 55 : 67– 70.
81. Jokic´, B. Mitric´, M. Radmilovic´, V. Drmanic´, S. Petrovic´, R. and Janac´kovic´, D. 2011. "Synthesis and Characterization of Monetite and Hydroxyapatite Whiskers Obtained by a Hydrothermal Method." *Ceramics International.* 37 : 167–173.

82. Yang, L.X. Yin, J.J. Wang, L.L. Xing, G.X. Yin, P. and Liu, Q.W. 2012. "Hydrothermal Synthesis of Hierarchical Hydroxyapatite: Preparation, Growth Mechanism and Drug Release Property." *Ceramics International.* 38 : 495–502.

83. Zhang, H. and Darvell, B.W. 2010. "Synthesis and Characterization of Hydroxyapatite Whiskers by Hydrothermal Homogeneous Precipitation Using Acetamide." *Acta Biomaterialia.* 6 : 3216–3222.

84. Parthiban, S.P. Kim, Y. Kikuta, K. and Ohtsuki, C. 2011. "Effect of Urea on Formation of Hydroxyapatite through Double-Step Hydrothermal Processing." *Materials Science and Engineering C.* 31 : 1383–1388.

85. Jinawath, S. Polchai, D. and Yoshimura, M. 2002. "Low-temperature, Hydrothermal Transformation of Aragonite to Hydroxyapatite." *Materials Science and Engineering C.* 22 : 35 – 39.

86. Zhang, X. and Vecchio, K.S. 2007. "Hydrothermal Synthesis of Hydroxyapatite Rods." *Journal of Crystal Growth.* 308 : 133–140.

87. Manafi, S. and Rahimipour, M.R. 2011. "Synthesis of Nanocrystalline Hydroxyapatite Nanorods via Hydrothermal Conditions." *Chemial Engineering Technology.* 34(6) : 972–976.

88. He, D. Xiao, X. Liu, F. and Liu, R. 2008. "Chondroitin Sulfate Template- Mediated Biomimetic Synthesis of Nano-flake Hydroxyapatite." *Applied Surface Science.* 255 : 361–364.

89. García, C. García, C. and Paucar, C. 2012. "Controlling Morphology of Hydroxyapatite Nanoparticles through Hydrothermal Microemulsion Chemical Synthesis." *Inorganic Chemistry Communications.* 20 : 90–92.

90. Zhu, A. Lu, Y. Si, Y. and Dai, S. 2011. "Frabicating Hydroxyapatite Nanorods Using a Biomacromolecule Template." *Applied Surface Science.* 257 : 3174–3179.

91. Ramedani, A. Yazdanpanah, A. Moztarzadeh, F. and Mozafari, M. 2014. "On the Use of Nanoliposomes as Soft Templates for Controlled Nucleation and Growth of Hydroxyapatite Nanocrystals under Hydrothermal Conditions." *Ceramics International.* 40 : 9377–9381.

92. Verma, G. Barick, K.C. Manoj, N. Sahu, A.K. and Hassan, P.A. 2013. "Rod-like Micelle Templated Synthesis of Porous hydroxyapatite." *Ceramics International.* 39 : 8995–9002.

93. Gopia, D. Indira, J. Kavitha, L. Sekar, M. and Mudali, U.K. 2012. "Synthesis of Hydroxyapatite Nanoparticles by a Novel Ultrasonic Assisted with Mixed Hollow Sphere Template Method." *Spectrochimica Acta Part A.* 93 : 131–134.

94. Li, Y. Tjandra, W. and Tam, K.C. 2008. "Synthesis and Characterization of Nanoporous Hydroxyapatite Using Cationic Surfactants as Templates." *Materials Research Bulletin.* 43 : 2318–2326.

95. Amera, W. Abdelouahdi, K. Ramananarivo, H.R. Zahouily, M. Fihri, A. Yannick, C. Varma, R.S. and Solhy, A. 2013. "Synthesis of Mesoporous Nano-Hydroxyapatite by Using Zwitterions Surfactant." *Materials Letters.* 107 :189–193.

96. Liu, C. Ji, X. and Cheng, G. 2007. "Template Synthesis and Characterization of Highly Ordered Lamellar Hydroxyapatite." *Applied Surface Science.* 253 : 6840-6843.

97. Kawakita, H. Gyotoku, A. Seto, H. Ohto, K. Harada, H. and Inoue, K. 2008. "Dextran Formation on Hydroxyapatite by Immobilized Dextransucrase to Control Protein Adsorption." *Carbohydrate Polymers.* 74 : 627–631.

98. Zhang, N. Gao, T. Wang, Y. Wang, Z. Zhang, P. and Liu, J. 2015. "Environmental pH-Controlled Loading and Release of Protein on Mesoporous Hydroxyapatite Nanoparticles for Bone Tissue Engineering." *Materials Science and Engineering C.* 46 : 158–165.

99. Matsumoto, T. Okazaki, M. Inoue, M. Yamaguchi, S. Kusunose, T. Toyonaga, T. Hamada, Y. and Takahashi, J. 2004. "Hydroxyapatite Particles as a Controlled Release Carrier of Protein." *Biomaterials.* 25 : 3807–3812.

100. Tomoda, K. Ariizumi, H. Nakaji, T. and Makino, K. 2010. "Hydroxyapatite Particles as Drug Carriers for Proteins." *Colloids and Surfaces B: Biointerfaces.* 76 : 226–235.

101. Yin, G. Liu, Z. Zhan, J. Ding, F. and Yuan, N. 2002. "Impacts of the Surface Charge Property on Protein Adsorption on Hydroxyapatite." *Chemical Engineering Journal.* 87 : 181–186.

102. ISO 10993-5. 2009. **Biological evaluation of medical devices Part 5: Tests For *in vitro* cytotoxicity by the International Organization for Standardization.** 24-28.

103. Clinical and Laboratory Standards Institute. 2011. **Performance Standards for Antimicrobial Susceptibility Testing: Twenty-First Informational Supplement.** M100–S21.

104. Song, Y. W. Shan, D. Y. and Han, E. H. 2008. "Electrodeposition of Hydroxyapatite Coating on AZ91D Magnesium alloy for Biomaterial Application." *Materials Letters.* 62 : 3276-3279.

105. Sadat-Shojai, M. Mohammad-taghi, K. Dinpanah-Khoshdargi, E. and Jamshidi, A. 2013. "Synthesis Methods for Nanosized Hydroxyapatite with Diverse Structures." *Acta Biomaterialia.* 9 : 7591-7621.

106. Cengiz, B. Gokce, Y. Yildiz, N. Aktas, Z. and Calimli, A. 2008. "Synthesis and Characterization of Hydroxyapatite nanoparticles." *Colloids and Surfaces A: Physicochem.Eng.Aspects.* 322 : 29-33.

107. Xiao, X. Liu, R. Liu, F. Zheng, X. and Zhu, D. 2010. "Effect of Poly(sodium 4 styrene-sulfonate) on The Crystal Growth of Hydroxyapatite Prepared by Hydrothermal method". *Materials Chemistry and Physics.* 120 : 603-607.

108. Luo, Q. and Andrade, A. D. 1998. "Cooperative Adsorption of Proteins onto Hydroxyapatite". *Journal of Colloid and Interface Science.* 200 : 104-113.

109. Gad, S. C. 1999. Alternatives to *in vivo* Studies in Toxicology. 178.

Author Biography

Name	Miss Pakvipar Chaopanich
Date of birth	14 December 1978
Address	351 Moo 3 Tha Wang Tong Muang Phayao 56000
Education	2001 Bachelor of Science in Chemistry GPA 2.76 King Mongkut's University of Technology Thonburi 2005 Master of Science in Inorganic Chemistry GPA 3.27 Kasetsart University
Scholarship	The Office of the Higher Education Commission, Ministry of Education, Thailand under the Research Project Title "Higher Education Research Promotion"
Academic Publications	1. Chaopanich, P. and Siriphannon, P. 2015. Facile Refluxing Synthesis of Hydroxyapatite Nanoparticles, *Australian Journal of Chemistry*. 68: 1293-1298. 2. Chaopanich, P. and Siriphannon, P. 2016. Sodium Sulfonate Template Assisted Hydrothermal Synthesis of Hydroxyapatite Nanorods. *Indian Journal of Chemistry*. 55A: 1084-1089.